PALACKY UNIVERSITY OLOMOUC

Faculty of Science

Department of Biochemistry

Differential organization of MAP65-2 and MAP65-3 in Arabidopsis

Diploma thesis

Author:	**Bc. Renáta Šnaurová**
Study programme:	B1406 Biochemistry
Field of study:	Biotechnology and Gene Engineering
Form of study:	Full
Supervisor:	**Georgios Komis, Ph.D.**
Year:	2019

I declare that I developed this diploma thesis separately and showing all the sources and authorship. I agree with the publication of the thesis by Act no. 111/1998 Coll., about universities, as amended. I was aware that the rights and obligations arising from the Act no. 121/2000 Coll., the Copyright Act, as amended, are applied to my work.

At Olomouc …… ……..……

Acknowledgments

I wish to express my sincere gratitude to my supervisor Georgios Komis, PhD. for his continuous professional guidance and help throughout the study, teaching, the patient time he gave me, his constructive criticism and suggestions during the preparation my diploma thesis and for his unique attitude toward people. Thanks are also extended to all members of the Department of Cell Biology under the leadership of Prof. Jozef Šamaj for the constructive working atmosphere, the help that I received and scientific discussions. I also want to thank my family and friends who have been supportive to me throughout the entire study, their understanding, patience, and encouragement. And I also thanks Mgr. Věra Frgálová for her good notifications and corrections during writing my thesis. During this work, I was funded by GACR project 503103671/33 and IGA projects IGA_PrF_2018_031 and IGA_PrF_2019_011.

Bibliography identification

Author's name and Surname	Renáta Šnaurová
Title	Differential organization of MAP65-2 and MAP65-3 in Arabidopsis
Type of thesis	Diploma
Department	Department of Biochemistry
Supervisor	Georgios Komis, Ph.D.
The year of presentation	2019

Abstract

In the present thesis, I study the differential localization and the dynamics of two dominant microtubule associated proteins of *Arabidopsis thaliana* with a role in microtubule bundling. The first protein MAP65-2 is ubiquitous and associated with cortical microtubule systems and with the developing cytokinetic apparatus the phragmoplast. The second, MAP65-3 exclusively associates with mitotic and cytokinetic microtubule systems. We followed the distribution of both proteins in seedlings of *A. thaliana* expressing tagged versions of either protein. We followed the dynamics of MAP65-2 by means of spinning disc or structured illumination microscopy and we identified a novel mechanism of MAP65-2 loading in the developing phragmoplast. In appropriately transformed living cells and by means of immunolabeling we were able to covisualize both MAP65-2 and MAP65-3 in relation to microtubules and to show that both proteins have non-overlapping patterns of localization

Keywords	Arabidopsis, cell division, microtubules, roots, MAP65-2, MAP65-3
Number of pages	87
Number of attachments	1
Language	English (Czech)

Bibliografická identifikace

Jméno a příjmení autora	Renáta Šnaurová
Název práce	Diferenciální lokalizace MAP65-2 a MAP65-3 v Arabidopsis
Typ práce	Diplomová
Pracoviště	Katedra biochemie
Vedoucí práce	Georgios Komis, Ph.D.
Rok obhajoby práce	2019

Abstrakt

V této diplomové práci se zabývám diferenciální lokalizací a dynamikou dvou dominantních proteinů asociovaných s mikrotubuly *Arabidopsis thaliana* tvořících svazky mikrotubulů. První proteinem je MAP65-2, který je všudypřítomný a je spojen s kortikálním mikrotubulárním systémem a s vyvíjejícím se cytokinetickým aparátem – fragmoplastem. Druhým je MAP65-3, který asociuje výhradně s mitotickými a cytokinetickými systémy mikrotubulů. Sledovali jsme distribuci obou proteinů v semenáčcích *Arabidopsis thaliana* exprimujících značené verze obou proteinů. Pozorovali jsme také dynamiku MAP65-2 pomocí konfokálního mikroskopu s rotujícím diskem nebo mikroskopie se strukturovaným osvětlením a identifikovali jsme nový mechanismus distribuce MAP65-2 ve vyvíjejícím se fragmoplastu. Byli jsme schopni vizualizovat MAP65-2 i MAP65-3 a jejich vztah k mikrotubulům ve vhodně transformovaných živých buňkách a pomocí imunoznačení ukázat, že se vzory lokalizací obou proteinů nepřekrývají.

Klíčová slova	Arabidopsis, buněčné dělení, mikrotubuly, kořeny, MAP65-2, MAP65-3
Počet stran	87
Počet příloh	1
Jazyk	Anglický (Český)

Table of Contents

Aims of the thesis

Theoretical Part

− Study of literature regarding the major classes of protein kinases regulating microtubules in plants and MAP65 proteins

Experimental Part

− Microscopic characterization of dynamics of MAP65-2 and MAP65-3 fusions with eGFP

− Covisualization of MAP65-2 and MAP65-3 in defined microtubule systems

− Covisualization of MAP65-2, MAP65-3, and microtubules in immunolabeled root wholemounts

− Crossings between MAPK mutants and lines expressing eGFP-MAP65-2 or eGFP-TUA6

1 Introduction

Higher plant cells are immobile and encased in a rigid cell wall, prohibiting large scale cell movements. However, the interior of the cell is highly dynamic with components of intracellular architecture undergoing rapid and vast rearrangements in space and time. The plant cell is overcrowded with cellular components, and these components are translocated from site to site by a highly organized and sophisticated regulated process. Such movements are largely owing to widespread components of the plant cytoskeleton, which is comprising of microtubules and actin microfilaments. Both cytoskeletal elements exhibit unique features of intracellular organization and play a wide range of roles, supporting fundamental cellular functions such as cell growth and cell division.

Although cytoskeletal proteins of eukaryotic cells are highly conserved they exceptionally show differences in their overall structure between plant and animal kingdoms. The microtubular cytoskeleton in higher plants participates in cell division and growth, determines the shape and polarity of cells, and also participates in vesicular transport and programmed cell death.

The microtubular plant cytoskeleton is intimately associated with both the formation and the patterning of rigid cell walls and hence is essential for defining cell growth directionality and blueprinting cellular morphogenesis. The guided formation of the cell wall is important for plant development – it defines the orientation of cell growth by means of directed cellulose deposition. Moreover, by controlling the cell division symmetry and cell division plane orientation, microtubules are implicated in tissue pattern formation.

The plant cytoskeleton is able to be very rapidly remodeled and is promptly responsive to conditional and developmental cues. The cytoskeleton is targeted by mechanisms of cell signaling, including reversible protein phosphorylation of specific cytoskeletal substrates, interaction with secondary messengers such as bioactive phospholipids (Pleskot *et al*., 2013), cyclic nucleotides (Means *et al.*, 1982), and intracellular Ca^{2+} (Means *et al.*, 1982).

The implication of the cytoskeleton in cell division, cytoskeletal rearrangements during the process are regulated by temporally controlled protein phosphorylation which is of key significance to drive transitions of the mitotic spindle and the movement of chromosomes and sister chromatids. Many microtubular proteins regulations are done by cyclin-dependent kinases (Sato and Toda, 2010) as well as by MAPKs and AURORA

kinases during the process of mitosis and cytokinesis (reviewed in Vavrdová *et al*., 2019). The above protein kinases belong to a group that encompasses classes sharing common targeting mechanisms.

The theoretical part of this thesis, is an overview of the current knowledge of microtubular cytoskeleton, microtubule-associated proteins and their regulation during cell cycle with a focus on the plant cell. The experimental part then deals with practical experiments performed mainly to characterize organization and dynamics of MAP65-2 and MAP65-3 fusions with eGFP, covisualize MAP65-2 and MAP65-3 in defined microtubule systems and covisualize MAP65-2, MAP65-3 and microtubules in immunolabeled root wholemounts.

2 The Current State of the Topic

2.1 An Overview of the Plant Microtubule Cytoskeleton

Higher plant cell motility is prohibited in the classical sense because cells are bound by a rigid cell wall. Definition of tissue patterning and organ identity are aspects of cell specification which require decisions at the cellular level which will occur *in situ* (Robert *et al.*, 2015) and not through migration of cells as it happens during the development of animals (Naylor and Davidson, 2017; Nagy and Goldstein, 2017). Pivotal role of the microtubule cytoskeleton in this context is that it underlies three key features of plant development: it controls cell division positioning and symmetry by defining the cell division plane at any stage of plant development (Kimata *et al*., 2016; Shao and Dong, 2016; Martinez *et al*., 2017); it defines directionality of cell growth by directing deposition of cellulose microfibril (Chen *et al*., 2016; Griffiths *et al*., 2015; Gutierrez *et al*., 2009; Paredez *et al*., 2006); and it drives the genetic material partitioning to two physically separated daughter cells via the cytokinetic deposition of the nascent cell plate through the successive processes of mitosis and cytokinesis (Miart *et al.*, 2014; Murata *et al.*, 2013).

2.2 Microtubules

Microtubules (MTs) have an outer diameter about 25 nm (Choi *et al.*, 2009). The internal diameter of these hollow polymeric cylindrical structures is 14 nm (Tilney *et al.*, 1973). The microtubule is usually composed of 13 longitudinal protofilaments, each formed by polymerization of α- and β-tubulin heterodimers (see Fig. 1A). These heterodimers are the basic building blocks of the microtubular cytoskeleton. The heterodimers of individual adjacent protofilaments engage into homotypic lateral interactions when two α- and two β-subunits always interact. However, the first and the last protofilaments form only a heterotypic junction (interaction of α-subunit with adjacent β-subunit; see Fig. 1A) arising from the shift between protofilaments (Vleugel *et al.*, 2016). Thus, a so-called seam is formed at the point of displacement, which is involved in the dynamics of microtubules, as it may be the site of their dissociation or association (Vleugel *et al*., 2016; Wade, 2009; Wade and Hyman, 1997).

α- and β-Tubulins belong to the tubulin superfamily. Six isotypes of α-tubulin (Kopczak *et al*., 1992), nine β-tubulin isotypes and two functionally redundant γ-tubulin isoforms are known in *A. thaliana* (Snustad *et al.*, 1992; Liu *et al.*, 1994). The diversity

of tubulin isoform is enhanced through post-translational modifications (PTM; Magiera and Janke, 2014).

Together they form stable heterodimers. Both α- and β-tubulin have a binding site for guanosine triphosphate (GTP) on their molecules, with α-tubulin binding GTP firmly, unlike β-tubulin, which has GTP-like activity and where GTP is hydrolyzed to GDP. The energy released by the cleavage of this macroergic bond is utilized to bind the tubulin heterodimer molecule to a second heterodimer to form longitudinal protofilaments. When GTP is bound to β-tubulin, the heterodimer assumes a direct conformation that facilitates lateral protofilament binding. In the hydrolysis of GTP to GDP, conformation changes from direct to curved and protofilaments are suddenly prone to disintegration (Muller-Reichert *et al*., 1998; Rice *et al*., 2008). All the above-mentioned properties of tubulins and their polymers point to two important and interrelated aspects.

First, the microtubules show polarity. This means that αβ-tubulin heterodimers are bound to each other by the "head-tail" rule and thus one end of the microtubules is formed by the α-tubulin ring (the (-) end), the other end of the microtubules is formed by the β-tubulin ring (the so-called "end") (+) end; see Fig. 1A).

Second, microtubules exhibit dynamic instability. Dynamic instability is characterized by rapid growth or shortening of microtubules, in response to immediate cell requirements (Mandelkow *et al*., 1991; Shaw *et al.*, 2003). The rapid depolymerization of microtubules is called "catastrophe", a return to "rescue" growth, a sustained "suspended" microtubule. Microtubules are often found in the cell in the form of microtubule bundles. Microtubule dynamics have also been described in these bundles (see Fig. 1B; Komis *et al*., 2014; Shaw *et al*., 2003).

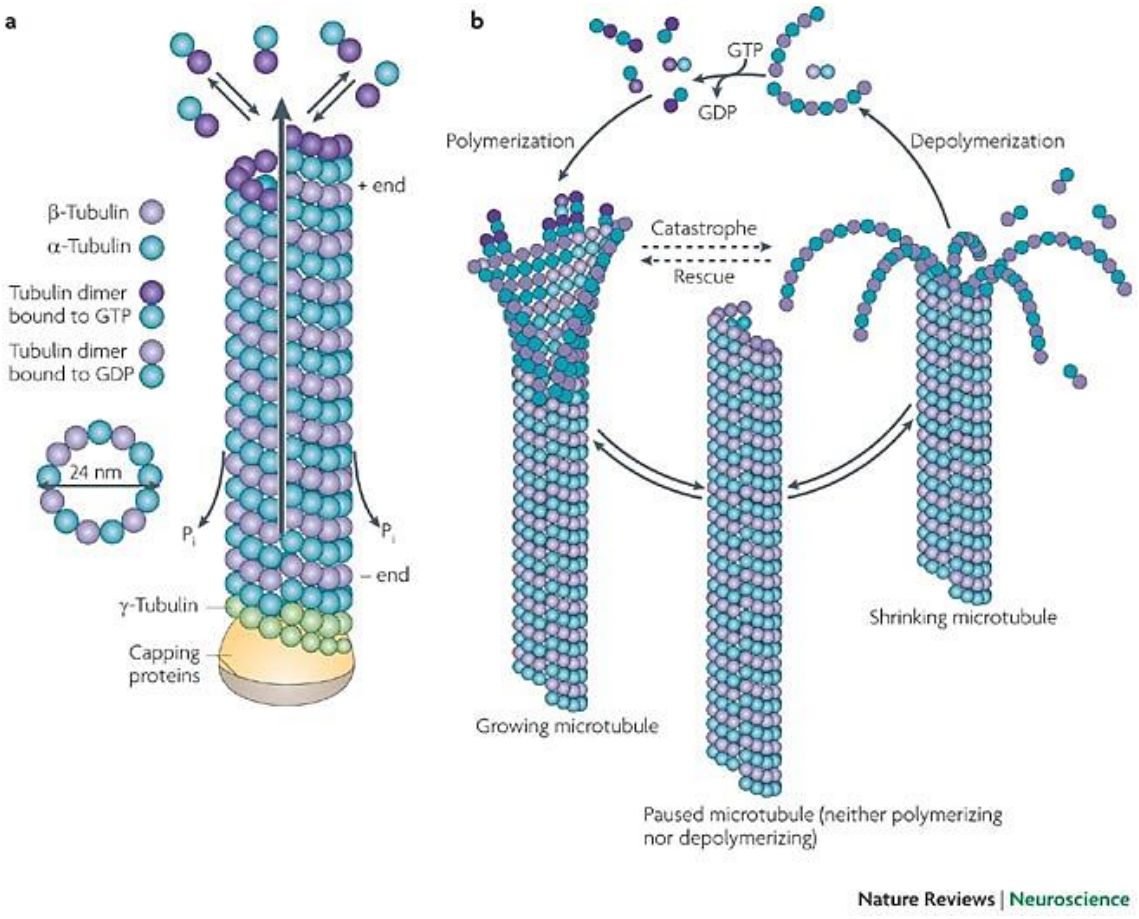

Figure 1. Microtubule structure and dynamics. **A.** Representation of tubulin subunits by different-colored spheres – blue for α-tubulin and purple for β-tubulin, γ-tubulin is in green. The hollow cylindrical MT is made of 13 linear protofilaments created of vertically-stacked tubulin heterodimers. The (+) end is shown at the top and the (-) at the bottom while β-tubulin faces the (+) end and α-tubulin the (-) end. The seam is shown by a vertical black arrow. The diameter 24 nm of MT is shown as a cross-section off to the left. The γ-tubulin ring complex for nucleation is at the (-) end and labeled with capping proteins. **B.** MT transition scheme for transition from growing (polymerizing) to shrinking (depolymerizing), and paused state. GTP-bound tubulin subunits are present in the growing end of the microtubule. Taken from Rochlin *et al*., 1999.

Plant cells have different microtubule configurations compared to animal cells. During interphase, microtubules are oriented predominantly along the plasma membrane, where they form a network of cortical, highly dynamic microtubules (Wasteneys, 2002). Among other things, the function of cortical microtubules is closely linked to the formation of the cell wall. It is believed that the cellulose-synthase enzyme (CESA), which is directly involved in cell wall construction, is transported to the target site on the microtubules (Paredez *et al*., 2006). In most cell types, during the G2 phase, the cortical network of microtubules is reorganized and microtubules begin to concentrate in a thin ring around the nucleus upon transition to the prophase. Thus, a preprophase band (PPB) is created, which defines the future plane of division (Nogami and Mineyuki, 1999; Pickett-Heaps

and Northcote, 1966). PPB gradually disappears and a mitotic spindle is formed, dividing chromosomes into two daughter cells. In the course of mitosis, acentrosomal spindle passes by a series of changes (there are no centrosomes in which the (-) ends of the microtubules are anchored).

2.2.1 The Microtubule Cytoskeleton during Cell Growth and Cell Cycle

The plant cells do not have centrosome, but we can find other plant-specific microtubule structures. During interphase, plant microtubules are arranged by self-organization into a highly dynamic network of cortical microtubules (see Fig. 2F) located on the inside of the cytoplasmic membrane and capable of reorganizing according to the actual needs of the cell (Komis *et al.*, 2014; Ma *et al.*, 2016; Shaw, 2013; Wasteneys and Ambrose, 2009). Cortical microtubule cytoskeleton serves as the draft for appropriate spatial deposition of cellulose microfibrils in the overlying cell wall to sustain cell growth and cytomorphogenesis (Komis *et al.*, 2015; Li *et al.*, 2015). Cellulose microfibril patterns coincide with cortical microtubules which furnish tracks for the regulation of the transmembrane cellulose synthase complexes trajectories as they catalyze the nascent cellulose microfibrils polymerization (Paredez *et al.*, 2006). A vesicular delivery of cellulose synthases to the plasma membrane is assisted by microtubules during targeted exocytosis (Gutierrez *et al.*, 2009).

As the cell goes through the cell cycle and enters the cell division phase, drastic changes at the subcellular and molecular level are required. The cortical MTs are concentrated into parallel bundles in a narrow band around the cell nucleus – structure called the preprophase band (see Fig. 2A) which indicates the position for subsequent cell division (Rasmussen *et al.*, 2013), but there are apparently other mechanisms for determining PPB-independent positioning (Rasmussen *et al.*, 2013; Zhang *et al.*, 2016). The beginning of the PPB formation seems like a broad ring of parallel microtubules and then narrows before the onset of mitosis (Dhonukshe and Gadella, 2003). The PPB coexists with the precursor of the mitotic spindle – a polar, perinuclear microtubule array – for a while, then the PPB disassembles and mitosis is initiated, but a trace remains at the original site for the later formation of a cellular plate (Rasmussen *et al.*, 2013), a breakdown of the nuclear envelope occurs and condensed chromatin is exposed to cytoplasmic environment.

The bipolar mitotic spindle is formed (prophase to prometaphase) and is necessary for proper nucleus distribution, is acentrosomal in plants due to the absence of centrosome

and microtubules are organized by themselves. Chromosomes start interacting via kinetochores with MT bundles and are also involved in their organization (Dinarina *et al.*, 2009; Petrovská *et al.*, 2013). The purpose of the mitotic spindle at this stage is chromosomes orientation so that kinetochores will be aligned to the equatorial plane which is a random geometrical position which coincides with the cell division plane previously defined by the PPB (metaphase; see Fig. 2B). Accurate partitioning and positioning of the sister chromatids to the two opposite poles of the mitotic spindle are regulated by dramatic spatiotemporal rearrangements of microtubules (Yamada and Goshima, 2017).

Kinetochore-associated microtubules begin to shorten (anaphase) and pairs of identical chromosomes are pulled to the opposite poles of the cell. After the chromosomal division to the opposite poles of the cell (telophase) due to the mitotic spindle, their despiralization and nuclear membrane and nucleoli formation begin to occur.

The microtubules change the conformation from the mitotic spindle to the phragmoplast (see Fig. 2c,d), and from its center, a cell plate synthesis begins, giving rise to a new plasma membrane and a cell wall. Cell plate formation and positioning are predetermined on the signal of microtubules of the preprophase band (Lipka *et al.*, 2014; Murata *et al.*, 2013). Antiparallel bundles of both stable and dynamic phragmoplast microtubules are organized perpendicularly to the nascent cell plate and serve as pathways for molecular motors transporting material to form a new cell wall (de Keijzer *et al.*, 2014; Li *et al.*, 2010). The cell plate is subsequently centrifugally expanded by rearrangement of the nucleation complexes at the (-) ends of the microtubules and subsequent nucleation of the new microtubules at the margins of the plate (Murata *et al.*, 2013).

The whole process is completed by the cytokinesis, during which the phragmoplast reaches the cortical side, the cell plate, and the parent membrane fuse to complete cytokinesis; cytoplasm, individual organelles, proteins, and others are separated (see Fig. 2D,E; Smith, 2001; Van Damme *et al.*, 2007). In animal cells, the nuclear membrane is strangled from the outside towards the center by a contractile ring, whereas in plants the membrane is formed from the center to the edges, or centrifugally.

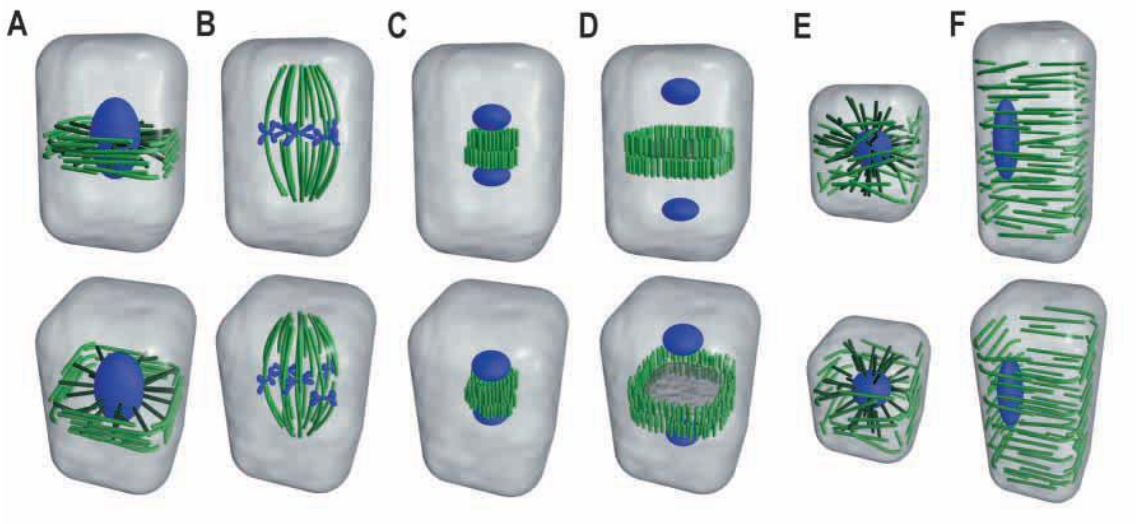

Figure 2. A schematic representation of a microtubule arrangement and its changes during the cell cycle in plants. **A.** A preprophase band indicating the upcoming division. **B.** Metaphase dividing spindle with dispersed polar regions. **C.** Phragmoplast formed between two daughter nuclei. **D.** Cytokinetic phragmoplast centrifugally expanding while forming a cell plate. **E.** At the end of cytokinesis, microtubules radiate from the nucleus towards the microtubules associated with the plasma membrane. **F.** Plant cell in interphase. During cell extension, the cortical microtubules are parallelly arranged. Taken from Wasteneys, 2002).

2.2.2 Nucleation

In eukaryotic cells, the (-) ends of microtubules are mostly anchored in the Microtubule Organizing Center (MTOC), where microtubule nucleation occurs. The major protein involved in microtubule nucleation is another of the tubulin family, γ-tubulin (Binarova *et al.*, 2006; Oakley *et al*., 1990) and proteins forming the complex with γ-tubulin (Drykova *et al*., 2003; Gunawardane *et al.*, 2000; Raynaud-Messina and Merdes, 2007). In animals or yeast, MTOCs are strictly defined, and microtubules nucleate from these particular sites (centrosomes in animals, pole bodies in yeast).

In plants, compared to animals, the situation is a bit different. Although microtubules are also nucleated from γ-tubulin complexes (Drykova *et al*., 2003) of very similar protein composition, they do not have a strictly defined MTOC. MTOC of plant microtubules can be said to be dispersed. Microtubule nucleation in plants occurs on the nuclear membrane (Stoppin *et al.*, 1994), on the plasma membrane (Schmit, 2002), and nucleation has also been shown to occur on the Golgi membrane (Drykova *et al*., 2003). Furthermore, kinetochore nucleation is expected (Binarova *et al*., 2000). Last but not least, microtubules are nucleating themselves – this is predominantly on the cellular cortex under the cell wall (Murata and Hasebe, 2007; Murata *et al.*, 2013; Murata *et al*., 2005). The γ-tubulin is also found at the phragmoplast and has a preference for (-) ends

of microtubules at the distal edges, which are facing the daughter nuclei, and it is not found at the midzone of the phragmoplast (Kong *et al*., 2010).

A template for microtubule nucleation is created of multiprotein γ-tubulin ring complexes (γ-TuRCs) within cells (see Fig. 3; Sulimenko *et al.*, 2017; Kollman *et al.*, 2011; Farache *et al*., 2018; Teixidó-Travesa, 2012). This complex has the γ-tubulin molecules organized in a single-turn helical pattern (Kollman *et al*., 2010) and interactions between γ-tubulin and α/β-tubulin heterodimers, the end-on, serves as the support for the assembly of lateral associated α/β-tubulin heterodimers into protofilaments. A short tubular structure (the microtubule seed) is thought to be promoted by the otherwise kinetically unfavourable formation, which can rapidly polymerise into a microtubule filament after achieving a specific size threshold (see Fig. 3; Kollman *et al*., 2010; Roostalu *et al.*, 2017). The γ-TuRCs are always localized at the MT (-) end containing α-tubulin and the highly dynamic β-tubulin is exposed at the MT (+) end expanding outwards and because of this localization appears to regulate the polarity of MTs (see Fig. 3). High regulation of nucleation of MT in space and time is required to establish the correct formation of MT networks (Sanchez and Feldman, 2016; Petry and Vale, 2015). The activation of the γ-TuRCs happens usually only once when they are recruited to MTOCs within the cell (Tovey and Conduit., 2018).

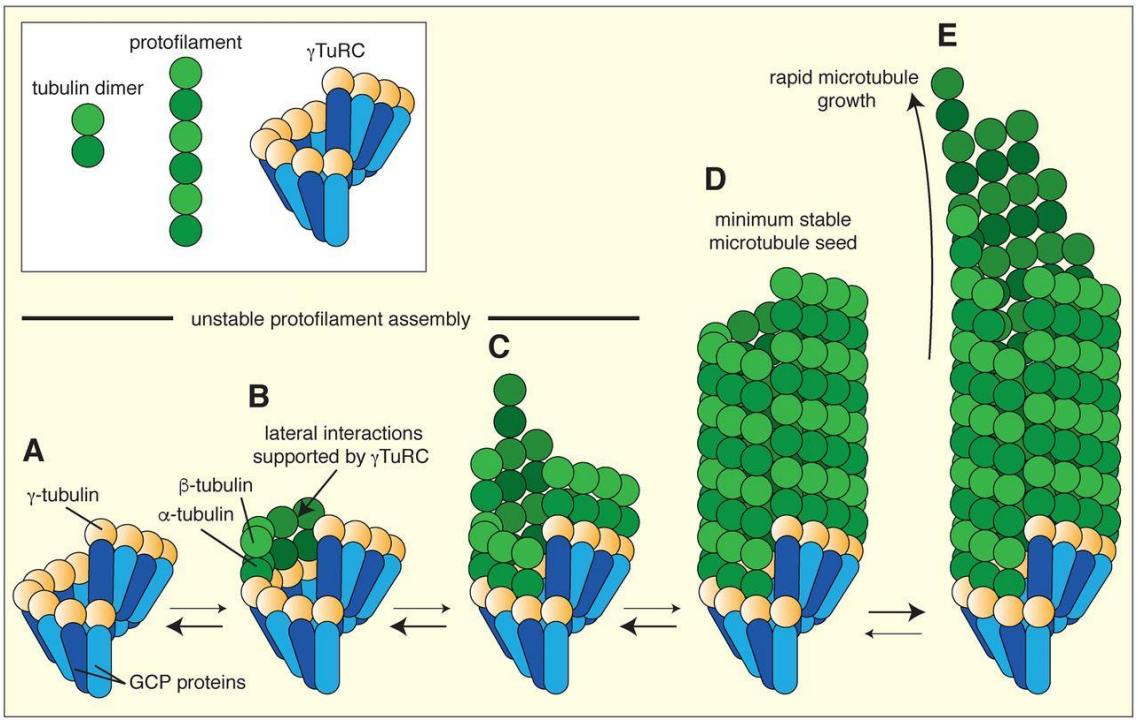

Figure 3. Nucleation of microtubule. **A**. The γ-TuRC is organized in a single-turn helix via their bond to γ-tubulin complex proteins (GCPs, blue), γ-tubulin molecules are in yellow. **B.** The

protofilament growth is promoted by binding of γ-tubulin molecules to α/β-tubulin heterodimers entering from the cytosol. **C.** An unstable and slow stage of MT assembly progresses where disassembly is more probable than continued assembly. **D.** A stable stage of the assembly, where is enough tubulin heterodimers to form a microtubule seed (stable seed size stay unclear). **E.** MT polymerisation progresses rapidly after the formation of the stable seed. Taken from Tovey and Conduit., 2018.

2.2.3 Regulation

Microtubules have many functions in the cell. Rapid adaptation of the cellular machinery is required for conditional and developmental responses of cell growth and division to such abrupt changes. Microtubule mitotic transitions (from the PPB to the mitotic spindle and to the phragmoplast) need to be adjusted on time during the cell division because delays in the progression of some stages can cause an abortion of the mitotic/cytokinetic process (e. g., Beck *et al*., 2011). One possibility of regulating microtubule function are posttranslational modifications of tubulins. A number of them are known (Hammond *et al*., 2008). These include, for example, tyrosine nitration of α-tubulin (Blume *et al.*, 2013), acetylation (Al-Bassam and Corbett, 2012), glycosylation (Hino *et al*., 2003), phosphorylation of α-tubulin by protein kinase C (De *et al*., 2014), interactions with bioactive lipids such as phosphatidic acid (Zhang *et al*., 2012), hydroxylation, methylation, and ubiquitination, and almost all processes at the cellular level are affected (Prabakaran *et al.*, 2012). Phosphorylation is executed by kinase enzymes that catalyze reaction when the γ-phosphate group of ATP is transferred to an acceptor site (typically a hydroxyl group of Ser, Thr or Tyr) in the substrate molecule. Such activated protein kinases target tubulin itself (Ban *et al.*, 2013; Bekešová *et al.*, 2015), as well as a variety of microtubule-associated proteins (e. g., EB1c, Kohoutová *et al.*, 2015; MAP65-1, 2 and 3, Beck *et al*., 2010; Sasabe *et al.*, 2011) are targeted by such and become controlled by reversible phosphorylation events.

Another possibility for regulating microtubules is the interaction with microtubule-associated proteins (MAPs), which will be addressed in the chapter 2.3 of the theoretical introduction belonging to MAPs. The affinity of these proteins to the surface of MTs is mostly regulated by reversible phosphorylation (Smékalová *et al*., 2014; Beck *et al.*, 2010; Kohoutová *et al*., 2015). Microtubule is a polyanion and has a negative charge on its surface under the physiological pH conditions in the cytoplasm, binding of MAPs is electrostatic and depends on the existence of microtubule binding domains with a positive charge (Yu *et al*., 2015).

For example, microtubule-associated protein MAP65-1, which is the founding member of the Feo/PRC1/MAP65 family. It has a bipartite microtubule-binding domain in its carboxyl-terminal end (Smertenko *et al*., 2004). Members of the CGMC group of protein kinases (which includes, cyclin-dependent protein kinases – CDKs; mitogen-activated protein kinases – MAPKs, glycogen synthase kinases – GSKs, and Cdc2-like kinase – CLK) is predicted to target and phosphorylate microtubule-binding domain of MAP65-1. Experimental verification of regulation of MAP65-1 dependent on phosphorylation and affinity for the surface of microtubules has been done (Smertenko *et al.*, 2006; Beck *et al*., 2010).

2.2.3.1 Mitogen Activated Protein Kinases and Its Interactions with Microtubule Cytoskeleton

Mitogen-activated protein kinases, MAP kinases, or MAPKs only, are multienzyme signaling cascade complexes that are highly evolutionarily conserved within eukaryotic organisms (Feng *et al*., 2016; Marangoni *et al*., 2015; Pincus *et al*., 2013). They play a particularly important role in plant signaling, as these immobile organisms react not only to substances from their internal environment, such as hormones or growth regulators but also to external stimuli – these may be different types of stress (Ovečka *et al.*, 2014) or interaction with symbionts and pathogens (Becker *et al.*, 2015; Jalmi and Sinha, 2016).

Mitogen-activated protein kinases are phosphorylation enzymes involved in signaling transduction, gene expression, and activation of various cytoskeletal proteins. MAPKs are involved in regulation of cellular processes such as cell survival, cell division, polarization, stress responses, and metabolism. Phosphorylation of cytoskeletal proteins results in cytoskeleton rearrangement and this leads to morphological changes and cell polarization. Some motor proteins (kinesins) can activate MAPK and participate in transduction of the signal to the correct cellular target (during cell division). Changes in the integrity of cytoskeletal elements have a direct impact on MAPK activity (Šamaj *et al.*, 2004).

MAP kinase signaling pathways function by reversible post-translational phosphorylation (Ovečka *et al*., 2014). At the imaginary peak of the cascade, the MAP kinase kinase kinase (MAP3K) is activated by an extracellular or intracellular stimulus and phosphorylating MAP kinase kinase (MAP2K), which then phosphorylates MAP kinase (MAPK). Phosphorylated MAP kinase then triggers a mechanism leading to

cellular response to a given stimulus (see Fig. 4) through activation/inactivation of transcription factors, cytoskeletal components or other signaling pathways (Smékalová *et al.*, 2014).

MAP3Ks include, for example, proteins of the ANP (*A. thaliana* homolog of nucleus- and phragmoplast-localized kinase) family involved in the organization of the microtubular cytoskeleton and the correct process of cytokinesis (Beck *et al.*, 2010, 2011; Takahashi *et al.*, 2010). The *A. thaliana* double mutant plants in the ANP2 and ANP3 genes showed impaired growth of vegetative organs with unusually branched root hairs (Beck *et al.*, 2010). The strongly bundled microtubules in these mutants have been found by an electron microscope, apparently due to impaired MAP kinase signaling (Beck *et al.* 2010).

MKK6 (mitogen-activated protein kinase 6) is a protein ranked between MAP2Ks and is also involved in cytokinesis in which it is localized in the equatorial portion of the phragmoplast. The MKK6 activator is ANP3 and mutation in the *mkk6* gene in *A. thaliana* leads to cytokinetic defects and premature growth arrest (Takahashi *et al.*, 2010).

Originally, MAPKs were discovered as a type of protein kinases that phosphorylate neuronal microtubule-associated MAP2 protein after insulin stimulation (Ray and Sturgill, 1988). Subsequently, the range of MAP kinase targets was found to be broader. The MAPK association with MTs was found in many mammalian cell types, including neurons and oocytes (Fiore *et al*., 1993; Mandelkow *et al*., 1992) and interacts also with MT in plants. In Arabidopsis, MPK4 and MPK6 are involved in the regulation of MT cytoskeleton (Kosetsu *et al.*, 2010; Takahashi *et al.*, 2010).

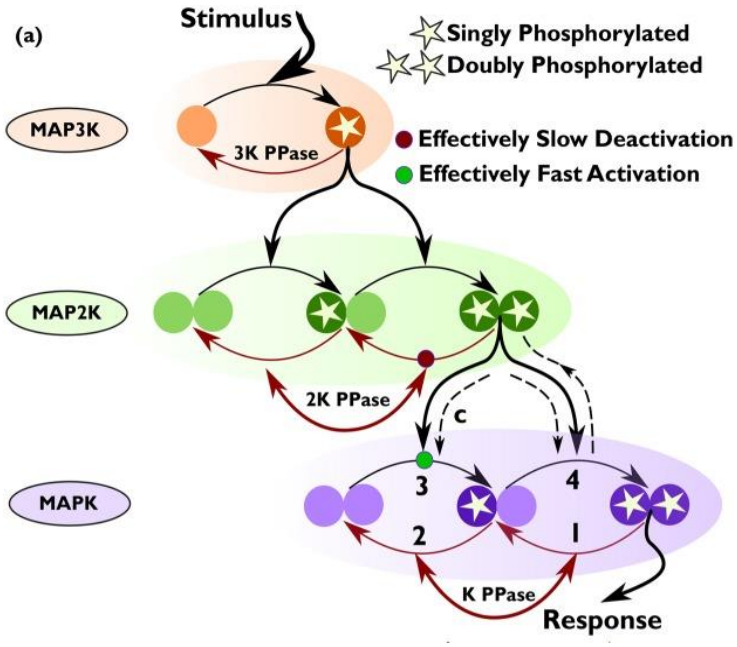

Figure 4. MAPK cascade adaptive response to stimulus. **A.** Linear three layered MAPK cascade scheme. Stimulus activates MAPK kinase kinase (MAP3K). Phosphorylation/dephosphorylation by adding/removing phosphate group is referred to as activation/deactivation of kinases. The activated MAP3K phosphorylates MAPK kinase (MAP2K) for its activation. The activation of MAPK is regulated by doubly phosphorylated MAP2K. The corresponding phosphatase (PPase) deactivatates a phosphorylated kinase in the corresponding layer of the cascade. Adapted from Mitra *et al*., 2018.

2.2.4 Dynamics

Both ends of the microtubules have different growth activity. The (+) end is a rapidly increasing/decreasing end, while the (-) end is much slower in increase/decrease in heterodimers. Growing microtubules have a stabilizing GTP cap at their (+) end because GTP to GDP hydrolysis occurs with a slight delay. If GTP hydrolysis is faster than the addition of new tubulin heterodimers, the GTP cap is lost and microtubules begin to shorten.

Tubulin heterodimers bind a GTP molecule that can be hydrolyzed to GDP. This hydrolyzable GTP carries a β-subunit in the so-called E-site, while a GTP molecule is bound to the α-subunit of the heterodimer at the so-called N-site and is not subject to hydrolysis and is hidden between both subunits (Vleugel *et al*., 2016). The names of both sites are based on their English terms E-site (exchangeable) and N-site (nonexchangeable), which show whether GTP hydrolysis can be exchanged for GDP at a given location (see Fig. 5). The heterodimer carrying GDP on the β-subunit is less tightly bound to the protofilament than the GTP-bearing heterodimer due to the conformational change caused by GTP hydrolysis (Alushin *et al*., 2014; Horio and

Murata, 2014; Wade, 2009). If free αβ-heterodimers are added to the emerging microtubule faster than GTP hydrolysis, the microtubule grows, a so-called GTP cap is formed at its plus end to prevent depolymerization (see Fig. 6; Dimitrov *et al*. 2008; Piedra *et al.*, 2016). Only after incorporation of the heterodimer into the microtubule is GTP hydrolyzed on the β-subunit, giving a lattice containing predominantly GDP on β-subunits (Dimitrov *et al*., 2008). However, if the new heterodimers are integrated more slowly into the microtubule, then, after GTP hydrolysis, the bonds between the heterodimers in the microtubule are destabilized, leading to its degradation and shortening. The transition from polymerization to depolymerization is called a disaster (see Fig. 6). In an extreme case, the microtubule can completely disintegrate. If microtubule growth resumes after a disaster, we are talking about a rescue.

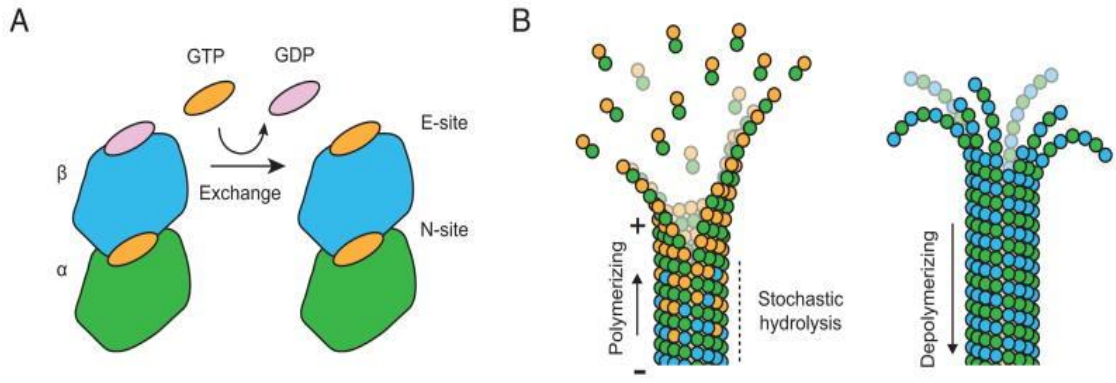

Figure 5. Dynamic and stabilized microtubules structures. **A.** Scheme of the αβ–tubulin heterodimer and its spontaneous exchange of GDP for GTP bond in solution. **B.** Scheme of microtubule polymerization and depolymerization structure intermediates. Adapted from Alushin *et al*., 2014.

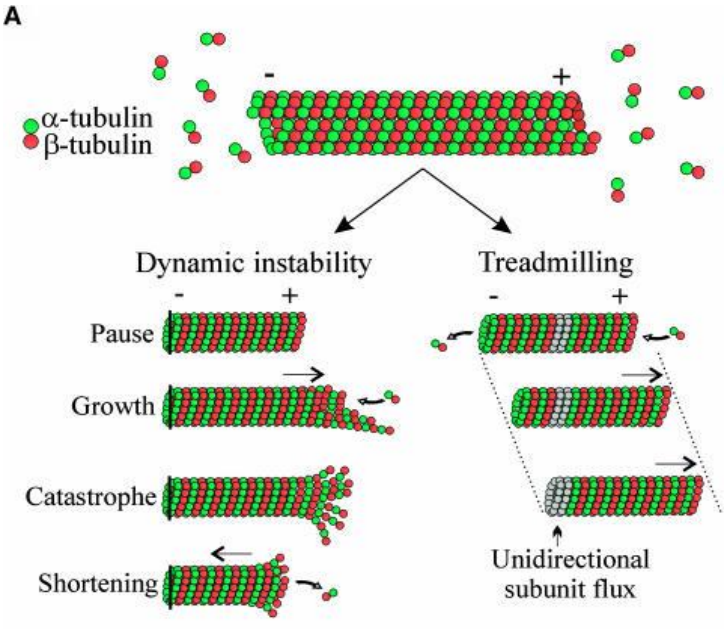

Figure 6. Dynamic instability and treadmilling of MTs. **A.** The MT (+) ends are usually not anchored in the cell and therefore grow more frequently than (-) ends due to the addition of tubulin heterodimers. In the case of too rapid hydrolysis of GTP on the added heterodimer, the (+) end becomes unstable and the microtubule depolymerize – catastrophe. Subsequent removal of the tubulin subunits shortens the microtubule. In the case of non-anchored microtubules, their removal at the (-) end may occur simultaneously with the attachment of the subunits at the (+) end. The result is an indirect flow of subunits within the microtubule. This movement of microtubule in space is called treadmilling. Adapted from Dixit and Cyr (2004).

2.3 Proteins Interacting with Microtubules

The functional and mechanical properties of microtubules are significantly influenced by the number of proteins that interact with both the polymerized microtubules and the separate tubulin dimers. Plant microtubule-associated proteins can be divided into microtubule-crosslinkers, microtubule (+) end-binding proteins, microtubular folding/dynamics regulators, motor proteins and tubulin folding regulators (Gu *et al*., 2008; Rodríguez-Milla and Salinas, 2009). The MAPs function is to modulate microtubule dynamics so that they can perform a wide variety of tasks in the cell. MAPs can react with microtubules directly or through interaction with other MAPs (Vleugel *et al.*, 2016). These include proteins stabilizing or destabilizing microtubules, proteins supporting microtubule nucleation, bundling or branching, or proteins mediating microtubule anchoring to cellular organelles (Horio and Murata, 2014). The most studied microtubule-crosslinkers that potentially associate cortical plasma membrane microtubules are CLASPs (CLIP-associated proteins; Wasteneys and Ambrose, 2009), to AtFH4 formin-bound membrane (Deeks *et al*., 2010), microtubule-binding proteins (CSI; Gu *et al.*, 2010) and proteins belonging to the MAP65 family.

There are 9 members of this family (AtMAP65-1 to AtMAP65-9) in the *A. thaliana* genome. MAP65-1 and MAP65-2 share significant homology, identical intracellular localization and functional redundancy in the microtubular organization (Lucas and Shaw, 2012). Other members of MAP65 family are cell cycle dependent (Smertenko *et al.*, 2008). Cloning the PLEIADE gene (PLE) showed identity with AtMAP65-3 (Müller *et al.,* 2004). Mutants in the PLE gene show defects in root and embryo morphology. Another well-studied family of molecular crosslinkers is MAP70. There are 5 members in Arabidopsis. MAP70-5 is involved in the regulation of anisotropic cell growth (Korolev *et al.*, 2007).

These interacting proteins include a group of molecular motors. In animals, we include kinesins, moving mostly to the (+) end of microtubules, and dyneins, moving to the (-) end (Marx *et al.*, 2005). Dyneins are not found in higher plant cells, therefore only kinesins that are diversified into many subgroups mediate movement to the (+) and (-) ends of microtubules (Richardson *et al.*, 2006; Wickstead and Gull, 2007). Molecular motors move along microtubules and gain energy by hydrolysis of ATP via their ATP-binding domain (Hirokawa *et al*., 2009; Vale, 2003) and allow the transport of cellular load, e. g. in the formation of a cell plate (de Keijzer *et al*., 2014; Li *et al*., 2010) or are involved in the reorganization of the microtubule network during the cell division (Lee *et al.*, 2007; Lipka *et al.*, 2014).

Among the MAPs, we also include microtubule (+) end interacting proteins, called (+) end tracking proteins (+TIPs), which are inherent in all eukaryotic organisms (Schuyler *et al.*, 2003). Because of their localization at the growing end of the microtubules, it is very likely that they will also interact with other proteins and cellular components during microtubule penetration through the plasma membrane (Vleugel *et al*., 2016).

2.3.1 Severing

Dynamic cellular processes have a basis in the remodeling of the microtubule cytoskeleton. Another mechanism of destabilizing and disassembling the microtubule cytoskeleton is represented by the severing of microtubules. One of the important classes of microtubule remodelers are the severases – katanin, spastin, and fidgetin – which are able to cut microtubules into shorter fragments. Severing enzymes are crucial for many biological processes, including the formation of meiotic and mitotic spindle (Zhang *et al*., 2007; McNally *et al*., 2006), cilia resorption (Rasi *et al*., 2009), organization of cortical

microtubule arrays in plants (Lindeboom *et al.*, 2013; Nakamura *et al*., 2010), neuronal morphogenesis, and axonal outgrowth (Jinushi-Nakao *et al.*, 2007; Trotta *et al*., 2004; Sherwood *et al*., 2004; Ahmad *et al*., 1999).

The microtubule-severing enzymes katanin, spastin, and fidgetin are members of the superfamily of AAA (adenosine triphosphatases - ATPases associated with diverse cellular activities) proteins that cut microtubules in an ATP-dependent manner and are widely conserved in animals and plants. Severases are different from other microtubule depolymerases, which have function primarily at the ends of microtubules (Howard and Hyman, 2007), by binding to and creating internal breaks in the microtubule grid (Roll-Mecak and McNally, 2010). Term dynamic instability is for a distinct feature of microtubules, which is switching between growing and shrinking phases. (Mitchison *et al*., 1984).

The AAA family members tend to assemble into ring-shaped oligomers, and only in this oligomeric state, they are allowed to bind their substrate with high affinity. Spastin and katanin are in the monomeric state when bound to ADP, and form hexamers only in the presence of ATP, unlike most AAA ATPases. This hexamerization is dependent on ATP and is also accompanied by a noticeable increase in microtubules binding affinity. The hexamer structure is labile, as both katanin and spastin mostly exist as monomers at submicromolar concentrations, even in the presence of ATP (Roll-Mecak and Vale, 2008; Hartman and Vale, 1999).

There is a paradox, that in many systems, the loss of the microtubule-severing enzyme leads to a decrease in microtubule mass. There might be expected break down of the microtubule cytoskeleton after severing, but inhibiting these enzymes *in vivo* decreases, rather increases, the number of microtubules and suggesting that there is a nucleation-like activity of severases. Rapidly generating microtubule mass mechanism, especially nucleation in the absence of centrosome-bases as in meiotic spindles or neurons. This microtubule amplification dependent on severing has been directly observed in cortical microtubule arrays in plants. The guanosine diphosphate (GDP)–tubulin lattice exposed through severing depolymerizes spontaneously in the absence of stabilizing guanosine triphosphate (GTP) cap, thus, it has to be stabilized for this amplification (Roll-Mecak and McNally, 2010).

During mitotic anaphase, identical sister chromatids divide and separate to opposite poles of the microtubule spindle. Anaphase motion of chromatids to poles (anaphase A) is firmly connected to depolymerization of the opposite ends of chromosome-associated

microtubules. Plus ends of microtubules are actively depolymerized by chromosomes, this "chewing" of their way poleward along microtubule tracks is a type of motility called Pacman. Meanwhile, microtubules associated with chromosomes serve as traction fibers, which are strained poleward via persistent depolymerization at their (-) ends. This process is termed poleward flux because of the resulting microtubule poleward flow (flux), reels in chromatids attached to poles of the spindle (Mitchison and Salmon, 2001). All three severases are incorporated into the anaphase Pacman-flux machinery used for chromosome separation. The functions of these proteins are segregated so that microtubule (-) end depolymerization and flux is stimulated by spastin and fidgetin, whereas (+) end depolymerization and Pacman-based anaphase A is stimulated by katanin. The activity of these proteins is segregated both temporally and spatially, that allows them to perform complementary functions throughout the spindle. This is most evident during anaphase A when the Pacman-flux machinery integrates all three proteins and is used to move chromosomes (Zhang *et al.*, 2007).

The founding member of AAA superfamily is katanin (from katana, the Japanese word for samurai sword), which was first purified from egg cytoplasm of sea urchin, where it was thought to break down the microtubules in interphase before the formation of the mitotic spindle during cell division. Katanin is a heterodimer consisting of an 80-kD targeting and regulatory subunit (p80) and a 60-kD AAA catalytic subunit (p60). Katanin is the only known ATPase associated with microtubules, other than the motor proteins dynein and kinesin (Hartman *et al.*, 1998) and requires ATP for severing and disassembling stable microtubules, ATP hydrolysis is necessary for this reaction. Katanin targets to centrosomes in many cell types and contributes to microtubule (-) end depolymerization and flux. Katanin acts substoichiometrically, as one molecule of katanin can release many tubulin dimers from a microtubule (see Fig. 7). Katanin does not seem to modify or proteolyze tubulin, since the tubulin, which is released from the disassembly reaction, is able to repolymerize (McNally and Vale, 1993; McNally *et al*., 1996).

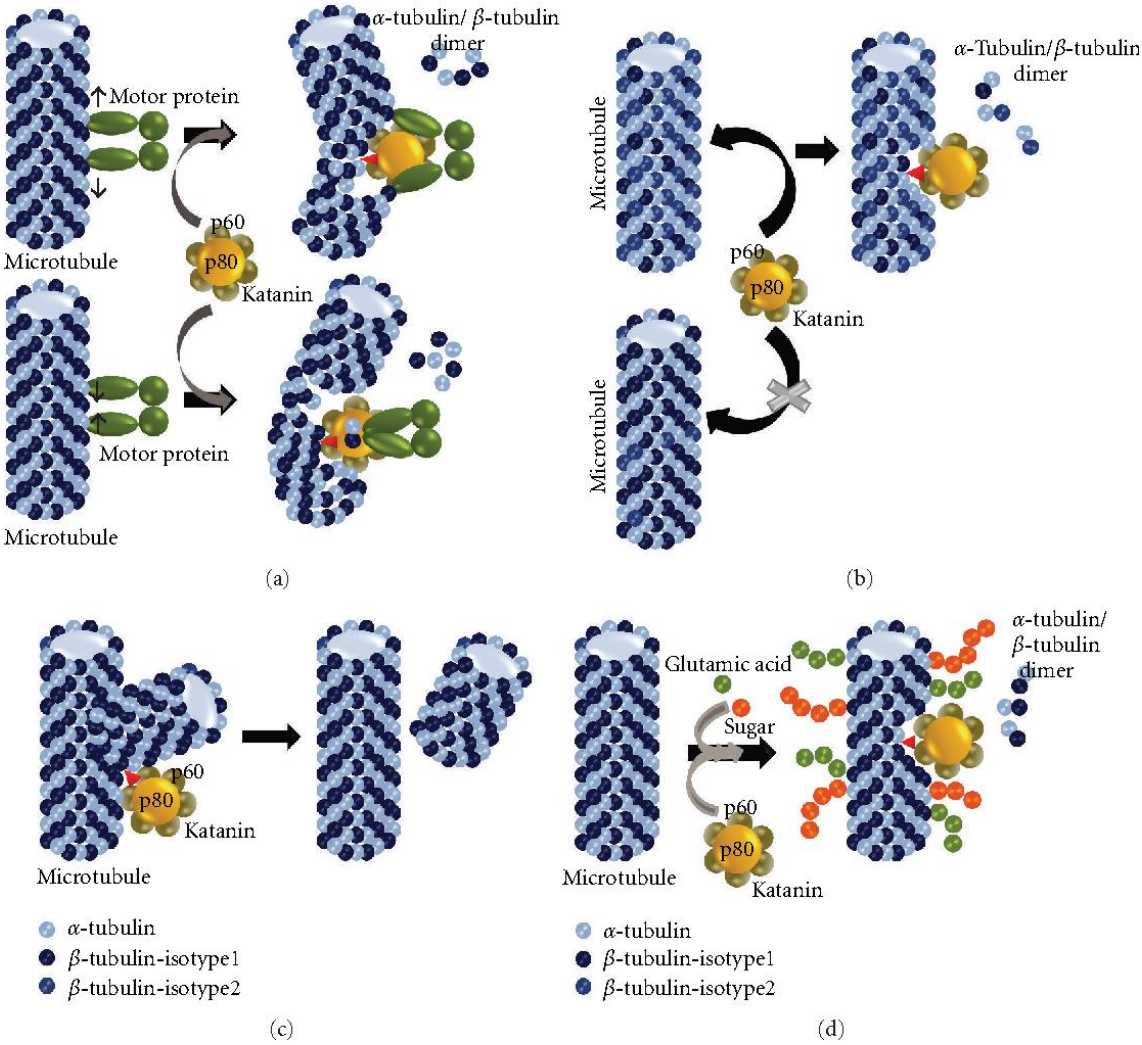

Figure 7. Katanin severing MTs models. **A.** Bending or deformation of MT is caused by bound and moving motor proteins. The severing process is enhanced by katanin at this site. **B.** The MT redundant isotype (isotype2/TBB2) of β–tubulin is preferable for katanin binding and severing. **C.** Branching sites of aberrantly branched MTs are severed by katanin. **D.** Post-translational modifications (polyglycation, poly-glutamylation) of MTs are preferred for severing by katanin. Taken from Ghosh *et al*., 2012.

Spastin is an ATP-independent regulator of dynamics of microtubules and slows shrinkage and increases rescue. Spastin is accumulated at shrinking ends; the increase in spastin concentration may underlie the increase in the frequency of rescues and the slowdown in shortening. Spastin switches microtubules into a state where the positive net flux of tubulin onto each polymer which leads to the exponential increase in mass of microtubules. Spastin can also increase the mass of MTs by using its severing activity to create new microtubules that can serve as templates to support the growth of new microtubules. (Kuo *et al*., 2019)

Fidgetin makes a close group with spastin and katanin showed by phylogenetic analysis (Frickey and Lupas, 2004) and is localized in cytoplasm and nucleus during

interphase. Fidgetin is the nuclear protein with a putative bipartite signal for nuclear localization. Fidgetin can make dimers with itself in vitro, deletion studies revealed that the full-length molecule integrity is required for the self-interaction, fidgetin operates in the nucleus as an oligomer. (Yang *et al*., 2005).

2.3.2 Motor Proteins

In eukaryotic cells, the motor proteins travel in the intended direction along microtubules which preferentially bind to stable fibers (Vaughan, 2005). These are enzymatic complexes that move on microtubules based on the energy obtained from ATP hydrolysis to ADP. Two families of motor proteins, dyneins and kinesins, their main functions are the directed movement of cellular components, transport of various cargos in the cytoplasm, but also the movement of cytoskeletal components towards each other, mRNAs, and protein and membranous complexes (Barlan and Gelfand, 2017). Motor proteins are present on almost all MT based structures which form during the cell cycle (Lee *et al*., 2015).

In animals and yeasts, kinesin and dynein move in the only single direction along the microtubules and in the opposite manner. Kinesin moves toward the (+) end of MTs (Asada *et al*., 1997; Paluh *et al*., 2000) and dynein moves toward the (-) end (Kikkawa, 2013).

In eukaryotes, kinesins are highly homologous. Mammalian kinesins are classified into 14 subfamilies according to sequence similarities (kinesin-1 – kinesin-14; Lawrence *et al*., 2004; Miki *et al*., 2005). Some kinesins are important during cell division – the establishment of spindle bipolarity, alignment of chromosomes to the metaphase plate, sizing of MT spindle, and cytokinesis which the coordinated actions of kinesins ensure. Higher plants lack (-) end-directed motor protein such as dynein (Wickstead and Gull, 2007). Nevertheless, the land plants encode more than 60 kinesins (Miki *et al*., 2014) and some of them are predicted to be (-) end-directed motor proteins (Yamada *et al*., 2017) that might compensate the lack of dynein. Kinesins in plants have a similar structure to (+) end-directed kinesins in other species but can differ between the individual kinesin subfamilies. The increased number of kinesins that play a role in mitotic cell division that should be accomplished with lack of centrosomes or another motor dyneins based on MTs in plants (Miki *et al.*, 2014).

In general, the kinesin molecule consists of two light chains (KLC) and two heavy chains (KHC). The light chains include tail domain and heavy chains stalk domain, that

is connected to the light chain, neck-linker and globular motor domain (see Fig. 8). The stalk domain constitutes of a coiled-coil structure and is in connection with a tail domain that enables bonded cargo transport and is highly divergent among different kinesins reflecting their diverse functions (see Fig. 8; Ogawa *et al.*, 2004). The direction of kinesin motility is determined by the amino acid sequence of neck-linker which is joined to the motor domain and also regulates activity (see Fig. 8; Woehlke and Schliwa, 2000; Endow and Waligora, 1998). The well conserved globular motor domain within the animals and plants is also marked as catalytic core and is characterized by the presence of ATP- and microtubule-binding site or "head" (see Fig. 8; Woehlke *et al*., 1997).

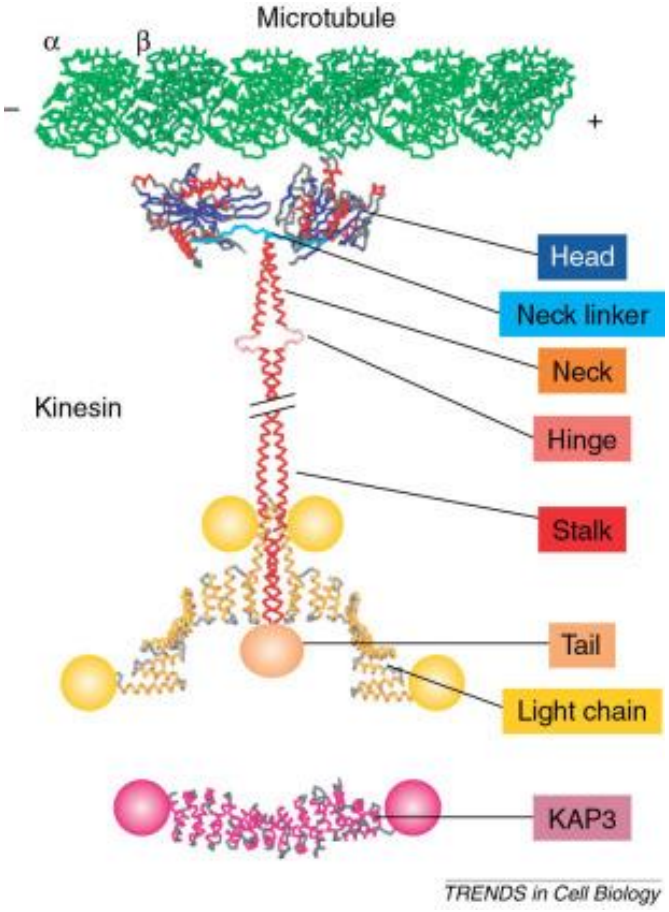

Figure 8. Structure of kinesin domains and associated proteins. The schema shows some known molecular structures in backbone. The structure on the top represents the MT protofilament. The structures in the middle (red and blue) represents a dimeric kinesin heavy chain (KHC) that consists of a motor domain ("head", α-helices red, β-strands blue), a neck linker (cyan), an α-helical neck and a stalk (red) which coiled-coil interaction causes dimerization. A nonhelical hinges disrupts the stalk and allow swivelling of the heads and the stalk bending in inactive "folded" conformation. A red sphere represent the globular tail domain. Two light chains (KLC, yellow) are linked to the tail. The N-terminal residues are in coiled-coil formation and connect the light chains to the heavy chains. The C-terminal residues are for cargo docking or for scaffolding transport vesicle proteins. Adapted from Mandelkow and Mandelkow, 2002.

The presence of two motor domains allows movement of kinesin which is capable of microtubule gliding activity dependent on ATP and is coupled to ATP hydrolysis activated by MTs. The stalk domain interacts with other subunits of kinesin or with the loaded molecules such as nucleic acids, lipids, and proteins (Hirokawa *et al*., 1989; Diefenbach *et al*., 1998; Kanai *et al.*, 2004). The motility of kinesin requires precise cooperation of motor domains to avoid slipping of the microtubules after the binding. The tight bound of ADP is necessary for both kinesin motor domains. The ADP is released of the attached catalytic core after the encounter with microtubules, the ATP binds quickly into empty nucleotide binding site and the movement is allowed after the ATP hydrolysis (Vale *et al.*, 1985, 1996).

2.3.3 Bundling of Microtubules

Bundling is a physical process of crosslinking of adjacent microtubules by virtue of microtubule binding proteins (Smertenko *et al.*, 2004). Owing to their polyanionic nature (Yu *et al.*, 2015), microtubules physically repel each other, therefore their tight alignment in the cortical cytoplasm of actively growing cells is depending on the mediation of appropriate crosslinking proteins. Microtubule bundles play a crucial role in the formation and maintenance of organized MT arrays in eukaryotic cells. The highly bundled acentrosomal interphase MTs at the cell cortex and their spatial organization dictates the cell expansion direction in plant cells (Wasteneys and Ambrose, 2009). The MT cortical array and an assembly helping in the organization of the cell wall growing diffusely over a large surface (Cyr, 1991). Microtubules are generally highly organized and occur in same oriented parallel groups long over hundreds of micrometers even without fixed microtubule organizing centers (Chan *et al*., 2003) rather than in radial orientation of microtubules. Cross-bridges between these MTs and the plasma membrane provides that the cortical array is formed as a sheet instead of three-dimensional bundles (Cyr and Palevitz, 1995). Although these cross-linked MTs stay dynamic inside the bundles (Bratman and Chang, 2008).

Bundles of microtubules are built through the cross-linking protein's activity, including motor and/or non-motor MAPs, also the members of the MAP65/Ase1/PRC1 family (65kDa MT-associated protein/Anaphase Spindle Elongation 1/Protein Regulator of Cytokinesis 1; Chan *et al*., 1996, 1999; Smertenko *et al*., 2004; Gaillard *et al*., 2008). MAP65s are major cross-linkers of MT in plant cells (MAP65-1 to MAP65-9; Hussey *et al*., 2002), fungi (Ase1; Schuyler *et al.*, 2003) and in vertebrate (PRC1; Jiang *et al.*, 1998).

All these MAP65 have the common ability for MTs bundling in vitro, but they have the difference in their physical interactions with the lattice of MTs and/or in the cross-linking between adjacent MTs. MAP65 proteins form a homodimer for the promotion of bundling of antiparallel MT in the phragmoplast and in other MT arrays during cell division (Smertenko *et al.*, 2004; Gaillard *et al*., 2008). MAP65 seem to create filamentous crossbridges, keeping the minimal spacing of 25–30 nm between microtubules (Chan *et al*., 2003). The cross-bridges are spaced regularly and show a regular axial spacing compatible with 13 protofilaments MTs in symmetrical helical superlattice (Chan *et al*., 1999). The array is composed of MTs which overlap and can keep a parallel relationship over several micrometers (Hardham and Gunning, 1978; Seagull and Heath, 1980). The MT bundling is dependent on a C-terminal domain that is also responsible for dimerization (Smertenko *et al.*, 2004).

MAP65-1 and PRC1 cross-link anti-parallel MTs in vitro and the space between microtubules is 30 nm. The cross-links between MTs have diagonal orientation and have an angle of ca. 60° relative to the lattice of microtubules (Gaillard *et al.*, 2008; Subramanian *et al*., 2010). PRC1, Ase1, and MAP65-4 do not have an effect on velocities of growth and shrinkage of bundled MTs (Loïodice *et al*., 2005; Fache *et al.*, 2010; Janson *et al*., 2007; Bieling *et al.*, 2010). So MTs in bundles are longer than the unbundled MTs, and they show a collective behavior characterized by a coordinated growth of ends of MTs, which grow close to each other (see Fig. 9; Stoppin-Mellet *et al*., 2013). In animal cells and fission yeast, these proteins play a role in mitosis to define a zone of MT overlap between the poles of the spindle by crosslinking anti-parallel MT spindle fibers (Mollinari *et al*., 2002; Schuyler *et al*., 2003; Yamashita *et al*., 2005). In fission yeast, Ase1 participates in interphase by keeping a short antiparallel microtubule bundle at each nuclear-associated MTOC (Loïodice *et al.*, 2005).

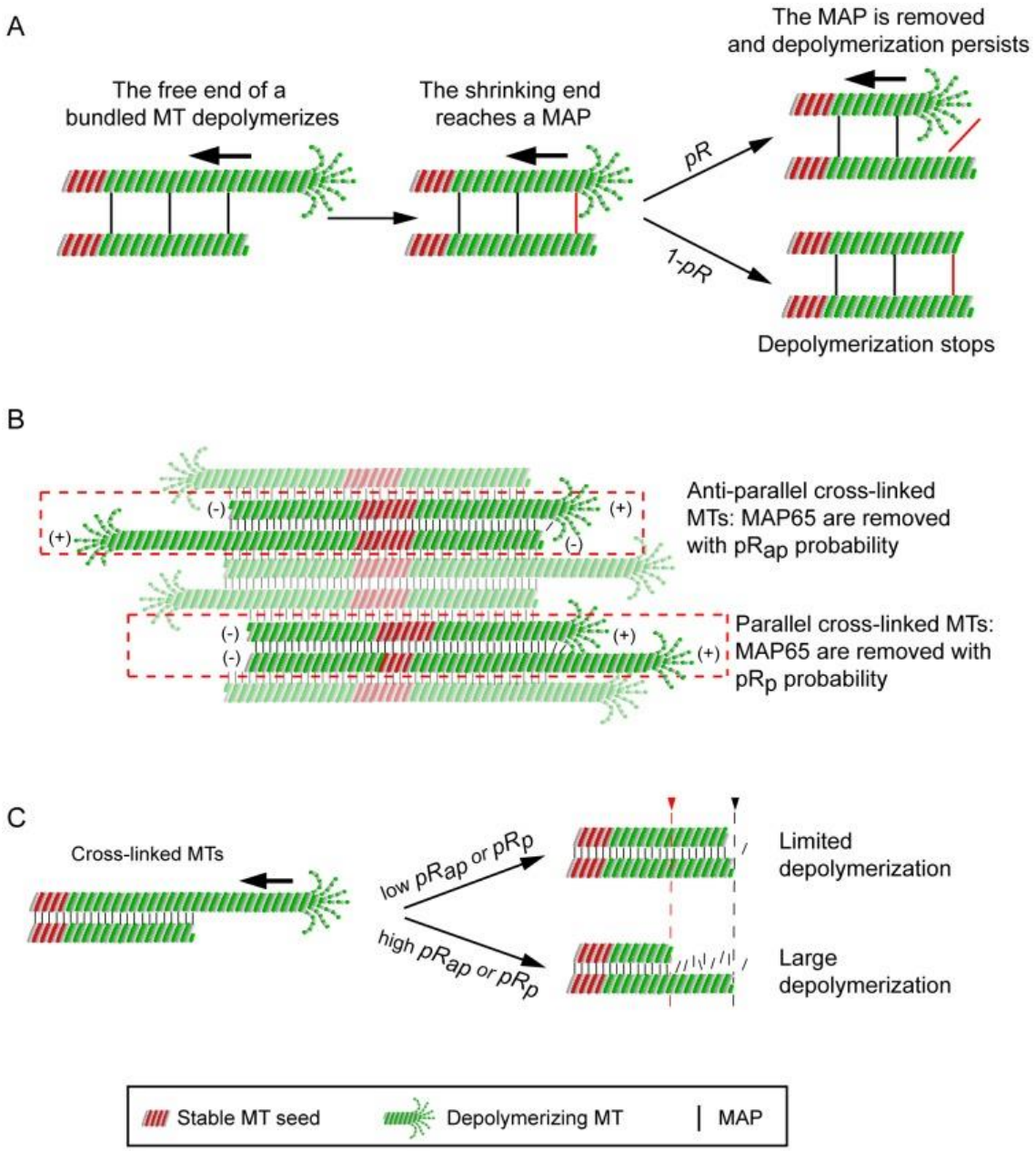

Figure 9. Model of MT growth in bundles. **A.** The effect of a MAP65 bond on depolymerization of MTs. Stable MT seeds are in red, dynamic MTs are in green. The bars represent 3 MAP65 proteins crosslinking one pair of MTs for simplicity. A catastrophe event (left panel) is for the upper MT end and MT depolymerizes until it reaches a bond with MAP65 (red bar) at the end of the cross-linked MT (middle panel). The MAP65 can detach from MT with probability pR (right, top panel), or can stay bound to the MTs with a probability (1-pR) (right, bottom panel). The bond with MAP65 can be removed and the MT continues at shrinking in the first case or the MAP65 bond can resist to MT depolymerization, which can stop in the second case, **B.** The MAP65 (black bars) can detach from anti-parallel MTs with a probability pRap, or can detach from parallel bundled MTs with a probability pRp during depolymerization. **C.** The pRap and pRp value affect the amplitude of MT depolymerization. The catastrophe event occurs for upper MT end and MT depolymerizes (left panel) before reaching the end of a cross-linked MT (right panel). The most of the MAP65 molecules stay bound to the MT at low pRap or pRp (top panel), consequently, MT depolymerization stops at the vicinity of the end of the adjacent MT (black broken line). In high values of pRap or pRp (labile MAP bonds; bottom panel), depolymerization of MTs may

remain behind the cross-linked MT end, thereby generating short bundles (red broken line). Taken from Stoppin-Melet *et al*., 2013.

2.4 65-kDa Microtubule-Associated Proteins

Microtubules form bundles fitting up cells with specific mechanisms for shape controlling or force generating; in cooperation with microtubule-associated proteins (MAPs). The first purification of MAP65 was from tobacco suspension cells as a 65 kDa MAP that binds to and bundles MTs (Chang-Jie and Sonobe 1993). MAP65-1 restrains the amplitude of microtubule bundle depolymerization and increases the elongation phases. MAP65-1 is the plant ortholog of vertebrate PRC1 and yeast Ase1. The following persistent elongation of bundles is controlled by the coordination of microtubule growth, so that microtubule ends come in close vicinity. The frequencies of rescue are higher between parallel than between anti-parallel MTs. So the MTs polarity bundled by MAP65 controls the bundle's growth amplitude (Stoppin-Mellet *et al.*, 2013). MAP65 proteins are necessary for the maintenance of bipolarity of the mitotic spindle during formation of midzone in anaphase and for cytokinesis in vivo (Mollinari *et al.*, 2002; Müller *et al*., 2004; Loïodice *et al*., 2005; Caillaud *et al*., 2008).

All plant studied MAP65s so far are associated with MT bundles in vivo, but their localization in cell varies. For example, MAP65-1 is in association with cortical MTs, the preprophase band and the mid-zone of spindle (Smertenko *et al*., 2004; Van Damme *et al*., 2004), while MAP65-4 is in association with the forming spindle (prophase) and the fibers of kinetochore (prophase to anaphase; Fache *et al*., 2010). In plant living cells, bundled MTs in association with MAP65-1 have growth and shortening velocities comparable to unbundled MTs (Lucas *et al*., 2011).

Plant MAP65s regulate the dynamics parameters of MTs while bundling MTs that causes the overall increase of the bundle length. MAP65-1 and MAP65-4 decrease MT frequency of catastrophes so that cross-linked MTs spend more time on growing than unbundled MTs, and increase the number of rescue events because they reduce the distance over which cross-linked MTs depolymerize (Stoppin-Mellet *et al*., 2013). Conversely, MAP65 do not affect the velocities of growth and shrinkage of MTs (Lucas *et al.*, 2011). The orthologs PRC1 and Ase1 have similar tendencies which are comparable to plant MAP65s (Loïodice *et al*., 2005; Janson *et al.*, 2007; Bieling *et al.*, 2010). Parallel groups of MTs occur interconnected by cross-bridges of filaments which lengths are similar to the diameter of the MTs (Hardham and Gunning, 1978; Seagull and Heath, 1980; Lancelle *et al.*, 1986; Tiwari *et al*., 1984).

The sequences of the nine forms of AtMAP65 have an identity from 28% to 79% (Hussey *et al*., 2002), so AtMAP65 proteins can have different activities and functions (Van Damme *et al.*, 2004). The sequence identity of AtMAP65-1 with AtMAP65-2 is 78%, but the sequence identity with AtMAP65-6 is about 44% (Hussey *et al*., 2002). AtMAP65-1 has significant divergence in sequence with AtMAP65-6 at both N- and C- termini and both affect the stability of microtubules in different ways and interact in different manners. AtMAP65-1 interact with microtubules continuously and ladder-like so allows microtubules to gain a fortress-like structure. This structure could be much more resistant to depolymerization that can be caused by cold or dilution treatments than AtMAP65-6 induced mesh-like network of individual MTs (Mao *et al.*, 2005). AtMAP65-1 and AtMAP65-5 are associated with a subset of the array of cortical microtubules (Van Damme *et al.*, 2004). The AtMAP65-1 and AtMAP65-2 proteins are highly similar (90%), have a redundant function in the axial extension of the hypocotyl cells (Lucas *et al*., 2011), are important for the function of the cortical microtubule array, without necessarily being required for organization of the microtubule array, and co-localizes with throughout the cell cycle (Lucas and Shaw, 2012). AtMAP65-1 and AtMAP65-2 localize in pre-mitotic and cell division arrays (Smertenko *et al*., 2000, 2004, 2008; Chang *et al*., 2005; Mao *et al*., 2005; Li *et al*., 2009; Meng *et al*., 2010; Sasabe *et al*., 2011). During cytokinesis, the AtMAP65-1, AtMAP65-2 and AtMAP65-3 act redundantly (Sasabe *et al*., 2011).

Distinct roles in plant mitosis and cytokinesis are played by the MAP65-3 and MAP65-4 proteins providing structure to the acentriolar microtubule arrays (Müller *et al*., 2004; Caillaud *et al*., 2008; Fache *et al*., 2010; Ho *et al*., 2011). The cortical array and the preprophase band (PPB) are not labeled by AtMAP65-4 protein, but its strong association is with the perinuclear microtubules and the mitotic spindle (Van Damme *et al.*, 2004). Cytokinesis is given rise by the phragmoplast, which assembles the cell plate until the nuclear division is completed. In the phragmoplast, microtubules are aligned perpendicularly to the division plane and are organized in an antiparallel manner. The (+) ends of antiparallel MTs are located at or near the site of cell division and (-) ends are facing two reforming daughter nuclei. The bipolar MT array organization allows directional transport of Golgi-derived vesicles to the division site (Staehelin and Hepler, 1996; Jürgens, 2005). The array of MTs with mixed polarities is resulting from polymerization/depolymerization and reorganization of MTs in the central spindle (Zhang *et al.*, 1990).

AtMAP65-3 is localized at the midzone of the spindle and the phragmoplast midline and is not localized in the interphase array or in the prophase, metaphase, or early anaphase spindle (see Fig. 10; Smertenko *et al*., 2000; Müller *et al*., 2002, 2004). The AtMAP65-3/PLE localization suggests that protein has a role in cell division but not in cell expansion. AtMAP65-3 is also identified as PLEIADE which is involved in cytokinesis and, when mutated, leads to the formation of incomplete cell walls, multinucleated cells, and the phragmoplast is deformed. MAP65-3 loss causes a wider dark central gap in the phragmoplast and frequent cytokinesis failures (Müller *et al.*, 2004; Caillaud *et al*., 2008). Nevertheless, the bipolar appearance of phragmoplast MTs does not require MAP65-3 and suggests that MAP65-3 bundles parts of MT (+) ends in the phragmoplast and cross-links antiparallel MTs near their (+) ends during telophase and cytokinesis. This bundling is necessary for the formation of the cell plate. MAP65-3 seems to plays a more important role than other isoforms of MAP65 which are also involved in cross-linking of antiparallel MTs in the phragmoplast (Van Damme *et al.*, 2004; Smertenko *et al.*, 2008). The MAP65 cross-linking activity of MTs is necessary for the interaction of kinesins which are implicated in cytokinesis with (+) ends of MT and thus is critical for cytokinesis. (Ho *et al*., 2011). The bundling of antiparallel MTs at the (+) end is brought about by the dimerization of MAP65-3/PLEIADE member of MAP65 family and comes from opposite sides of the division plane that occurs selectively at the phragmoplast periphery (Müller *et al*., 2002, 2004; Ho *et al.*, 2012; Murata *et al*., 2013). The phosphorylation of MAP65-3/PLEIADE by MAP kinases cause debundling of MTs towards the center of the phragmoplast (Takahashi *et al*., 2004).

In Arabidopsis, PLEIADE/AtMAP65-3 interacts also with spindle assembly checkpoint (SAC) proteins. The SAC establish chromosome segregation without errors by preventing the beginning of anaphase as long as any unattached or incorrectly attached chromosomes are present (Paganelli *et al*., 2015). Therefore, the cell cycle progression and the chromosome attachment to phragmoplast MTs are involved in PLEIADE/AtMAP65-3 function in the end (Steiner *et al*., 2016).

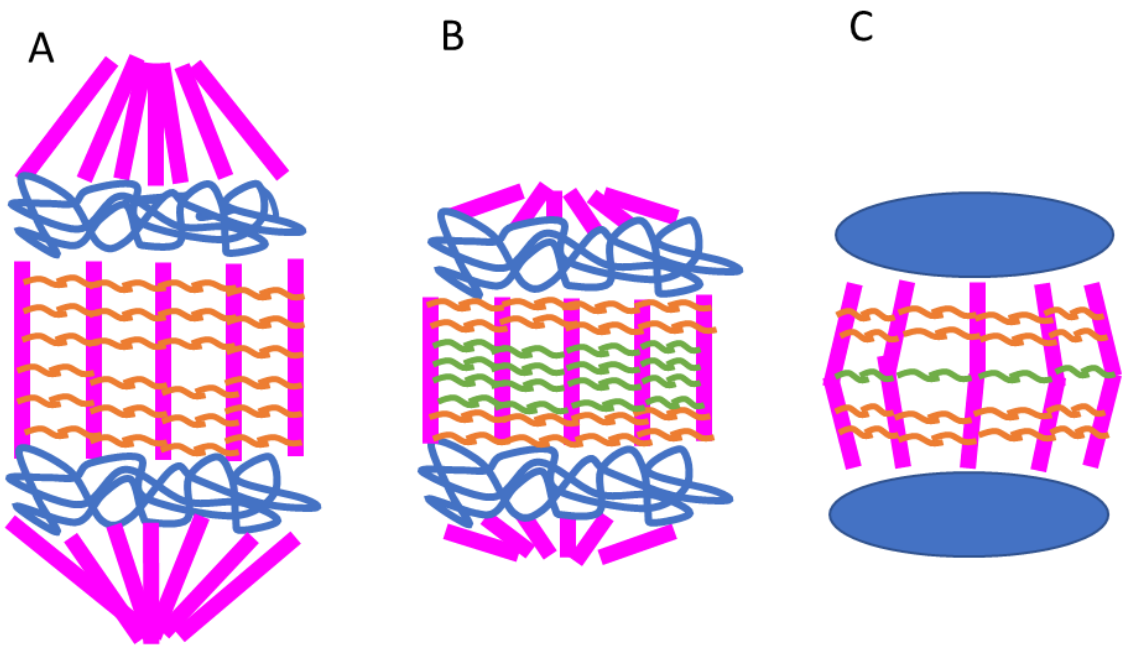

Figure 10. Model of MAP65-2 and MAP65-3 distribution during late anaphase, telophase and cytokinesis. **A.** The MAP65-2 protein (orange) crosslinks MTs (magenta) during late anaphase. **B.** The MAP65-3 protein (green) is accumulated broadly in a midzone of telophase spindle. **C.** The MAP65-3 protein is restricted in a midline of phragmoplast. DNA is in blue.

2.5 Superresolution Microscopy

Studying of subcellular structures and dynamics of specific compartments requires a powerful methods for examination, one of them is a fluorescence microscopy (Combs, 2010). Addressing of dynamics of various compartments and intracellular architecture at a wide range of spatiotemporal resolution depend on existence of various confocal or widefield platforms and using different labeling strategies. It is necessary to have adequate resolving power of microscopy, because many of such structures occupy a relevant volume (Komis *et al.*, 2018; Ovečka *et al.*, 2018).

Different superresolution methods get over Abbe's diffraction limitation of widefield or confocal scanning fluorescence microscopy (Komis *et al.*, 2015a, 2018). Structural information below this limits are overcome by the patterned light illumination strategies (such as stimulated emission depletion microscopy, STED; Hell and Wichmann, 1994; or structured illumination microscopy, SIM; see later; Gustafsson, 2000), and others which exploit photochemical effect of fluorophores and extremely sensitive acquisition systems for enhancing the localization of individual molecules, e. g. photoactivation localization microscopy (PALM; Betzig *et al.*, 2006) and stochastic optical reconstruction microscopy (STORM; Rust *et al.*, 2006). For these methods, the

resolution of dimensions can be isotropic (PALM/STORM and STED) or moderately poor at the Z-dimension (SIM; Komis *et al*., 2015a). The actual Z-range and temporal resolution of such superresolution methods are within limits for the ability to resolve subcellular structures of living cells that are labeled with genetically encoded fluorescent markers.

2.5.1 Structured Illumination Microscopy

The difference between SIM and PALM or STORM, which are TIRF-based (total internal reflection fluorescence) methods, is that SIM works widefield manner and can extend superresolution at large fields of view (FOVs). The imaging of relatively large tissue areas and easing of quantitative deductions of organelles in subcellular level in many cells is allowed by SIM. And effective Z-range (more than 10 μm; Szczurek *et al*., 2018) can be offered by using 3D-SIM via commercially available SIM platforms, that allows studying of voluminous subcellular structures, e. g. plasmodesmata organization (Fitzgibbon *et al.*, 2010), interphase nuclei (Fišerová *et al*., 2017; Kraus *et al.*, 2017; Schmid *et al*., 2017; Schubert *et al*., 2014; Schubert, 2014, 2017), mitotic chromosomes (Schubert *et al*., 2014; Ribeiro *et al*., 2017; Marques *et al.*, 2016; Banaei-Moghaddam *et al.*, 2012; Antosch *et al*., 2015) or the meiotic and mitotic spindle (Marques *et al.*, 2012; Vyplelová *et al*., 2018). Computer-assisted image reconstruction is used for SIM and is subjected to miscellaneous errors that can be caused by the poor quality of the sample and mostly inconvenient signal-to-noise ratios (respective poor labeling, high background, etc.). Moreover, the refractive index mismatches in the optical path inducing spherical aberrations can cause artefactual reconstruction in 3D-SIM (Arigovindan *et al*., 2012; Demmerle *et al*., 2017; Komis *et al*., 2015b).

3 Material and Methods

Following chapters about material and methods are predominantly taken of my bachelor thesis, because of use of same or similar methods (Šnaurová R. (2017): *Role of GSK inhibitors on mitotic progression of plants*, bachelor thesis, UPOL, Czech Republic).

3.1 Plant Material

Arabidopsis thaliana (L.) Heynh,

- ecotype Columbia (Col-0)
- ecotype Columbia (Col-0) steadily expressing eGFP-MAP65-2
- ecotype Columbia (Col-0) steadily expressing eGFP-MAP65-3
- ecotype Columbia (Col-0) steadily expressing tagRFP-MAP65-2 x eGFP-MAP65-3
- ecotype Columbia (Col-0) steadily expressing tagRFP-MAP65-2 x eGFP-TUA6
- dominant heterozygous mutant *mpk4*
- recessive homozygous mutant *mpk6-2*

3.2 Observation of Seedlings Phenotype

Plant cultivation was accomplished under sterile conditions *in vitro* in a growth chamber. Seeds were sowed on the square Petri dishes with a solid MS medium (Murashige and Skoog) at half concentration of substances ($^1/_2$ MS) and without vitamins.

3.3 Preparation of Seeds

Seeds were put into 1,5ml Eppendorf tubes, then was made surface sterilization of seeds before sowing seeds on the solid ½ MS medium. The sterilizing solution was prepared by diluting a stock of 10% v/v solution of sodium hypochlorite (NaClO) at a 1% v/v solution and then one drop of the Tween 20 detergent was added. 1 ml of sterilizing solution was added into Eppendorf tube with seeds, incubation took around 10 minutes with occasional vortexing. Every manipulation with seeds was carried out in a sterile laminar flowbox and with the use of only sterile instruments and solutions then. For solution exchange was used an automatic micropipette after sterilization. The sterilization solution was almost completely removed and replaced with 1 ml of 70% v/v aqueous ethanol. The tube was inverted few times for a total of not more than 30 seconds and then the ethanol solution was removed. Seeds were then washed 3-5 times with 1 ml of sterile distilled water and after that were transferred to the solid ½ MS medium. It was necessary to shake

microtubes with water because of residues of ethanol solution and sterilizing solution which would cause problems with germination. A small volume of water after the last wash was allowed in the tube to be used for transferring the seeds to medium.

3.4 Preparation of Culture Medium and Sowing

Arabidopsis seeds were cultivated *in vitro* under sterile conditions on ½ MS medium. Sterile medium was poured into square Petri dishes (120 mm × 120 mm) in a sterile laminar flowbox. Thereafter, approximately 120 seeds were seeded on each sterile plate by using micropipette (100 µl). The tip of the pipette was slightly cut at the end for easier sowing of seeds on sterile plates. For genotyping and crossings later were seeded 30 seeds of Arabidopsis MAPK mutant lines in two lines. All instruments used for sowing seeds were sterile or were sterilized by 70% v/v aqueous ethanol or Spitaderm disinfectant solution. The closed dishes were sealed with parafilm and placed in a horizontal position in the refrigerator (4 °C, dark) for 1-4 days for stratifying seeds and synchronizing their germination and seedling growth. After this, the Petri dishes with seeds were transferred to a culture chamber (phytotron) where they were placed vertically and cultured for another 3-4 days to allow germination and seedling growth (23 °C, 16 h light / 8 h dark) for the wholemount method.

3.5 Selection of Arabidopsis Transformants

The 3-4 days old seedlings of transformants of MAP65-2 and MAP65-3 fusions and crosses tagRFP-MAP65-2 x GFP-TUA6 were selected by their fluorescence signal under an epifluorescence microscope. By using a laser of excitation wavelength 488 nm were selected plants emitting a green signal of GFP in the root tip (MAP65-2 and MAP65-3 fusions, and GFP-TUA6 of the cross line). Laser of excitation wavelength 545 nm was used for selection of tagRFP-MAP65-2 crossed with GFP-TUA6. Positive plants were then used for the whole mount method for immunofluorescence labeling.

3.6 Selection, PCR Genotyping and Agarose Electrophoresis of Arabidopsis Mutants

One week old Arabidopsis recessive homozygous mutant *mpk6-2* selection was based on lethal phenotype of this mutation for plants and were kept growing only surviving heterozygous individuals until flower formation.

One week old Arabidopsis dominant heterozygous mutant *mpk4* required genotyping for selection. First was necessary to isolate DNA followed by PCR reaction with specific primers and verification by agarose electrophoresis.

DNA Isolation

The 1,5ml Eppendorf microtubes were marked and filled with 20 µl of dilution buffer from Plant Direct PCR Kit on ice. Plates with on week old plants were in put into a sterile laminar flowbox. Always a small part of microtubes was moved into flowbox. For each sample was cut a piece of leave (2 × 2 mm) with sterile scissors, inserted into microtube and crushed with sterile micropipette tip. Treatment of sample in dilution buffer required another 30 minutes on ice then were microtubes moved to - 20 °C. Arabidopsis plants, ecotype Col-0 were used as negative control.

PCR Genotyping

Detection of the *mpk4* mutant was determined by polymerase chain reaction. A Phire Plant Direct PCR Kit was used for PCR genotyping. The composition of the PCR reaction mixture is shown in Table 1. Thermo scientific Phire Hot Start II DNA Polymerase and deionized Milli-Q® water was used for the reaction. In addition, primers were used: forward (F) LBb1.3 5'-ATTTTGCCGATTTCGGAAC-3' and reverse (R) 5'-CCGCTTCAACAGATGGTTACG-3'.

Procedure for preparing PCR reaction mixture: All components of the PCR reaction mixture were thoroughly thawed and vortexed. Components of the mixture according to Tab. 1 were pipetted into 1,5 ml microtube, vortexed and centrifuged. 19,1 µl of PCR reaction mixture were pippeted into the PCR tube, then were added 0,9 µl isolated DNA to each tube. All microtubes were vortexed, centrifuged and inserted in a cycler with time and temperature profile according to Tab. 2.

Table 1. PCR reaction mixture composition

PCR reaction mixture components	**Volume per one sample (RXN = 20 µl)**
ddH_2O	12,3 µl
5x Phire Reaction Buffer	4 µl
dNTPs	0,4 µl
F primer	1 µl
R primer	1 µl

Table 1. PCR reaction mixture composition *(continuation)*

Phire Hot Start II DNA Polymerase	0,4 µl

Table 2. Time and temperature profile of the PCR reaction

Step	Temperature, °C	Time	Number of cycles
Initial denaturation	98	5 min	1
Denaturation	98	5 s	
Annealing	65	5 s	39
Extension	72	10 s	
Final extension	72	3 min	1

Agarose Electrophoresis

After completion of the PCR reaction, the size of the products and the presence of heterozygous alleles was verified by agarose electrophoresis. 1% agarose gel was prepared by dissolving 1 g agarose in 100 ml 1x TAE buffer. Gel was left at room temperature for about 20 minutes to solidify. Midori Green was added to the gel for product visibility and comb, which created wells for sample application. The solidified gel was placed in an electrophoretic tray. 2 µl of 6x Loading Dye were added after PCR to individual samples and 10 µl of samples were applied to the gel. The gel was covered with 1x TAE buffer to the reminder line. After closing the lid with the voltage supply and attaching the electrodes to a voltage source triggered constant voltage electrophoresis 85 V, 400 mA electrical current and 30 min. After electrophoresis, the gel was removed and invoked in the visualizer Gel DocTM EZ Imager.

3.7 The Wholemount Method for Immunofluorescence Labeling

A variant of immunofluorescence techniques, which aims to the preservation of the entire organ integrity (in this particular case the root) while preserving immunoreactivity of the proteins of interest (in this case, tubulin as a constituent of microtubules and MAPs). A special procedure for sample preparation for this is required. For this study, a published protocol was followed (Sauer *et al.*, 2006) after certain modifications which are mentioned in the following sections.

1) Fixation

Fixation is the process of chemical immobilization of intracellular molecules aiming to the preservation of structure and antigenicity. For this purpose the ideal fixative comprises a mixture of a monovalent (formaldehyde) and a bivalent (glutaraldehyde) aldehyde, buffered at a pH and mixed in a solution with additives necessary (such as EGTA and $MgSO_4$) for the preservation of microtubules. Formaldehyde is derived from the alkaline hydrolysis of a 8% w/v paraformaldehyde solution. For the preparation of this solution, 16 g of powdered paraformaldehyde was dissolved in 150 ml of ultrapure Milli-Q® water under continuous stirring with a magnetic stirrer and gentle heating (at appx. 70 °C for about 30 min). The hot solution had a milky appearance. One tablet of solid pure KOH was dipped into the solution with the aid of tweezers to clear the solution and promote hydrolysis of PFA, until the latter was colorless and transparent. After the solution cooled down, 4-10 ml of glycerol was added and the solution was complemented to its final 200 ml volume by Milli-Q® water. The resulting solution contains monomeric formaldehyde and can be stored indefinitely at room temperature. The solution is toxic, so it is always necessary to work with it under a hood and with protective clothing.

The fixative used here (see List of Solutions, Tab. 3) was dispensed as required into the wells of twelve-well plastic plates for cell cultures (ca. 3 ml of fixative per well). Seedlings were transferred to hollow plastic baskets with their bottom lined with a 50 μm plastic net which were then placed in fixative-filled wells of the culture plate. Fixation was carried out under the hood for a minimum of 1 hour at room temperature and was extended in some occasions for overnight at 4 °C. Prior to fixation plastic baskets were very thoroughly washed with detergent, tap water and then Milli-Q® water. The fixative was removed from the plates by using a Pasteur pipette and the samples were washed at least 4 times by 10 minutes with buffer (½ MTSB). Solutions were exchanged from outside of the baskets to prevent damaging of the delicate root tips.

2) Enzymatic Digestion of the Cell Wall

Antibody molecules are impermeable to the plant cell wall which has a cut-off pore size of ca. 20 kDa (Fleischer *et al*., 1999). To ensure diffusion of antibody molecules within root cells and at considerable depth of the root it is necessary to degrade cell wall components post-fixation which is done by using an appropriate cell wall digesting enzyme cocktail. When all post-fixation washings were completed, baskets with fixed seedlings were removed from the ½ MTSB solution, carefully blotted on filter paper and

placed into other wells containing cell wall digesting enzyme cocktail (see List of Solutions, Tab. 3) and the seedlings were incubated for 25-30 min at 28 °C. After enzyme digestion, baskets with seedlings were placed to clean wells containing ½ MTSB. The enzymatic solution was stored at -20 °C and could be reused 5-6 more times. Seedlings were washed twice in MTSB for 10 minutes each and then two more times with phosphate buffered saline (PBS) for 10 minutes each. For working with a larger number of samples, plastic baskets were transferred using tweezers into ½ MTSB-, or PBS- prefilled wells. Same approach was also used after the reduction and antibody incubation (see below).

3) Reduction

Even after extensive washing it is expected that residual unreacted aldehyde groups are remaining in the sample and such groups can covalently bind antibody molecules to non-specific sites causing background fluorescence in the sample. A possible way to deal with this problem is to reduce aldehyde to non-reactive alcohol groups and this is done by treating the fixed samples with $NaBH_4$ as a reducing agent. Therefore, after the last wash with PBS, samples were treated with 1 $mg \cdot ml^{-1}$ of $NaBH_4$ in PBS for 15 min at room temperature. After reduction, the baskets were transferred into wells with PBS buffer (without $NaBH_4$) and then washed extensively with PBS until the solution stopped to effervesce.

4) Permeabilization

Although the barrier of the cell wall is breached by cell wall digesting enzymes, the diffusion of antibody molecules in the root cells is still hampered by the intact plasma membrane. This is circumvented by extracting the membrane lipids using a buffered detergent solution (see List of Solutions, Tab. 3). Samples were incubated in extraction solution for 30 min 1 h and subsequently the solution was removed with a Pasteur pipette and the samples were washed with PBS 4 times for 10 minutes each.

5) Blocking

Non-specific antibody binding can also occur non-covalently through hydrophobic or electrostatic interactions of immunoglobulin molecules with different subcellular structures. This type of non-specificity is prevented by incubating the sample with a solution of an inert protein such as bovine serum albumin (BSA; see List of Solutions, Tab. 3). The blocking solution was applied for at least 1 hr at room temperature but it was occasionally was prolonged to overnight incubation at 4 °C.

6) Incubation with Primary Antibody

The primary antibody is used to recognize the epitope of interest in the sample. For indirect immunofluorescence, this antibody is unconjugated. The primary antibody solution was prepared by diluting the antibody in 3% w/v BSA in PBS at a ratio of 1:500. As the primary antibodies was chosen rat monoclonal anti-α-tubulin, anti-eGFP nanobody (GFP-Booster) Atto488 conjugated and monoclonal rabbit anti-tagRFP (see List of Solutions, Tab. 3). Plastic baskets with seedlings were transferred directly from the blocking solution to the antibody solution which was placed into the wells of 24-well culture plates containing 700 µl of antibody solution in each well. The culture plate was covered with a lid and the samples were incubated overnight at room temperature. Following antibody incubation, samples were then transferred back into larger wells with PBS buffer and washed at least 6 times for 10 minutes each – the first 4 times with PBS and then 2 times with 3% w/v BSA in PBS. Frequently, the washing after primary antibody incubation was extended overnight. The diluted primary antibody was stored at -20 °C and could be reused for 4-6 more times with no evident decline in labeling efficiency.

7) Incubation with Secondary Antibodies

In the indirect variant of immunofluorescent detection the primary antibody is recognized by fluorophore-conjugated species specific immunoglobulins. Each secondary immunoglobulin molecule can be derivatized with 3-9 fluorophore molecules and each primary immunoglobulin can bind up to 3 secondary immunoglobulin molecules. Therefore and by comparison to direct immunofluorescence where the primary antibody is directly conjugated, the indirect regime provides the means for a tremendous enhancement of the signal and markedly increased signal-to-noise ratios in the final image. Prior to application of the secondary antibodies the samples were blocked with 3% w/v BSA in PBS as in step 6 for at least 1 hour. After this the plastic baskets were lightly blotted on filter paper and transferred into the wells of a 24-well plate filled with 700 µl of the solution of the secondary antibodies. The solution was made by diluting the secondary antibodies (Alexa Fluor 647 anti-rat IgG, Alexa Fluor 488 anti-mouse, and Alexa Fluor 546 anti-rabbit) in 3% w/v BSA in PBS at a ratio of 1:500 and the incubation of the seedlings was carried out for 3 hours at 37 °C and was continued overnight at 4 °C. As the secondary antibody was chosen Alexa Fluor 488 anti-rat. After incubation, the

secondary antibody solution was discarded and the samples were washed at least 6 times for 10 minutes each in PBS buffer.

8) DAPI Staining

Samples were counterstained with the DNA dye 4',6-diamidine-2'-phenylindole dihydrochloride (DAPI). DAPI binds to the minor groove of AT-rich stretches of DNA and exhibits a characteristic blue fluorescence with a λem_{max} at 461 nm and after excitation at a λexc_{max} at 358 nm. Conveniently, DAPI emits fluorescence only when bound to DNA. The DAPI working solution was prepared by dilution of stock solution (10 mM in DMSO) at a ratio of 1:2000 with PBS buffer and then the seedlings were incubated for 10-15 min at room temperature. The samples were then washed 3 times for 10 minutes each with PBS.

9) Mounting of Samples

During imaging with the laser light sources used to excite the fluorophores of the sample, free radicals are produced and these can irreversibly destroy the fluorophores (photobleaching). To protect the fluorophores and preserve fluorescence emission, samples must be mounted in the presence of a strong antioxidant which in this case is paraphenylene diamine. The solution is prepared as shown in Tab. 1 and containing a strong buffering agent (100 mM Tris-Cl pH 8.8) and high concentrations of glycerol (up to 90% v/v). The alkaline pH is chosen because it allows maximum quantum yield of the fluorophores, while the glycerol content is adjusted to such high values as it offers a refractive index close to that of the coverslip, the immersion oil and the objective thus minimizing potential spherical aberrations that may confound the final image. For the mounting three to five seedlings were carefully transferred onto glass slides into a drop (ca. 50 µl) of mounting medium (see List of solutions, Tab. 3), covered with 22×34 mm rectangular coverslips and sealed with clear nail polish. Thus prepared samples were stored in appropriate microscopy sample cassettes (e. g. Heathrow Scientific) at -20 °C and then observed using a confocal spinning disc microscope, structured illumination microscope and laser scanning confocal microscope.

3.8 MAPK Mutants Crossing with Transformants Carrying Molecular Cytoskeleton Markers

The selected plants of mutant lines *mpk4* and *mpk6-2* and transformants expressing cytoskeleton markers (tagRFP-MAP65-2 x eGFP-TUA6) were transferred from the Petri

dishes to the soil after 3 weeks of growing on solid ½ MS medium. After another one week, the plants were ready for crossing. The mother plant (MAPK mutants) bud was opened with the help of tweezers (before self-pollination) and all sticks were removed under microscope. From the father plant (transformant), sticks were taken to dust the piston on the parent plant. The fruits were matured and seeds were harvested.

Dried seeds of F1 were prepared and sowed as mentioned in chapters 3.3 and 3.4 and selected first by fluorescence as mentioned in chapter 3.5.

3.9 Plant Preparation for Microscopic Study of Cytoskeleton *in vivo*

The 3-4 days old seedlings of transformants were used for *in vivo* study of organization, dynamics and localization of microtubules and two dominant microtubule associated proteins MAP65-2 and MAP65-3. Seedlings were mounted between glass slide and coverslip, or at exceptional occasions in Attofluor cell chambers to ensure their immobility. In all cases of live imaging, seedlings were secured in ½ MS medium.

3.10 Quantitative Analysis

During this study we quantified aspects of both microtubule organization and dynamics by means of computer-assisted post acquisition image analysis. In terms of organization we quantified microtubule occupancy and skewness of fluorescence distribution. Occupancy of fluorescently labeled microtubules represents a measure of polymeric tubulin abundance and corresponds to the percentage of the total area occupied by positively identified fluorescent structures against the whole field of view. Skeweness corresponds to deviations of fluorescence distribution from uniformity and represents a measure of microtubule bundling. To decipher both measures we used the LPixel plugins for Image J (freely available for download and installation after registration https://lpixel.net/services/research/lpixel-imagej-plugins/).

Microtubule dynamics were strictly quantified in time series acquired from eGFP-MAP65-2 expressing cells. Briefly, kymographs were generated using the Kymograph plugin of Zeiss Zen Blue software, using regions of interest (ROIs) encompassing the entire length of microtubules occupied during the entire time series. Plus and minus ends could be easily identified in the resulting kymographs based on the range of length fluctuations. The slopes of growth and shrinkage phases were used to calculate growth and shrinkage rates while the duration of growth and shrinkage phases were used to

calculate catastrophe and rescue frequencies. All such measurements were done according to previously published methods (Komis *et al.*, 2014).

3.11 Programs and Databases for Outcome Analysis

- Microsoft Excel 2016

Processing of microscopic images – export and editing images by using programs:

- Image Lab software (Bio-Rad)
- Microsoft Powerpoint 2016
- ZEN Blue 2012 (Zeiss)
- ZEN Black 2012 (Zeiss)
- Image J (https://imagej.nih.gov/ij/download.html)

Databases

- National Center for Biotechnology Information: http://www.ncbi.nlm.nih.gov/
- The Arabidopsis Information Resource: http://arabidopsis.org/
- The Universal Protein Resource (UniProt) https://www.uniprot.org/

3.12 Instrumentation

- Analytical balance (XA 110/2X, RADWAG)
- Automatic pipettes (0,1 µl – 10 ml, Eppendorf)
- Laboratory fume hood (M 1200, MERCI)
- Incubator (Biotrade)
- The Culture chamber (phytotron, Weiss Gallenkamp)
- Laboratory fridge (ERB 34633W, Electrolux)
- Laboratory balance (S1502, BEL Engineering)
- Laminar flowbox biohazard (Faster, FERRARA)
- Magnetic stirrer (MSH-420, BOECO)
- Confocal laser scanning microscope with operating programme ZEN Blue 2012 (Spinning disc, Axio Observer Z1, ZEISS)
- Epifluorescence microscope with operating programme ZEN Blue 2012 (Axio Imager M2, ZEISS)
- Microwave (MGE21, HITACHI)
- Freezer (Liebherr)
- Desktop pH meter (PC 2700, Eutech Instruments)
- Combi-Spin (FVL-2400N, bioSan)

- Attofluor™ Cell Chamber, for microscopy, ThermoFischer Scientific, catalogue number: A7816
- Electrophoretic tray BioRad
- PCR cycler MyCycler™ Thermal Cycler, BioRad
- Gel Doc™ visualizer EZ Imager, BioRad
- Structured illumination microscope with operating programme ZEN Black 2012 (Elyra 7 with Lattice SIM, ZEISS)

3.13 List of Chemicals

- 6x DNA Loading Dye (Invitrogen)
- GeneRuler™ 100 bp Plus DNA Ladder (Invitrogen)
- Agarose (Sigma Aldrich)
- Immersion oil 518F (Zeiss)
- Midori Green (Nippon Genetics)
- Phire Plant Direct PCR Kit (Thermo scientific)

3.14 List of Solutions

Most of the chemicals used in the experiment come from Sigma-Aldrich unless otherwise stated.

Table 3. List of Used Solutions

The sterilizing solution	
1% v/v sodium hypochlorite, 0,05% v/v Tween 20	
10 ml	10% v/v sodium hypochloride
90 ml	Distilled water (dH_2O)
Supplemented with dH_2O to 100 ml with addition of drop of Tween 20	
Solid ½ MS medium without vitamins	
2,2 $g \cdot l^{-1}$	Murashige and Skoog medium (Duchefa)
10 $g \cdot l^{-1}$	Sucrose
8 $g \cdot l^{-1}$	Phytagel
Supplemented to 1 liter with dH_2O, pH adjustment to 5,8 (KOH), sterilized by autoclaving	

Table 3. List of used solutions (*continuation*)

Liquid ½ MS medium without vitamins	
2,15 $g \cdot l^{-1}$	Murashige-Skoog medium (Duchefa)
10 $g \cdot l^{-1}$	Sucrose
Supplemented to 1 liter with dH_2O, pH 5,8 (KOH), sterilized by autoclaving	
Solutions for whole mount	
PFA solution for fixation	
16 g	Paraformaldehyde
150 ml	Ultrapure Milli-Q® H_2O
Fixative solution	
2,5 ml	8% w/v paraformaldehyde
7,5 ml	1× MTSB
4,4 ml	Ultrapure Milli-Q® H_2O
300 µl	Glutaraldehyde
25 µl	Triton-X
A total of 15 ml of fixative solution for five wells of 12 well culture plates (3 ml for each well)	
1× MTSB	
3,775 g	PIPES
0,3075 g	$MgSO_4 \times 7\ H_2O$
0,475 g	EGTA
Supplemented to 250 ml with Milli-Q® H_2O, pH 6,8	

Table 3. List of Used Solutions *(continuation)*

0,025 g / 250 ml	sodium azide
Enzymatic solution	
0,2 g	2% w/v Meicelase
0,2 g	2% w/v Cellulase
0,1 g	1% w/v Macerozyme
10 mg	0,05% w/v Pectolyase Y23
10 ml	MTSB

Table 3. List of used solutions (*continuation*)

Incubation: 20-30 min, room temperature	
½ MTSB buffer for dissolving the enzymes	
100 ml	1×MTSB
100 ml	Ultrapure Milli-Q® H_2O
PBS (Phosphate-buffered saline)	
Stock solution (10× PBS)	
80 g	NaCl (0,8 M)
2 g	KCl (2,7 mM)
11,5 g	$Na_2HPO_4 \times 2\ H_2O$ (6,5 mM)
2 g	KH_2PO_4 (1,5 mM)
Supplemented to 1 l with Milli-Q® H_2O, pH 7,3 (0,1 M KOH)	
Working solution (1× PBS)	
100 ml	PBS (10×)
900 ml	Ultrapure Milli-Q® H_2O
Reduction solution	
15 ml	PBS (1×)
Add of aligned micro weighing spatula with $NaBH_4$ for each sample, total ca. 15 mg of $NaBH_4$ for 5 samples.	
Permeabilization solution	
10 ml	PBS (10×)
10 ml	DMSO (10% v/v)
2 ml	Nonidet P-40 (2% v/v)
78 ml	Ultrapure Milli-Q® H_2O
Blocking solution	
3% w/v BSA in PBS	
1,5 g	BSA
50 ml	PBS (1×)
Before use, store for a few minutes in a freezer (-20 °C) for better dissolution of BSA	

Table 3. List of used solutions (*continuation*)

Primary antibody solution	
15 ml	3% w/v Blocking buffer (BSA+PBS)
30 µl	Monoclonal rat anti-α-tubulin (clone YOL1/34; 1:500)
30 µl	Affinity purified polyclonal rabbit anti-tagRFP (1:500; Evrogen)
75 µl	Affinity purified polyclonal alpaca anti-eGFP nanobody (GFP-Booster) Atto488 conjugated (1:200; Chormotec)
700 µl of antibody solution for one sample (well). Antibody solution was kept at -20 °C	
Secondary antibody solution	
10 ml	3% w/v Blocking buffer (BSA+PBS)
20 µl	Secondary antibody: Alexa Fluor 647 anti-rat IgG (1:500)
20 µl	Secondary antibody: Alexa Fluor 488 anti-mouse (1:500)
20 µl	Secondary antibody: Alexa Fluor 546 anti-rabbit (1:500)
DAPI	
Stock solution	
10 $mmol \cdot l^{-1}$ in DMSO	
Working solution	
Dilution 1:2000, 0,5 µl of 10 mM DAPI/1 ml PBS	
30 ml	PBS
15 µl	DAPI
Mounting medium	
100 mg	Paraphenylenediamine
30 µl	DMSO
1 ml	Tris (1,5 M, pH 8,8)
9 ml	100% v/v Glycerol
Solution was mixed with a glass rod, pH ca 8,8, stored in dark at -20 °C	

4 Results and Discussion

4.1 Localization Patterns of MAP65-2 and MAP65-3

4.1.1 General Remarks

The MAP65 family of microtubule crosslinking/bundling proteins is a well conserved family of MAPs. Exemplified by the founding member, MAP65-1, it is expected that all MAP65 proteins form coiled-coil based homodimers with juxtaposing carboxylterminal microtubule binding domains capable of crosslinking antiparallel microtubules (Li *et al*., 2007; Smertenko *et al.*, 2008). This feature is conserved in non-plant homologues of MAP65 proteins present in fission yeast (Ase1; Anaphase spindle elongation 1) and other eukaryotes (PRC1; protein regulator of cytokinesis 1; Braun *et al*., 2011; Juanes *et al*., 2011; Courtheoux *et al*., 2009; Janson *et al*., 2007).

In the present study, the localization of MAP65-2 was addressed in all major organs of *Arabidopsis thaliana* seedlings expressing a eGFP-MAP65-2 fusion protein expressed under the native promoter of *MAP65-2*. Similarly we addressed MAP65-3 localization using a eGFP-MAP65-3 construct, again driven by the native promoter of MAP65-3. Transformations with the appropriate *proMAP65-2::eGFP-MAP65-2* and *proMAP65-3::MAP65-3-GFP* constructs were done on a wild type Columbia background, since apparently seedlings bear no discernible phenotype. Localization studies, were conducted by means of SIM or spinning disc microscopy on epidermal cells of cotyledons, hypocotyls, petioles and roots of living seedlings.

Further spatial relations between MAP65-2 and microtubules were pursued in plants coexpressing tagRFP-MAP65-2 and GFP-TUA6 markers while the differential localization of MAP65-2 and MAP65-3 was documented in cells coexpressing tagRFP-MAP65-2 and eGFP-MAP65-3 markers.

Where live imaging was not applicable due to bleaching issues with either SIM or spinning disc microscopy, spatial correlations between MAP65 proteins and microtubules were addressed in appropriately immunolabeled root wholemounts.

Both MAP65-2 and MAP65-3 have different expected subcellular localization patterns, but they represent ubiquitous members of the MAP65 family with global distribution within vegetative and generative tissues (See in Figs. 11 and 12).

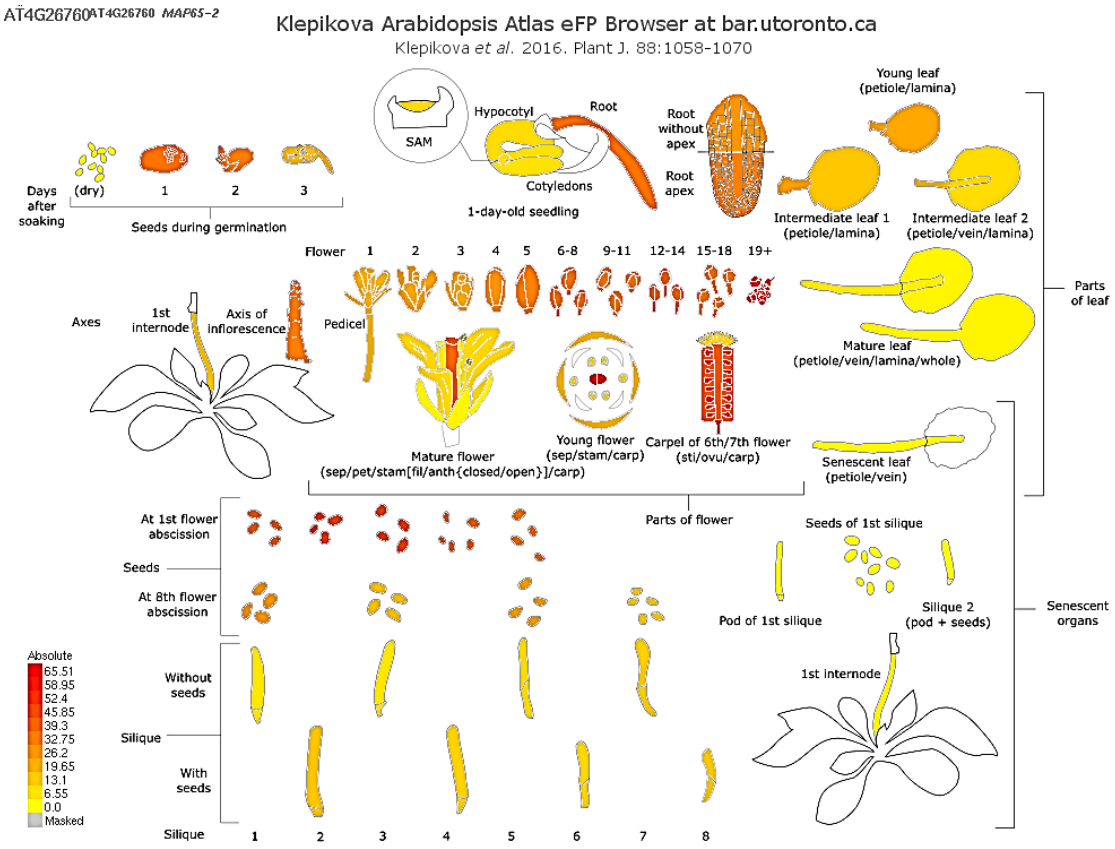

Figure 11. Heatmap demonstration of MAP65-2 expression via transcript analysis (source: https://www.arabidopsis.org/servlets/TairObject?id=126774&type=locus)

MAP65-2 is a predominant crosslinking protein in the cortical interphase array, while it is also expected to be found in mitotic and cytokinetic microtubular systems (see later). Although the interphase functions of MAP65-1 and MAP65-2 are well documented, similar deductions of their role in mitosis and cytokinesis cannot be deduced since single or double map65-1, map65-2 and map65-1map65-2 mutants, exhibit no relevant phenotypes (Lucas and Shaw, 2012)

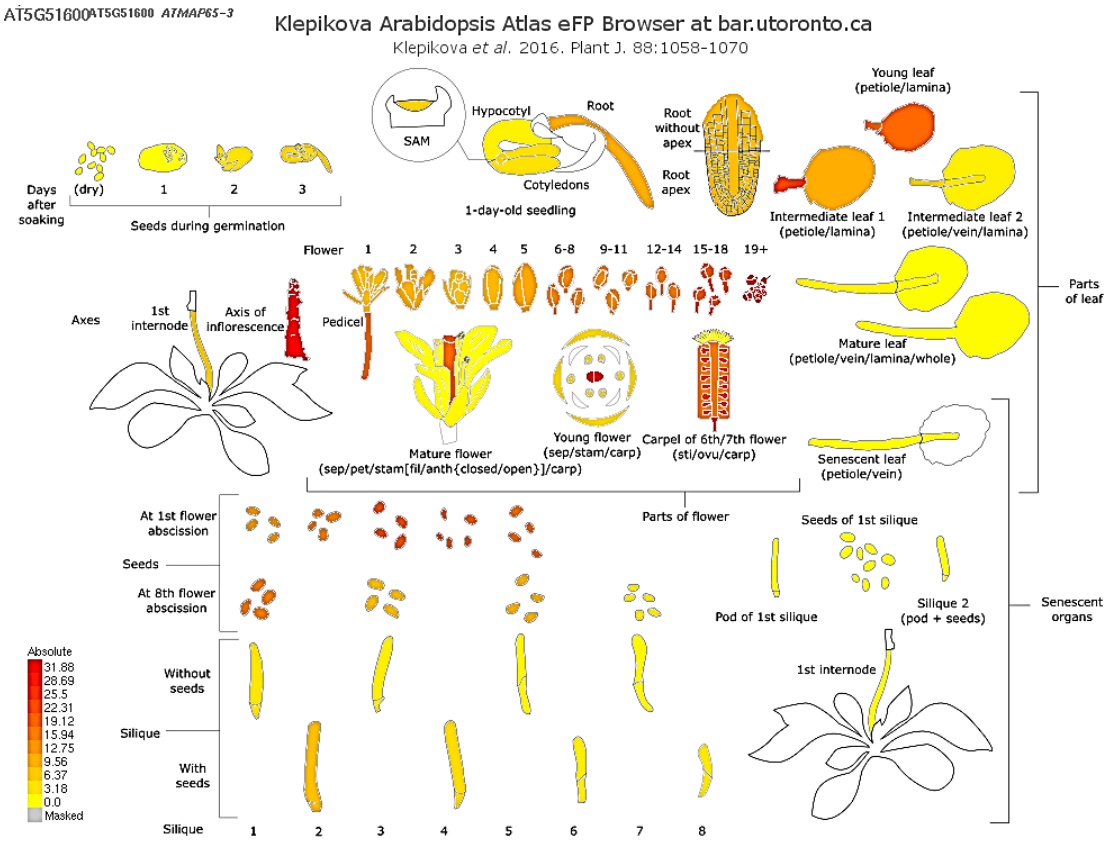

Data from A high resolution map of the Arabidopsis thaliana developmental transcriptome based on RNA-seq profiling: Klepikova et al., 2016, Plant J. 88:1058-1070. Total RNA was extracted with RNeasy Plant Kit and Illumina cDNA libraries were generated using the respective manufacturer's protocols. cDNA was then sequenced using Illumina HiSeq2000 with a 50bp read length. The read data are publicly available in NCBI's Sequence Read Archive under the BioProject ID 314076 (accession: PRJNA314076). Reads were aligned to the reference TAIR10 genome (Lamesch et al., 2012) using TopHat (Trapnell et al., 2009). Default TopHat settings and job resource parameters were used, with read groups unspecified. Reads per gene were counted with an in-house Python script using functions from the HTSeq package (Anders et al., 2015). Reads were filtered so that only uninterrupted reads corresponding to a region within exactly one gene were used for RPKM calculation. If a gene's expression level is not displayed, this indicates the reads for this gene did not pass the filtering criteria. RPKM values were compiled using an in-house R script.

Figure 12. Heatmap demonstration of MAP65-3 expression via transcript analysis (source: https://www.arabidopsis.org/servlets/TairObject?id=131797&type=locus)

MAP65-3 is also a universally expressed member of the MAP65 family but has more restricted roles during mitosis and cytokinesis (Herrmann *et al*., 2018; Li *et al*., 2017; Steiner *et al*., 2016; Ho *et al*., 2012). More importantly, map65-3 mutants exhibit robust cytokinetic phenotypes (Söllner *et al.*, 2002; Müller *et al.*, 2002, 2004) unlike single or double map65-1 and map65-2 mutants (Lucas and Shaw, 2012).

4.1.2 Overview of MAP65-2 Localization and Its Relation to Microtubule Bundles

Studies of single expressors of eGFP-MAP65-2 showed that the latter localizes at patterns corresponding to cortical microtubule arrays routinely encountered in epidermal cell types. In this sense eGFP-MAP65-2 follows the expected microtubule configuration in epidermal cells of the hypocotyl (see Fig. 13A), the cotyledon (see Fig. 13B), the petiole (see Fig. 13C,E), and the root (see Fig. 13D). Although MAP65-2 is ubiquitous in all vegetative tissues (Lucas *et al.*, 2011), particular cell types such as stomata guard cells

were nearly devoid of MAP65-2 despite a wealth of cortical microtubules (see Fig. 13F-I) as proven in double expressors of eGFP-TUA6 and tagRFP-MAP65-2 (Fig. 3G-I). This prompted us to quantify two important measures of microtubule organization, namely, skewness and occupancy (Higaki *et al.*, 2010). Skewness addresses divergence of fluorescence distribution of an assumed evenly labeled sample and thus serves as an indicator of bundling. Occupancy reflects the percent of thresholded fluorescent areas against to the whole field of view.

Survey of TUA6-GFP expressors, showed that principally, microtubule fluorescence is clustered and gave skewness values that were similar when comparing hypocotyl, cotyledon, petiole and root epidermal cells (see Fig. 13J). In terms of occupancy, however, there was a marked difference between the values obtained for TUA6-GFP and eGFP-MAP65-2 (see Fig. 13K). There are many plausible explanations which may be summarized as follows: (a) Not all microtubules are bundled. This is very consistent with the observation of rogue microtubules in cell types as those examined herein (e.g., Komis *et al*., 2014); (b) Microtubule bundling of interphase cortical arrays can be redundantly mediated by other members of the MAP65 family, such as MAP65-1 (e.g., Lucas *et al.*, 2011) or MAP65-5 (Van Damme *et al.*, 2004), thus the occupancy values obtained for MAP65-2 do not fully reflect the bundling extend in the cortical cytoplasm; (c) The polarity of adjacent microtubules cannot justify bundling as a major mechanism of cortical microtubule organization. This might represent an explanation of the MAP65-2 deficit in stomata guard cells that exhibit a radial array of cortical microtubules of uniform polarity (Marcus *et al.*, 2001) which is not favorable for bundle formation by MAP65 proteins that rather crosslink antiparallel microtubules (Li *et al.*, 2001; Smertenko *et al*., 2008; Gaillard *et al.*, 2008). Alternatively, MAP65-2 may not be expressed in stomata, hence the expression of the eGFP-MAP65-2 may not be adequate to visualize microtubule bundles in guard cells.

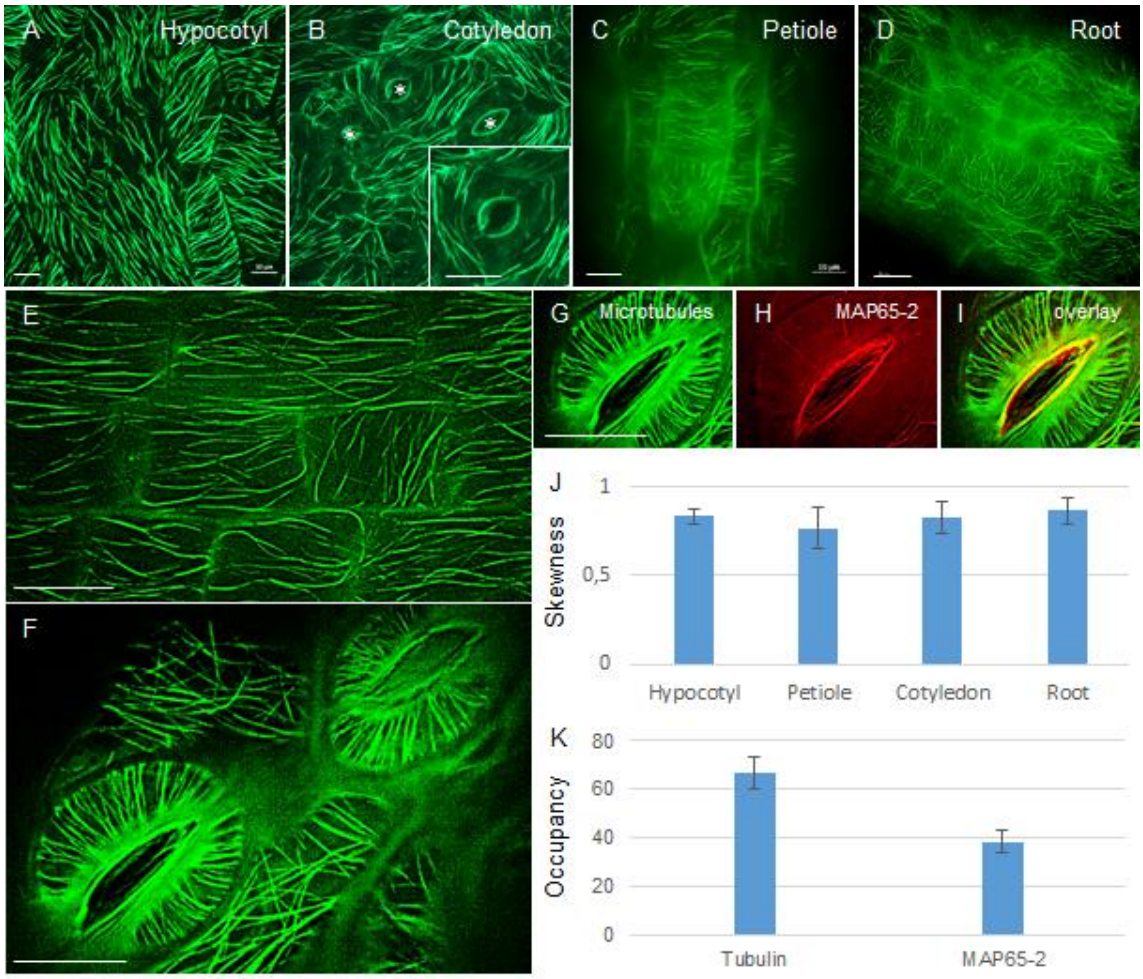

Figure 13. Overview and quantification of MAP65-2-based microtubule bundling in selected vegetative tissues and cell types. **A-D.** eGFP-MAP65-2 visualization in hypocotyl (A), cotyledon (B), petiole (C) and root (D) epidermal cells. **E.** Very regular and preferentially longitudinal formation of eGFP-MAP65-2 decorated bundles in petiole epidermal cells. **F-I.** Microtubule organization probed by TUA6-GFP (F,G,I) and tagRFP-MAP65-2 localization in cotyledon stomata guard cells. **J.** Overview of fluorescence distribution skewness in observed tissues of *A. thaliana* expressing a TUA6-GFP microtubule marker. **K.** Occupancy values of TUA6-GFP vs tagRFP-MAP65-2 signals averaged from all cell types examined. Scale bars: 10 μm for all cases.

The relation of MAP65-2 with the process of microtubule bundling was followed in quantitative and dynamic terms in both single eGFP-MAP65-2 expressors as well as in double TUA6-GFP and tagRFP-MAP65-2 transformants (see Fig. 14). By means of SIM, it became evident that signals arising from both TUA6-GFP and tagRFP-MAP65-2 are spatially close (e.g., see Fig. 14A-G) but not exactly overlapping (see Fig. 14H,K,L) and this was corroborated by means of normalized intensity profiling (see Fig. 14M,N) showing clear separation of the two signals. Since image acquisition of both channels was done sequentially, we excluded the possibility of channel mismatch by previously documenting subdiffraction Tetraspec beads for manual channel alignment as described before (Komis *et al.*, 2015c).

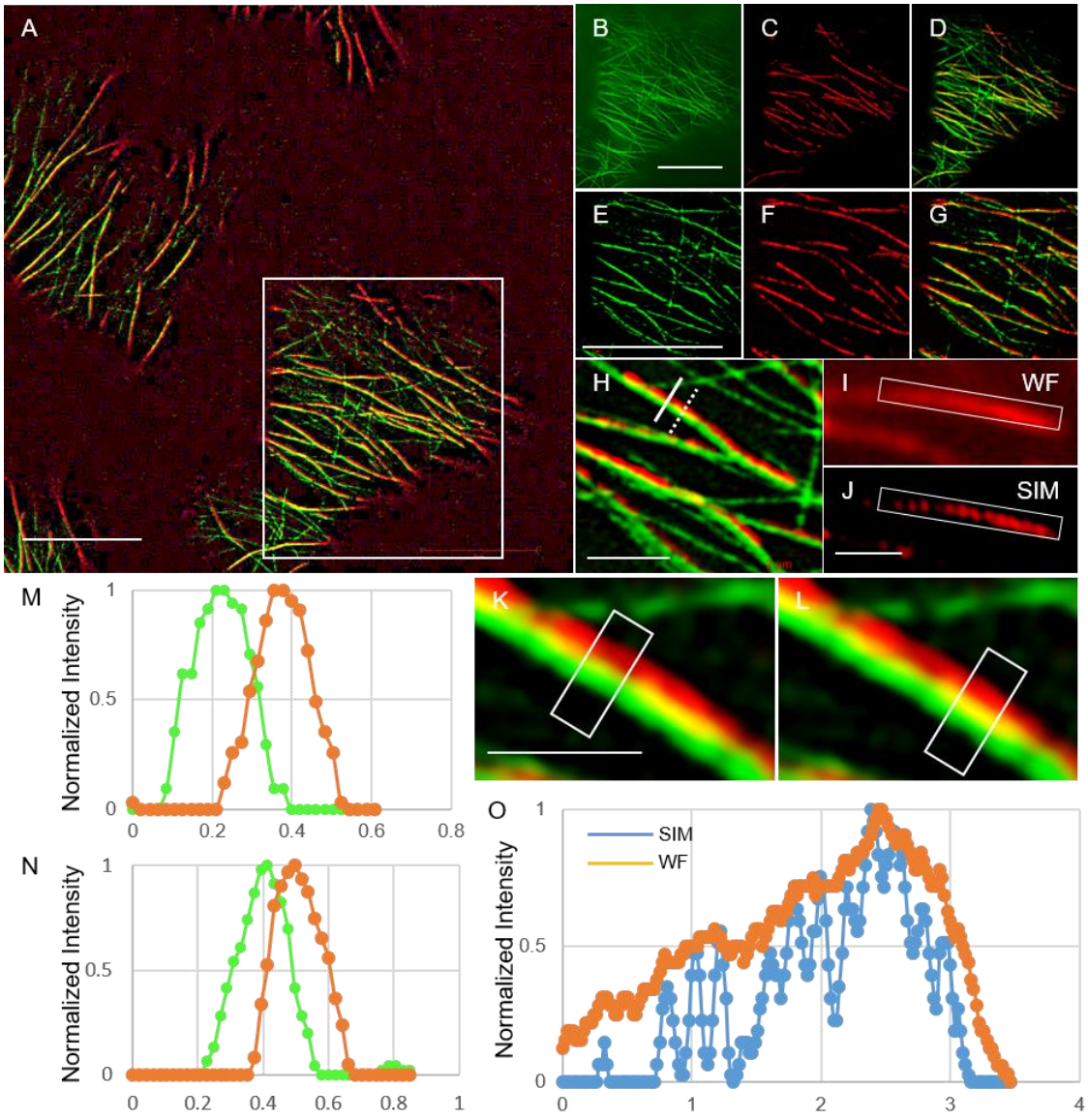

Figure 14. Spatial correlation between microtubules and MAP65-2. **A.** Overview of a cotyledon epidermal cell coexpressing TUA6-GFP (Green) and tagRFP-MAP65-2 (Red). **B-G.** Sequential magnification of the boxed area in A, showing microtubules (B,E), MAP65-2 (C,F) and their overlay (D,G). **H.** Double localization of TUA6-GFP and tagRFP-MAP65-2 showing clear signal separation after high resolution SIM imaging. **I,J.** Widefield epifluorescence and SIM comparison showing how superresolution can resolve the uneven distribution of MAP65-2 within microtubule bundles. **K,L.** High magnification view of the line profiles shown in (H) further proving the spatial separation between TUA6-GFP and tagRFP-MAP65-2 signals. **M-O.** Graph representation of normalized fluorescence intensity, quantifying signal separation of TUA6-GFP and tagRFP-MAP65-2 profiled in H,K,L and the discontinuous distribution of tagRFP-MAP65-2 profiled in I,J. Scale bars: 10 µm (A-G); 2 µm (H); 1 µm (I-L)

Moreover, we used SIM to demonstrate that MAP65-2 is not uniformly labeling microtubule bundles (see Fig. 4J) as it might be erroneously inferred by diffraction-limited widefield epifluorescence imaging of the same sample (see Fig. 14I). This is not

a surprising outcome since microtubule bundling can be redundantly regulated by other members of the MAP65 family, including MAP65-1 (which reportedly coincides with MAP65-2 after diffraction-limited imaging by means of the spinning disc; Lucas *et al*., 2011), or MAP65-5 (Van Damme *et al.*, 2004). At this stage, we assume that microtubule bundling occurs by following fundamental rules of constructive microtubule encounters (Tulin *et al.*, 2012; Stoppin-Mellet *et al*., 2013) by stochastically allowing the recruitment of different MAP65 proteins present at that time. Thus, microtubule bundles might be fully decorated by different MAP65 molecules cannot be visualized at the current setup. Moreover, the eGFP-MAP65-2 may be diluted to a pool of unlabeled MAP65-2 which should be expressed in the wild type background used for the transformation.

4.1.3 Dynamics of MAP65-2 in the cortical array

Being strictly focused on MAP65-2 we tracked in a time-lapsed manner the evolution of contiguous eGFP-MAP65-2 signals in elongating hypocotyl epidermal cells of *A. thaliana*. By means of tracking of fluorescence intensity (see Fig. 15) it became evident that MAP65-2 accumulation is not precisely following the previously published end-based dynamics of microtubules (Shaw *et al*., 2003), but rather accumulates at the center of bundles and spreads in a minus-end directed manner (see Fig. 15A-M)

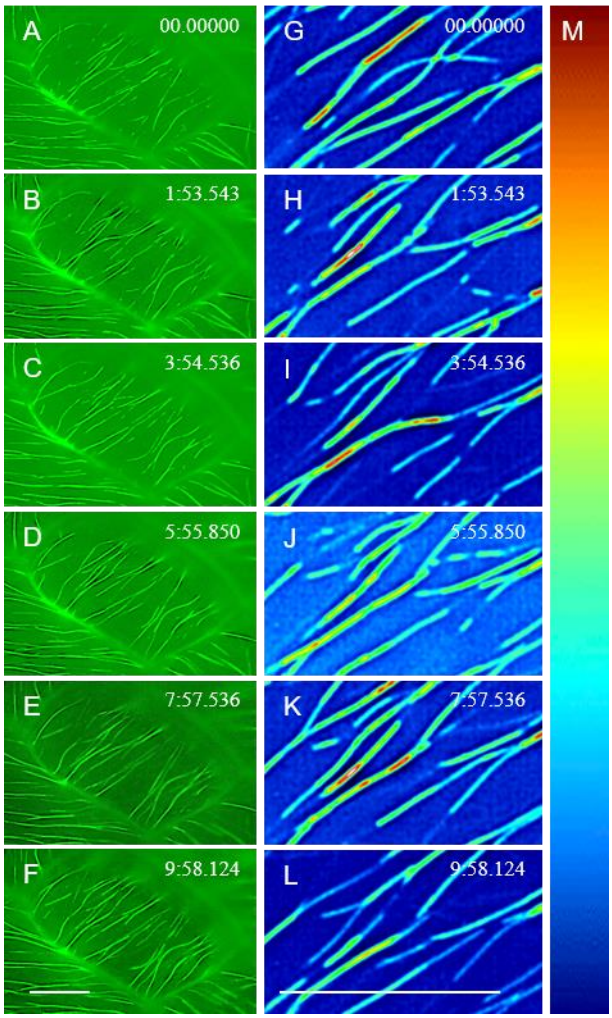

Figure 15. Progressive evolution of MAP65-2 accumulation during bundle formation in the cortical cytoplasm of petiole epidermal cells. **A-F.** Monochrome time-lapsed series showing progressive formation of bundles. **G-L.** Fluorescence intensity based color-coded depiction of a blow up of (A-F) stills quantitatively showing how MAP65-2 endeavors within microtubule bundles. **M.** The color scale used. Scale bars: 10 µm for all cases.

Microtubule bundling is a stochastic process which depends on spatial aspects of microtubule encounters (Tulin *et al*., 2012). When incoming microtubules encounter each other at angles equal or greater to 40°, either a crossover forms or a tip-wise catastrophe event occurs (Mace and Wang; 2015). In the latter case, crossover clearance may occur through the severing function of katanin (Wightman *et al.*, 2007; Deinum *et al.*, 2017; Zhang *et al*., 2013). The decoration of cortical microtubule bundles by means of MAP65-2 was temporally resolved in single transformants expressing eGFP-MAP65-2. In epidermal cells of hypocotyls, cortical microtubules are frequently bundled at variable degree of complexity, which can be followed by means of SIM imaging. Owing to the mechanisms of microtubule bundle formation, the association of MAP65-2 with such

structures is rather dynamic, as has been shown before in the case of its closest homologue, MAP65-1 (Portran *et al.*, 2013; Stoppin-Mellet *et al*., 2013).

Based on the increased resolution and optical sectioning potential of SIM we documented the dynamics of eGFP-MAP65-2 in microtubule bundles of different bulk and depicted the output by means of kymography. Kymographs generated as described (see Materials and Methods) were used to extrapolate plus- and minus- end dynamics of eGFP-MAP65-2 and decipher catastrophe and rescue frequencies (see Fig. 16).

In this line, we used SIM to provide adequate means discriminating fluorescence intensities of overlapping intrabundle microtubules (Komis *et al.*, 2014). This allowed the generation of very well discriminated kymographs (life history plots of individual microtubules/bundles decorated by means of eGFP-MAP65-2) and use these kymographs to decipher certain measures of eGFP-MAP65-2 including rates of growth and shrinkage and frequencies of catastrophes and rescues. In particular, we observed differential behaviors between the two different microtubule ends and thus extrapolated such measures for both. Thus the growth and shrinkage rates of (+) ends were calculated to be 7.9±2 μm/min and 14.4±1.55 μm/min respectively (mean±SD; N=25), while for the same end catastrophe and rescue frequencies were 0.027 events/min and 0.053 events/min respectively (N=25). For the (-) end, growth and shrinkage rates were 1.8±1.05 μm/min and 1.27±0.97 μm/min (mean±SD; N=25), while catastrophe and rescue frequencies were not calculated. The measures determined herein, are in good accordance with previous studies of microtubule dynamics of *A. thaliana* hypocotyl cells expressing different markers, such as GFP-MBD (a GFP fusion of the microtubule binding domain of the non-neuronal mammalian MAP4), EB1a-GFP (a GFP fusion of the End Binding 1a protein) and TUA6-GFP (Van Damme *et al.*, 2004; Komis *et al.*, 2014; Shaw *et al*., 2003).

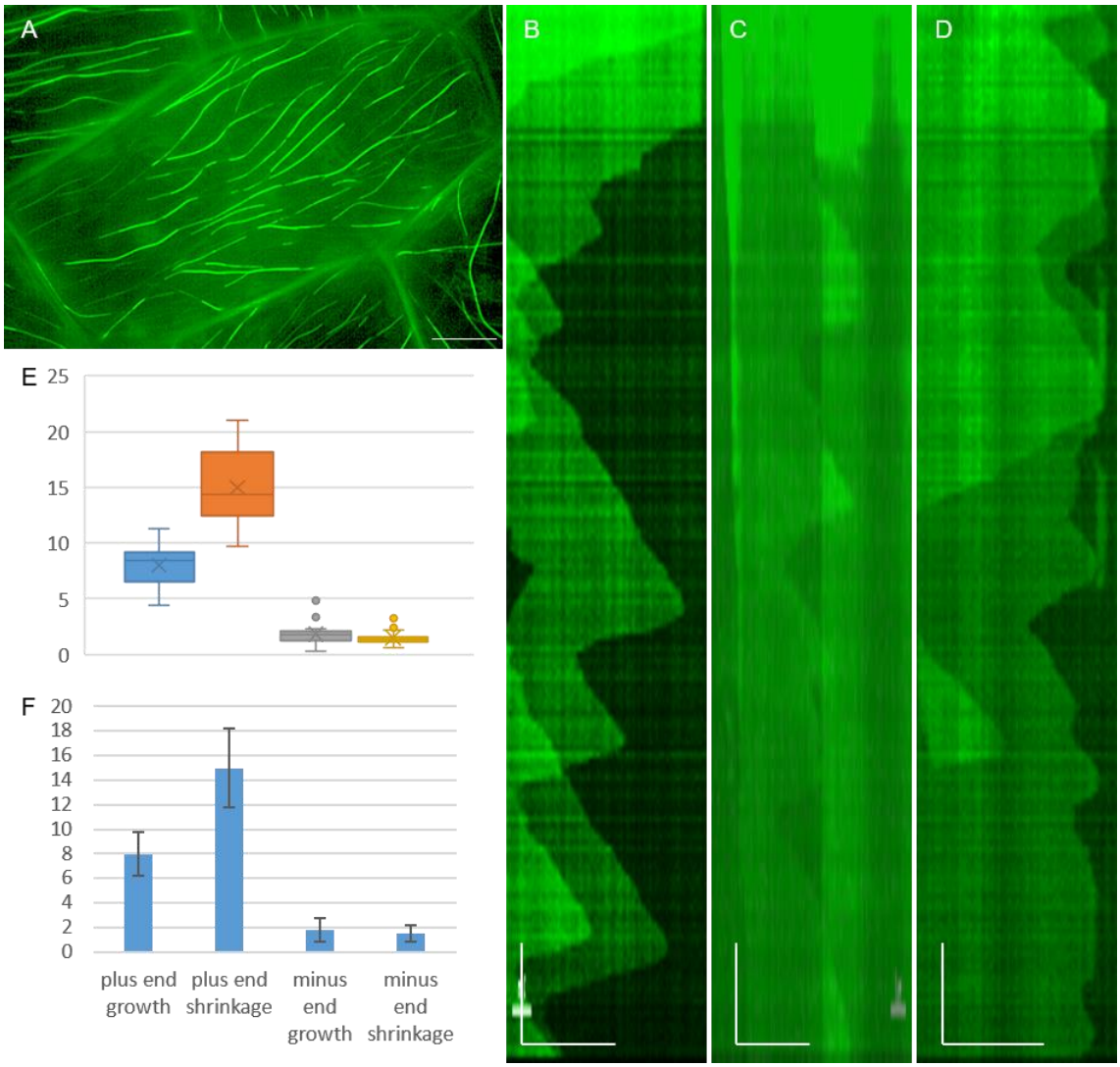

Figure 16. Dynamics of MAP65-2 in the cortical microtubule array. **A.** SIM overview of a living hypocotyl epidermal cell of *A. thaliana* expressing an eGFP-MAP65-2 marker observed in a time series. **B-D.** Representative kymographs. **E,F.** Box plot and bar chart documentation of growth and shrinkage rates averaged from several measurements from both plus and minus ends of microtubules. Scale bars: 10 µm (A), 5 µm (B-D). Time bars: 1 min (B-D). Part of this figure is adapted from Vavrdová *et al*. submitted to ACS Nano (under review).

4.1.4 Localization of MAP65-2 in Mitotic and Cytokinetic Arrays

The redundant MAP65-1 and MAP65-2 microtubule crosslinkers (Lucas *et al*., 2011) are also reported to colocalize with antiparallel microtubules within PPBs and telophase/cytokinetic microtubule systems such as the phragmoplast (Sasabe *et al*., 2011; Boruc *et al*., 2017; Smertenko *et al*., 2006; Mao *et al*., 2005). To characterize the occurrence of MAP65-2 in mitotic and cytokinetic systems, we followed the localization of eGFP-MAP65-2 in areas of cotyledons or petioles with vigorously dividing cells. As known from its closest homologue, MAP65-1, MAP65-2 was found to be enriched in PPBs (see Fig. 17A) and to be differentially distributed within the PPB array depending

on the extend of bundling (see Fig. 17B). Importantly, eGFP-MAP65-2 distribution follows the narrowing of the PPB as documented in time-lapse experiments (see Fig. 17C-F, Fig. 18).

The participation of MAP65-2 (according to what has been described for MAP65-1) is somewhat expected since earlier studies based on transmission electron microscopy have revealed the presence of electron dense crossbridges between adjacent microtubules of the PPB (Gunning *et al.*, 1978; Takeuchi *et al*., 2016). However other proteins have been also implicated in PPB formation through microtubule bundling and such is the mitotic kinesin calmodulin binding protein (KCBP; Kao *et al.*, 2000).

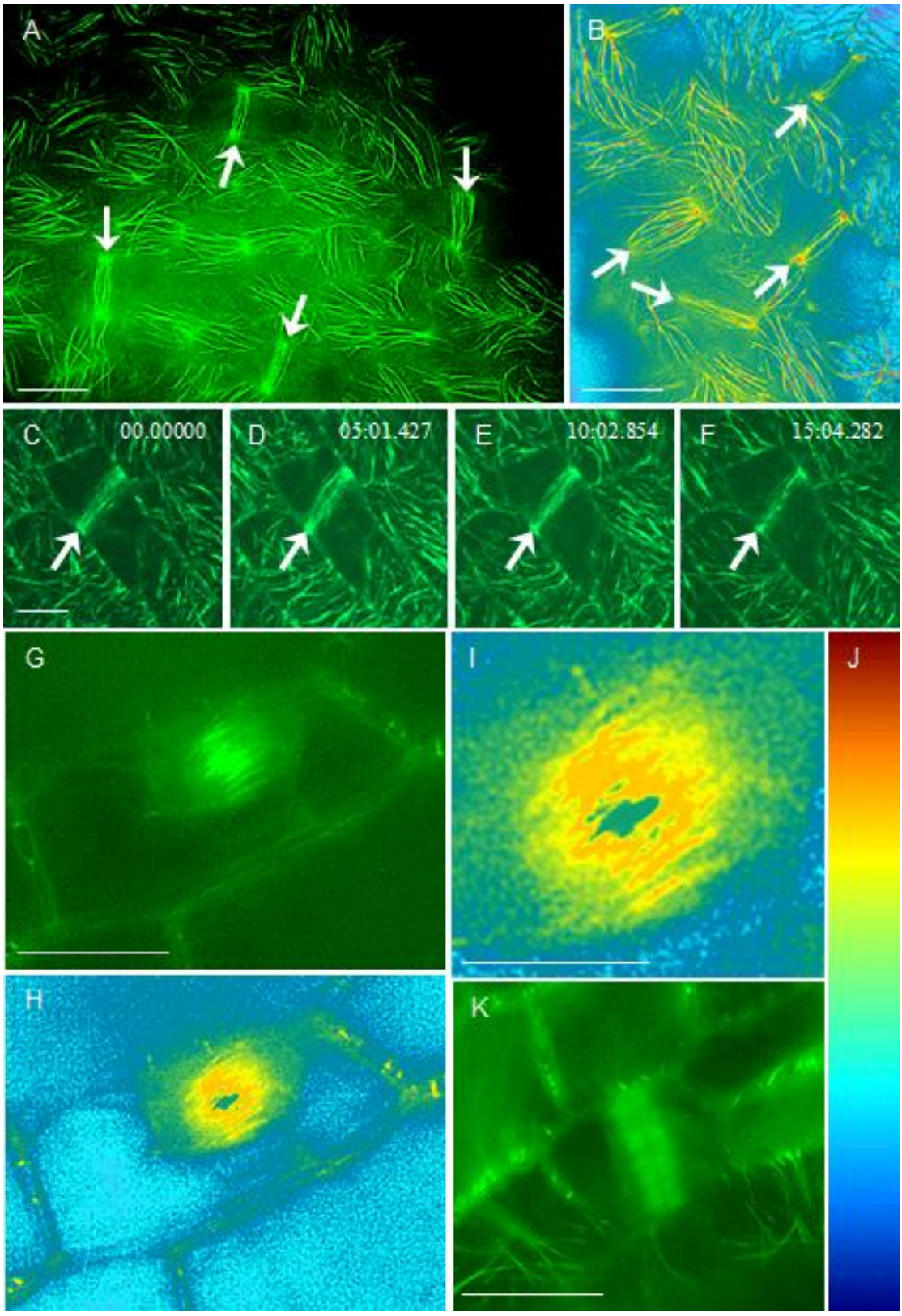

Figure 17. Localization of eGFP-MAP65-2 in the PPB and the phragmoplast. **A.** Overview of a cotyledon area exhibiting several PPBs (arrows). **B.** A similar area using intensity color coding to demonstrate different bundling extend within several PPBs (shown by arrows). **C-F.** Selected frames of a recorded time series, showing the progressive narrowing of a PPB (arrow). **G-I.** Localization of eGFP-MAP65-2 in a telophase interzonal system using the monochrome display (G) or intensity heat map (H-I) allowing the better visualization of how eGFP-MAP65-2 is more

concentrated within the midzone and progressively diminishes towards the poles. **J.** The heat map scale used in (B,H,I). **K.** A well-developed phragmoplast fully decorated with eGFP-MAP65-2. Scale bars: 10 μm (A-H, K), 2 μm (I).

The importance of MAP65-2 in PPB formation cannot be deciphered by the present findings and only its presence can be corroborated throughout the entire course of PPB formation (e.g., see Fig. 18).

As previous studies reported MAP65-1 is also inadvertently localizing to the PPB (Chang *et al.*, 2005; Van Damme *et al.*, 2004), although it is not clear how necessary this localization is for the initiation and the progressive narrowing of the PPB which is characterized by tighter association of the microtubules comprising it. The formation or progression of the PPB has been studied in terms of events such as the control of dynamicity (Vos *et al.*, 2004), the regulation of katanin-based microtubule severing (Komis *et al.*, 2017) or the presence of other effectors such as actin microfilaments (Takeuchi *et al.*, 2016; Kojo *et al.*, 2013; Panteris *et al.*, 2009) while the importance of microtubule bundling is currently underrated. Additionally, single map65-1 or map65-2 mutants do not exhibit discernible phenotypes (Lucas and Shaw, 2012) suggesting that alone these two isoforms are not critical for mitotic/cytokinetic progression. As will be discussed later, most critical appears to be MAP65-3 the largest member of the MAP65 family, mutants of which exhibit very robust phenotypes (see later).

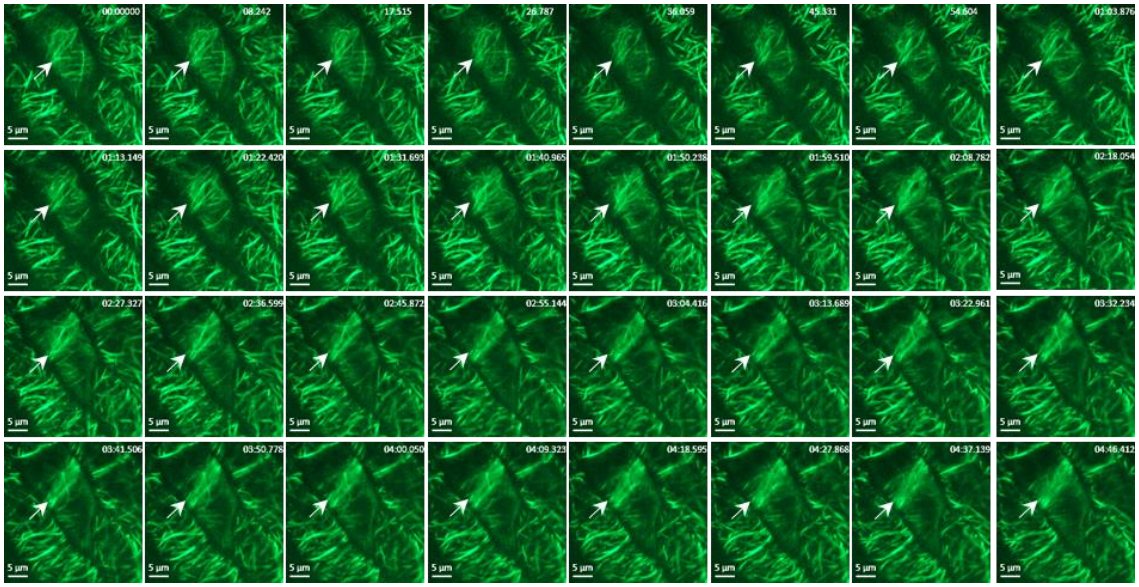

Fig. 18. Time-lapse imaging of progressive PPB formation starting from a discordant cortical interphase array and ending with the formation of a well-developed PPB. Scale bar: 5 μm

4.1.5 Dynamic Loading of MAP65-2 During Telophase/Cytokinesis

Dynamics of MAP65-2 relocalization during mitosis and cytokinesis were followed in single expressors of eGFP-MAP65-2. Although we used both spinning disc (see Figs. 19, 20) and SIM (see Fig. 21) imaging, we deemed the latter more relevant to the expected biological output since the temporal resolution was much better.

By means of SIM imaging, it became clear that loading of eGFP-MAP65-2 starts during telophase when the microtubule interzonal system succeeds the mitotic spindle during the end of anaphase. eGFP-MAP65-2 localization follows the entire interzonal system and thereon decorates the cytokinetic phragmoplast. During cytokinesis, eGFP-MAP65-2 localizes to the phragmoplast and follows the centrifugal expansion of the latter, being restricted at its margins until it reaches the daughter cell wall.

Documentation of mitosis and cytokinesis using the spinning disc, drastically improved the sampling frequency, allowing the observation of eGFP-MAP65-2 recruitment dynamics during the early stages of interzonal system/phragmoplast formation (see Figs. 19, 20). Such observations proved that the accumulation of eGFP-MAP65-2 starts at the midzone of the interzonal telophase system and expands outwards towards the poles in a minus-end directed manner until it occupies the entirety of the interzonal system. On the other hand, SIM by means of superior optical sectioning contributed to visualize in better detail the eGFP-MAP65-2 gradient formed during the progression of the telophase interzonal microtubule system before the emergence of the phragmoplast (see Fig. 21).

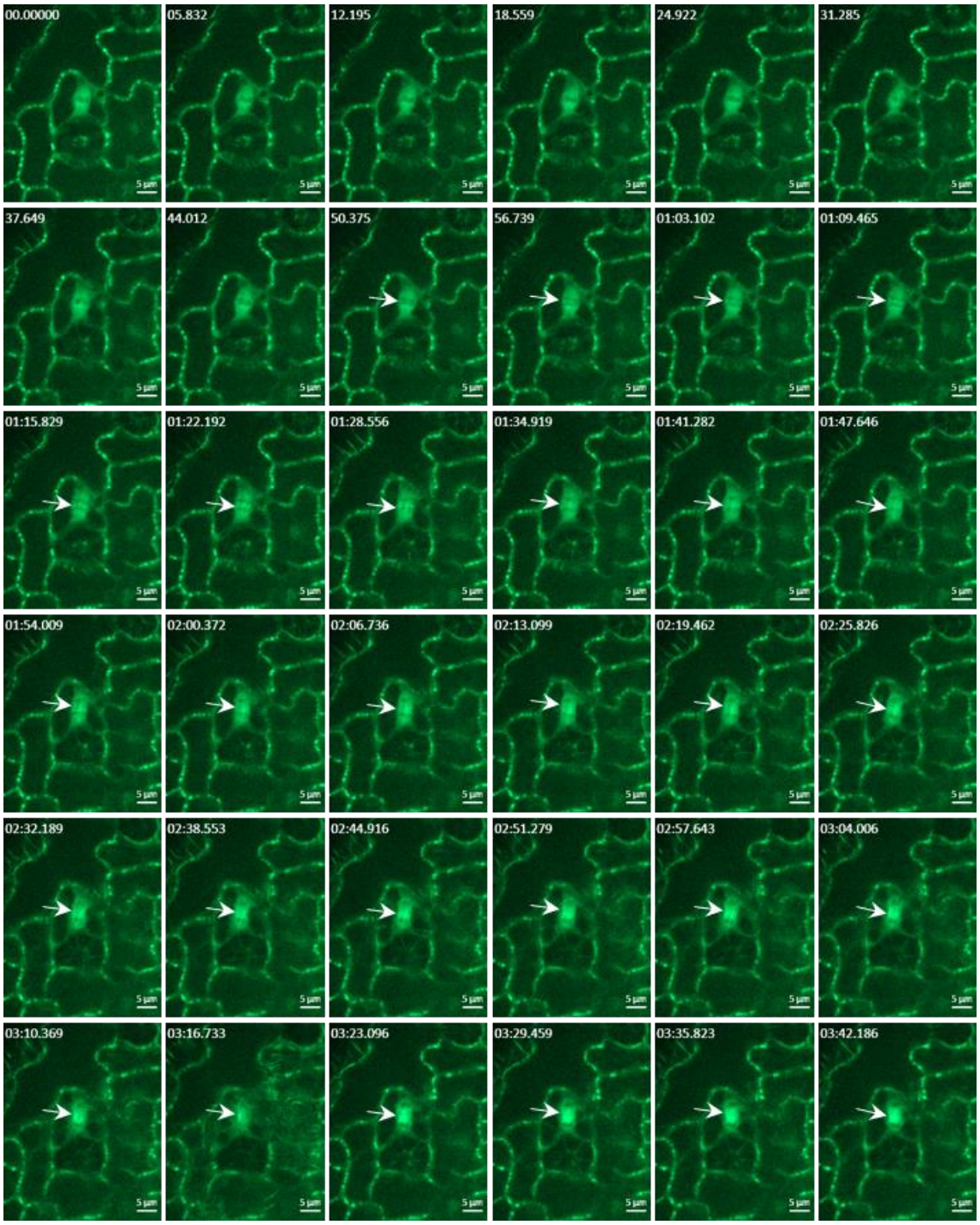

Figure 19. Progressive accumulation of eGFP-MAP65-2 at the last stages of mitosis and the onset of cytokinesis. The positive signal starts to appear as a thin line at the equatorial plane (arrows) which is progressively widening during the gradual formation of the microtubule interzonal system until the emergence of the cytokinetic phragmoplast. Scale bars: 5 µm.

To our knowledge, this is the first time that a MAP65 member is kinetically tracked in such a restricted stage of cell division. The frame rates of spinning disc acquisitions revealed mechanistic details of the bundling process showing that eGFP-MAP65-2 signal migrates in a poleward fashion at a minus-end directed manner. We know from earlier

studies that the interzonal microtubule system is not polymerized *de novo*, therefor MAP65-2 localization is not following microtubule polymerization but rather follows preexisting microtubule tracks.

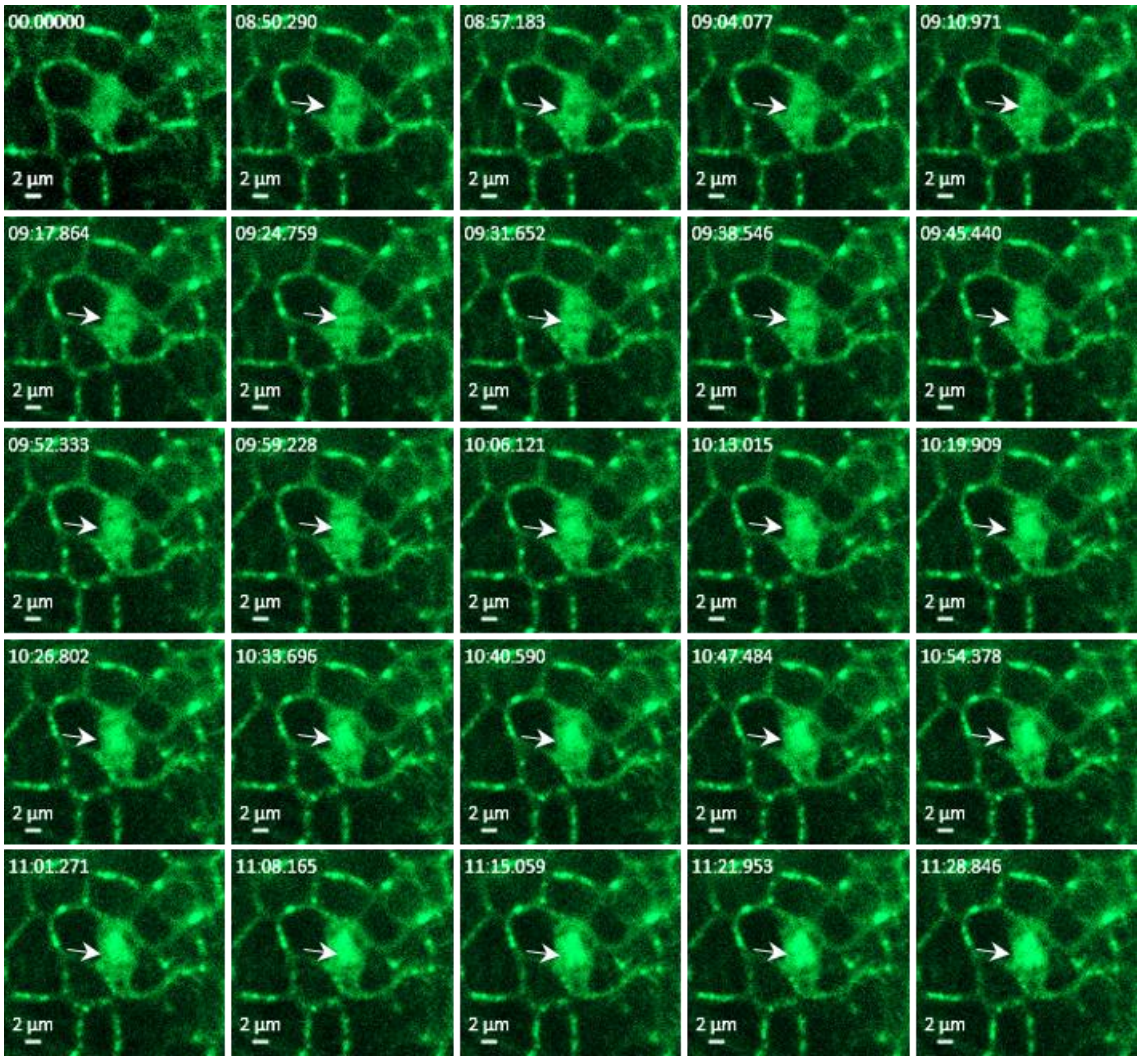

Figure 20. Closer view of the same process of eGFP-MAP65-2 loading at the end of anaphase until the onset of cytokinesis. The signal originally appears as a thin line at the cell equator and then spreads in a poleward fashion until it occupies the entire midzone (arrows). Scale bars: 2 µm.

By means of SIM, we verified that during the progress of cytokinesis and especially at the early stages preceding phragmoplast formation, eGFP-MAP65-2 forms a declining poleward gradient that progressively smoothens during the formation of the early phragmoplast until it disappears suggesting that thereon the distribution of eGFP-MAP65-2 is rather uniform along phragmoplast microtubules.

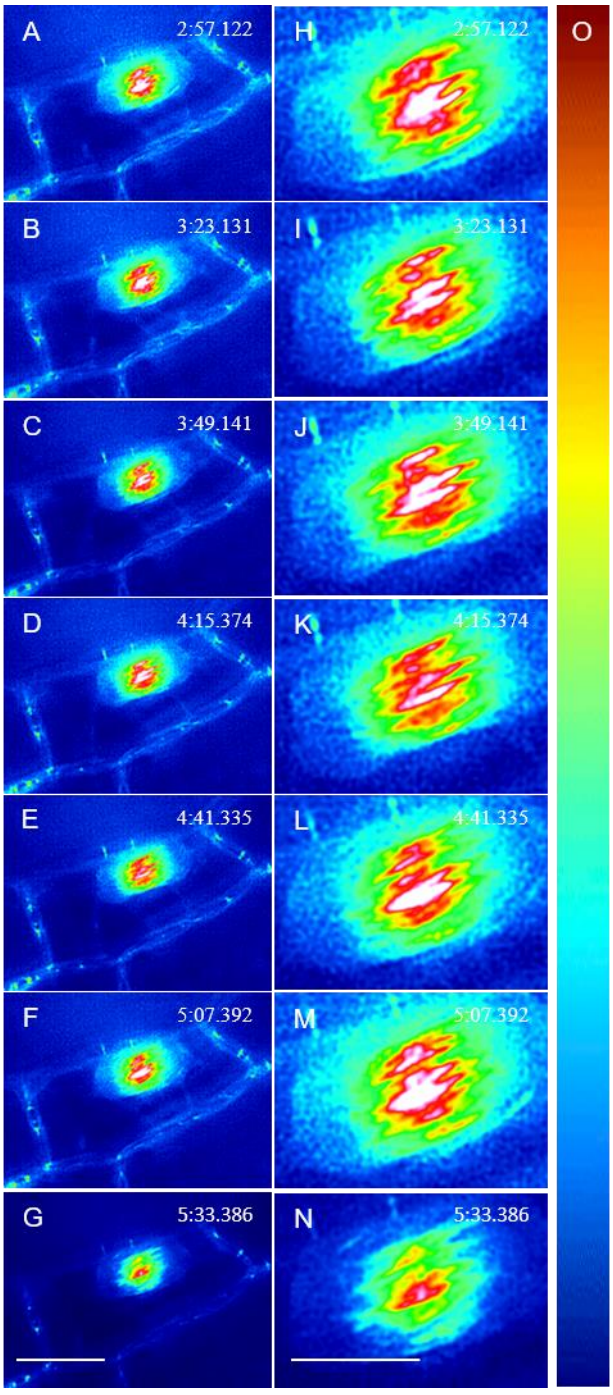

Figure 21. Intensity-based, color-coded documentation of the telophase cell shown in Fig. 17G. The signal corresponding to eGFP-MAP65-2 appears strongest at the midzone and declines progressively in a poleward fashion. Scale bars: 5 μm for all cases.

At present we cannot deduce a meaningful function of this mechanism of MAP65-2 localization, although it is reminiscent of the minus-end directed spreading previously described for cortical microtubules (see Fig. 15 and relevant discussion). This similarity provides a hint, that MAP65, as has been previously described, provide the means for a polarity based microtubule organization mechanism working in synergy with kinesin

motors (Pringle *et al*., 2013; Braun *et al*., 2011; Lansky *et al*., 2015). This possibility will be discussed later in the case of MAP65-3 where recent literature proved to be more informative (see later).

4.1.6 Localization of MAP65-3 in Living and Fixed Dividing Cells and Correlation with MAP65-2 Localization

As stated before MAP65-3 is the largest of the nine members of the Arabidopsis MAP65 family, with an apparent molecular weight of ca. 80 kDa (e.g., Beck *et al.*, 2010). As it was described before it functions selectively during mitosis/cytokinesis, being reportedly localized at all relevant arrays (Caillaud *et al*., 2008). In accordance with the mode of interaction between MAP65 proteins and microtubules, MAP65-3 also forms coiled-coil homodimers and crosslinks antiparallel microtubules (Ho *et al.*, 2011). And similarly to MAP65-1 (and presumably MAP65-2), its interaction with microtubules is tuned through reversible phosphorylation by at least mitogen activated protein kinases (Beck *et al*., 2010; Sasabe *et al*., 2011).

In the present work, we studied eGFP-MAP65-3 fusion transformed in a native background (*A. thaliana* ecotype Columbia). Importantly the expression of the fusion was driven by the native promoter of the protein. As MAP65-3 is an exclusively mitotic/cytokinetic microtubule crosslinking protein and this was proven by observations of single expressor lines of the eGFP-MAP65-3 marker, showing restricted localization of MAP65-3 in the PPB (see Fig. 22A) and the midzone of the expanding phragmoplast (see Fig. 22B).

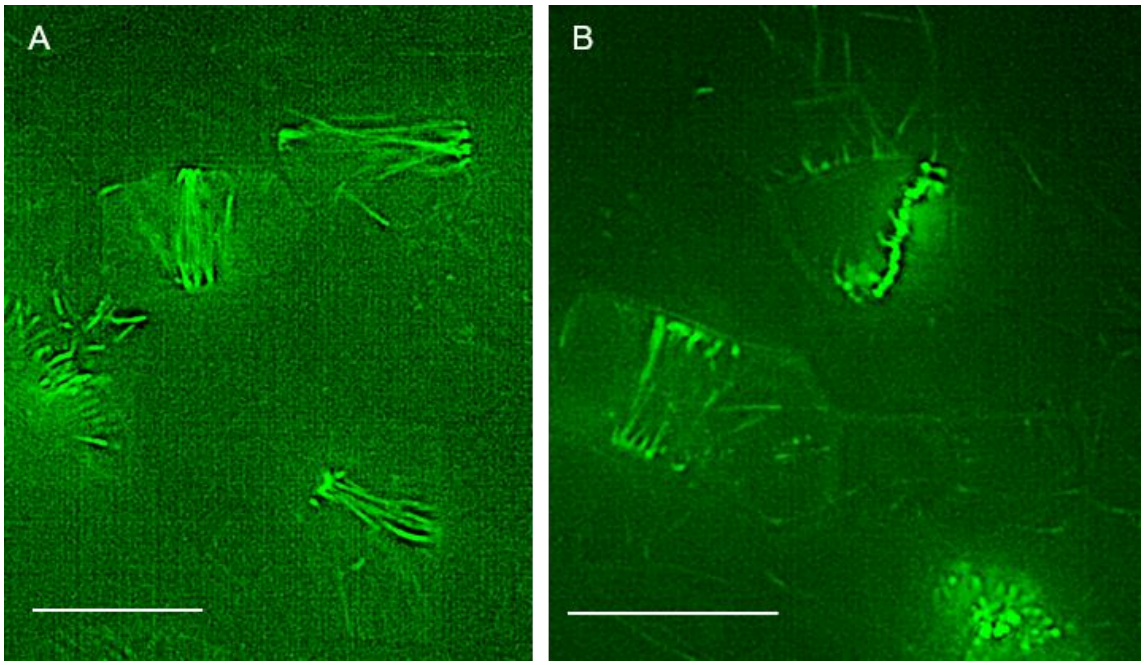

Figure 22. Conspicuous localization of MAP65-3 with PPBs and phragmoplasts in living, dividing cotyledon epidermal cells expressing an eGFP-MAP65-3 fusion protein. **A.** Localization at the PPB. **B.** Localization at the midplane of the phragmoplast, corresponding to the cell plate. Scale bars: 10 μm for all cases.

From the live imaging experiments of eGFP-MAP65-3, it became apparent that it exhibits a unique localization pattern compared to that of MAP65-2. Unfortunately, we were not able to document this in living seedlings expressing both microtubule and MAP65-3 markers and for this reason, we used the single eGFP-MAP65-3 expressor to colocalize both entities in appropriately immunolabeled root wholemounts. In this case, we observed that eGFP-MAP65-3 localization probed with an Atto488-conjugated anti-GFP nanobody, was restricted to the final stages of cell division and it was confined at the midzone not following the entire microtubule length as was previously shown for MAP65-2. In detail, the signal corresponding to eGFP-MAP65-3 appeared as a fairly broad zone during telophase which progressively narrowed as the interzonal microtubule system reorganized to the early phragmoplast.

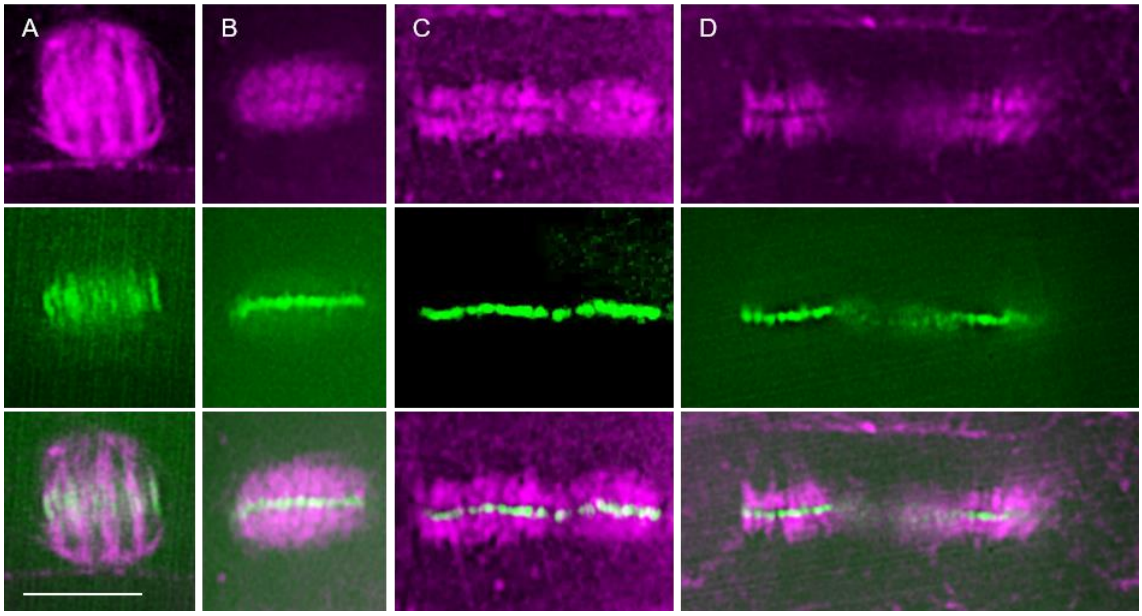

Figure 23. Progressive accumulation of MAP65-3 within telophase/cytokinetic microtubule structures, visualized in immunolabeled root wholemounts of *A. thaliana*. **A.** During telophase microtubules (top panel) form the interzonal system wherein MAP65-3 (middle, bottom panels) acquire a broad distribution. **B.** In early phragmoplast microtubules (top panel) form a conspicuous array with MAP65-3 (middle, bottom panels) is restricted to the midzone. **C.** During the onset of centrifugal expansion phragmoplast microtubules (top panel) and MAP65-3 (middle, bottom panels) occupy the entirety of the cell division plane. **D.** At later stages when phragmoplast approaches the parent wall, microtubules (top panel) and MAP65-3 become confined to the phragmoplast margins (middle, bottom panels). Scale bars: 5 µm for all cases. This figure is adapted from Vavrdová *et al.*, 2019.

The specific localization of MAP65-3 with developing cytokinetic arrays, was most prominently documented by means of three dimensional SIM of adequately immunolabeled wholemounts, proving that MAP65-3 follows the centrifugal expansion of the phragmoplast and becomes restricted to its margins (see Fig. 24).

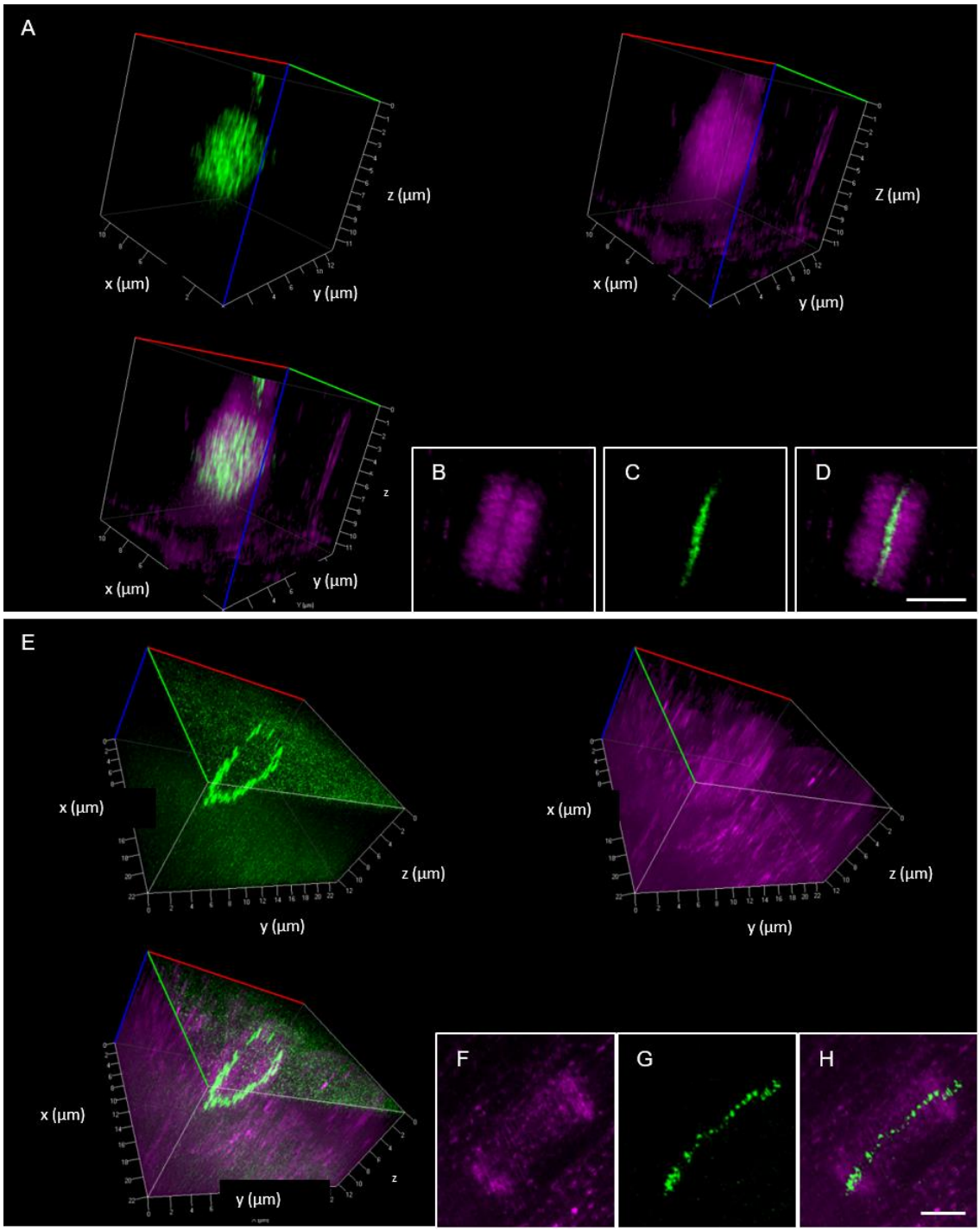

Figure 24. Three-dimensional rendering of MAP65-3 localization in *A. thaliana* root wholemounts. **A-D.** Early phragmoplast showing full occupancy of its area by both MAP65-3 and microtubules. **E-H.** Late phragmoplast showing the marginal restriction of both MAP65-3 and microtubules. Scale bars: 2 µm (B-D; F-H). This figure is adapted from Vavrdová *et al.*, 2019.

The trend of MAP65-3 localization during the progress of cytokinesis appears to be opposite to that described for MAP65-2. Based on our immunolocalization experiments, it seems that the MAP65-3 is trending towards a plus-end directed accumulation pattern, converging to the midplane and moving away from the poles. A recent study proved that

MAP65-3, interacts with PHRAGMOPLAST ORIENTING KINESIN 2 (POK2; Herrmann *et al*., 2018). POK2 belongs to the N-group of kinesin motor proteins exhibiting a motor domain at its N-terminus. All such kinesins (Kinesin-1 to Kinesin-12) are plus-end directed motors (Yamagishi and Yajima, 2018), and although directionality of POK2 has not been experimentally demonstrated, it might be assumed to follow the same trend of its class. These results taken together with the mode of eGFP-MAP65-2 localization in mitotic/cytokinetic systems, allow the assumption that microtubule bundling is a function facilitated by microtubule-based motor proteins with different directionality (Pringle *et al.*, 2013).

4.1.7 Differential Localization of MAP65-2 and MAP65-3

Previously published work has shown that MAP65 proteins may have redundant or unique functions during stages of cell growth requiring microtubule bundling. Based on the most studied members of the family, namely MAP65-1 and MAP65-3, it may be assumed that the mode of MAP65-based microtubule crosslinking, first requires the formation of MAP65 homodimers which then crosslink antiparallel adjacent microtubules, which represents a conserved mechanism among all eukaryotes expressing MAP65 homologues (e.g., Ho *et al*., 2011, 2012; Fache *et al.*, 2010; Subramanian *et al*., 2010).

The above presented results clearly show that MAP65-2 and MAP65-3 differentially localize within mitotic and cytokinetic microtubule structures and this was further sought in double Arabidopsis thaliana expressors of tagRFP-MAP65-2 and eGFP-MAP65-3.

The preprophase band is a microtubular structure wherein both proteins reside and for this reason, we addressed their possible colocalization (see Fig. 25).

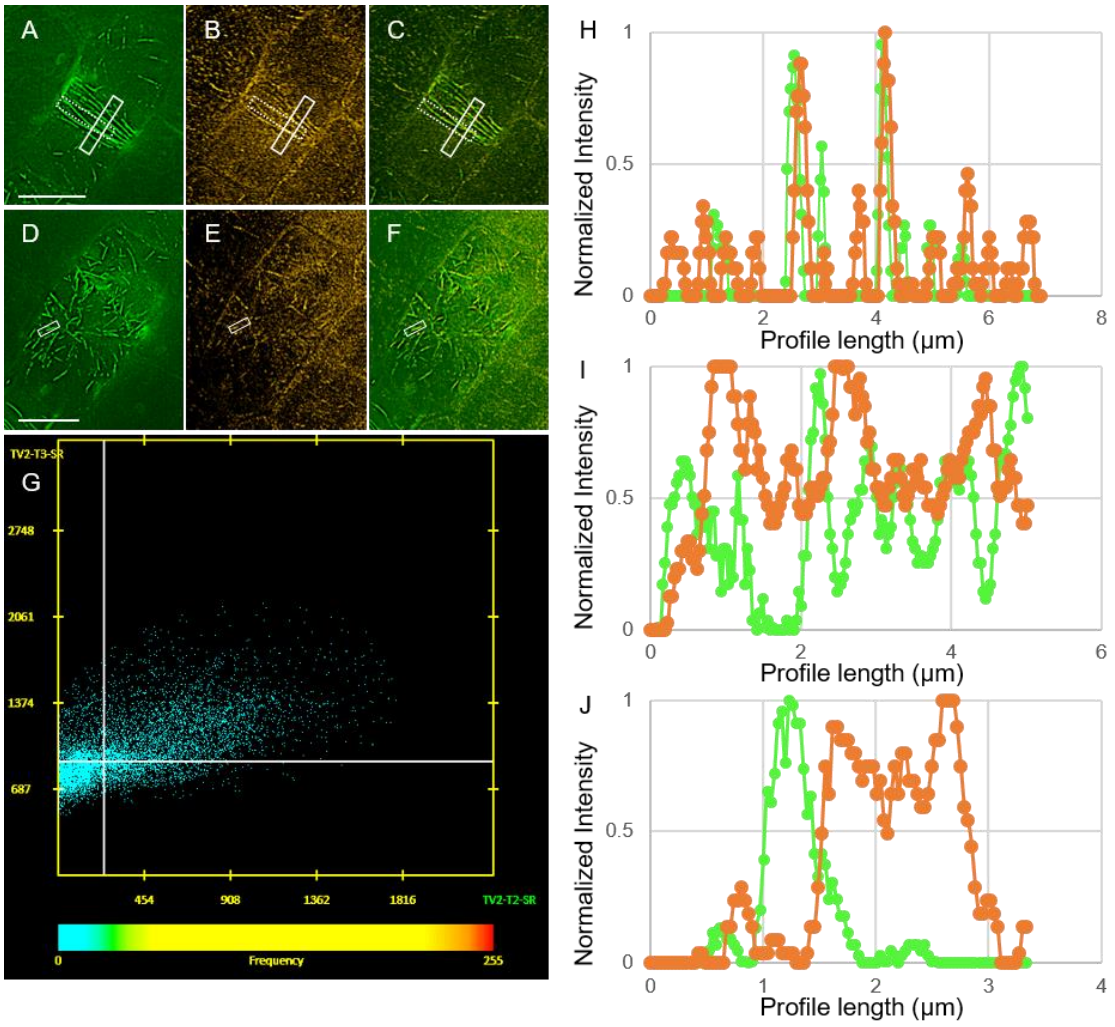

Figure 25. Colocalization of MAP65-2 and MAP65-3 within the PPB and radial-perinuclear post-cytokinetic microtubule arrays. **A-C.** Colocalization of MAP65-3 (A), MAP65-2 (B) and their overlay (C) within the PPB of a preprophase petiole epidermal cell coexpressing eGFP-MAP65-3 and tagRFP-MAP65-2. **D-F.** Colocalization of MAP65-3 (D), MAP65-2 (E) and their overlay (F) within postcytokinetic perinuclear microtubules. **G.** Scatterplot showing colocalization of both signals in the entire field of view in (A-C). **H.** Normalized fluorescence intensity profile of the fully outlined boxed area of (A-C) showing relative coincidence between the two signals. **I.** Normalized fluorescence intensity profile of the dotted outlined boxed area of (A-C) showing a relative absence of overlap between the two signals. **J.** Normalized fluorescence intensity profile of the fully outlined boxed area of (D-F) showing the relative absence of overlap between the two signals. Scale bars: 10 µm for all cases.

In both cases, we found that although both proteins are colocalized along straight lines corresponding to individual microtubules, or microtubule bundles (see Fig. 25A-F; H), their linear occupancy was nonoverlapping, either within PPBs (see Fig. 25I) or along post cytokinetic microtubules (see Fig. 25J).

Similarly, we followed the differential distribution of MAP65-2 and MAP65-3 in more advanced stages of cell division and particularly within the fully developed cytokinetic phragmoplast. In this case, we again employed immunofluorescence localization using

the anti-tagRFP antibody to probe tagRFP-MAP65-2, atto488-conjugated anti-GFP antibody to probe eGFP-MAP65-3 and anti-α-tubulin antibody to probe overall microtubule organization.

In this case, it was possible to verify the differential localization of MAP65-2 and MAP65-3 within the phragmoplast (see Fig. 26).

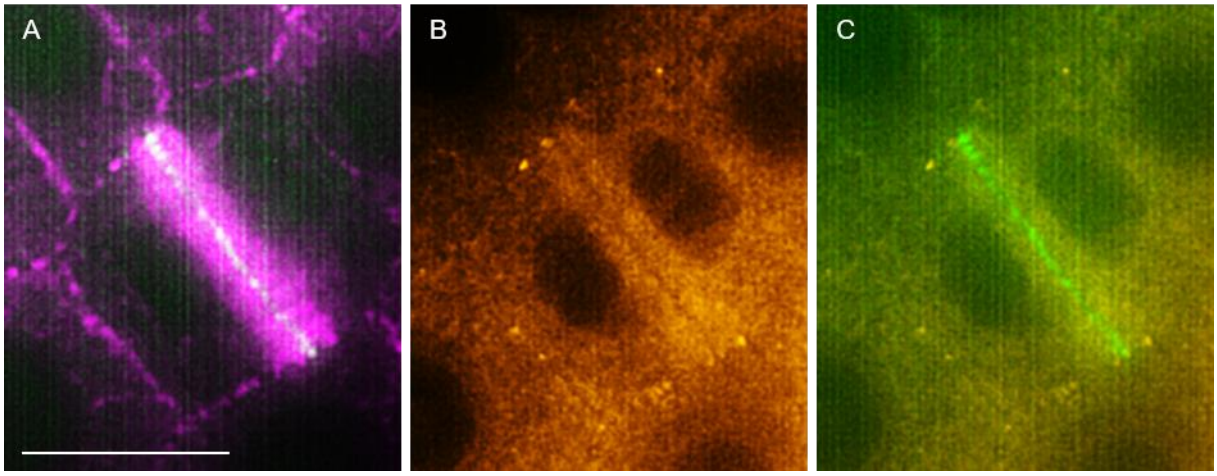

Figure 26. Differential localization of microtubules, tagRFP-MAP65-2, and eGFP-MAP65-3 in the phragmoplast of an immunolabeled root cytokinetic cell. Scale bar: 10 µm for all cases.

4.2 The *mpk4* Mutant Genotyping and Crossings

The genotyping of *mpk4* Arabidopsis mutants was used for selection of positive plants for subsequent crossings with transformant double line tagRFP-MAP65-2 x eGFP-TUA6. For *mpk6* Arabidopsis mutant selection and crossings, only control by observation of dwarf phenotype of heterozygous plant was used, homozygous mutants are lethal.

4.2.1 The *mpk4* Mutant Genotyping

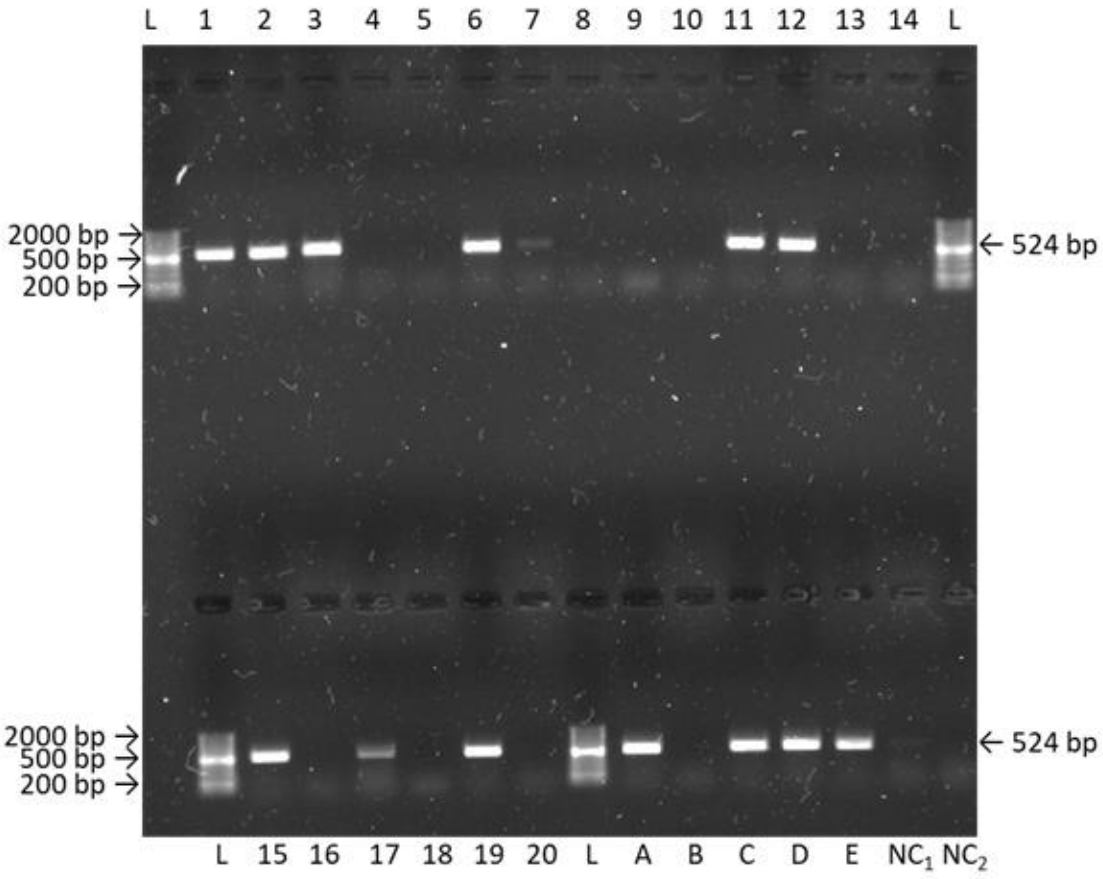

Figure 27. Electropherogram of PCR genotyping of Arabidopsis *mpk4* mutant. **1-20.** heterozygous *mpk4* mutant samples with the presence of band for 524 bp in some cases referring to the size of the insert of this mutant. **A-E.** Positive control – homozygous *mpk4* mutant samples with the presence of band for 524 bp in some cases referring to the size of the insert of this mutant. **NC_1 & NC_2.** Negative controls – samples of WT Arabidopsis, ecotype Col-0. **L.** 100 bp standard.

The results of genotyping have shown insert size 524 bp for Arabidopsis *mpk4* mutant. In heterozygous plants, phenotype is similar to WT Arabidopsis, ecotype Col-0 and can be easily confused, thus, genotyping is required for proving the presence of insert. The homozygous *mpk4* mutants exhibited above ground dwarf phenotype (e. g. Kosetsu *et al*., 2010) and were used as positive controls for genotyping. However, one of homozygous *mpk4* plants have not show band corresponding to the size of insert. There is some possibility that some contamination of different Arabidopsis mutant seed was in tube with *mpk4* mutant seeds and does not show desired band. Negative WT Arabidopsis controls have not shown desired band.

4.2.2 Crossings

The crossing experiment was done as option for *in vivo* studies of localization and dynamics of microtubules, MAP65-2, and MAP65-3 in MAPK mutants. The selection of F1 was done under conditions mentioned in chapter 3.5. However, the fluorescence of F1 plants was very weak or absent, which ensues that crossings were not successful.

5 Conclusion

Microtubule bundling is a major mechanism of biased microtubule organization during all stages of cell division, growth and differentiation. Based on the mechanism of function of the major microtubule bundling protein family of plants (MAP65), it is relying on the crosslinking of antiparallel microtubules (Ho *et al.*, 2011, 2012; Tulin *et al*., 2012; Gaillard *et al.*, 2008; Loïodice *et al.*, 2005). Proteins selected in the present study are tunable with microtubule affinities regulated through reversible phosphorylation at their carboxyl-terminal microtubule binding domain and this may explain their differential localization throughout cell division (Smertenko *et al.*, 2006; Mao *et al*., 2005; Sasabe *et al.*, 2011; Boruc *et al*., 2017).

What emerged however as an important research topic is the mechanism of their differential and non-overlapping coexistence within certain microtubule arrays such as the PPB, the telophase interzonal system and the expanding phragmoplast.

We believe that in this case different members of the MAP65 protein family developed unique interaction schemes with kinesin motors of different directionality. In plants the only documented interaction so far was proven between POK2 kinesin and MAP65-3, directing the latter to a plus-end directed fashion during phragmoplast formation and expansion, explaining the restriction of MAP65-3 at the cell plate plane shown herein and in other studies (Lin *et al*., 2019; Herrmann *et al*., 2018; Zhang *et al*., 2018; Steiner *et al*., 2016).

The role of MAP65-based microtubule bundling should be further sought in another cell division hallmark, namely the formation and the maturation of the PPB. The latter appears to be a collector of hind sights for cell division plane orientation (Martinez *et al*., 2018; Zhang et Dong, 2018) either be regulating mitotic spindle positioning (Komis *et al*., 20217; Schaefer *et al*., 2017) or by marking the future sites of daughter wall fusion with the parent outline (Rasmussen *et* Bellinger, 2018; Lipka *et al.*, 2015).

The attempts of crossing MAPK with transformants expressing cytoskeleton markers were unfortunately unsuccessful. However, these experiments will be repeated in the future but they are not included in this thesis.

By using advanced microscopies such as SIM and spinning disc and by employing different localization schemes it was possible to address the microtubule bundling process in various aspects of cell life ranging from growth and differentiation, to the regulation of cell division. Open questions regarding the role of microtubule bundling, the specific

mechanisms underlying it and the molecular partners specifying its spatiotemporal prerequisites are matters under investigation.

6 References

Ahmad F. J., Yu W., McNally F. J., Baas P. W. (1999): An essential role for katanin in severing microtubules in the neuron. *J Cell Biol* **145**, 305-315.

Al-Bassam J. and Corbett K. D. (2012): alpha-Tubulin acetylation from the inside out. *Proc Natl Acad Sci USA* **109**, 19515-6.

Alushin G. M., Lander G. C., Kellogg E. H., Zhang R., Baker D., Nogales E. (2014): High-resolution microtubule structures reveal the structural transitions in αβ-tubulin upon GTP hydrolysis. *Cell* **157**, 1117-29.

Ambrose J. C., Wateneys G. O. (2008): CLASP modulates microtubule-cortex interaction during self-organization of acentrosomal microtubules. *Mol. Biol. Cell* **19**, 4730-4737.

Antosch M., Schubert V., Holzinger P., Houben A., Grasser K. D. (2015): Mitotic lifecycle of chromosomal 3xHMG-box proteins and the role of their N-terminal domain in the association with rDNA loci and proteolysis. *New Phytol* **208**, 1067-77.

Arigovindan M., Sedat J. W., Agard D. A. (2012): Effect of depth dependent spherical aberrations in 3D structured illumination microscopy. *Opt Express* **20**, 6527-41.

Asada T., Kuriyama R. and Shibaoka H. (1997): TKRP125, a kinesin-related protein involved in the centrosome- independent organization of the cytokinetic apparatus in tobacco BY-2 cells. *Journal of Cell Science* **110**, 179-89.

Ban Y., Kobayashi Y., Hara T., Hamada T., Hashimoto T., Takeda S., Hattori T. (2013): α-tubulin is rapidly phosphorylated in response to hyperosmotic stress in rice and Arabidopsis. *Plant Cell Physiol* **54**, 848-58.

Banaei-Moghaddam A. M., Schubert V., Kumke K., Weiβ O., Klemme S., Nagaki K., Macas J., González-Sánchez M., Heredia V., Gómez-Revilla D., González-García M., Vega J. M., Puertas M. J., Houben A. (2012): Nondisjunction in favor of a chromosome: the mechanism of rye B chromosome drive during pollen mitosis. *Plant Cell* **24**, 4124-34.

Barlan K., Gelfand V. I. (2017): Microtubule-Based Transport and the Distribution, Tethering, and Organization of Organelles. *Cold Spring Harbor Perspectives in Biology* **9**, pii: a025817.

Beck M., Komis G., Müller J., Menzel D., Šamaj J. (2010): Arabidopsis homologs of nucleus- and phragmoplast-localized kinase 2 and 3 and mitogen-activated protein kinase 4 are essential for microtubule organization. *Plant Cell* **22**, 755-71.

Beck M., Komis G., Ziemann A., Menzel D., Šamaj J. (2011): Mitogen-activated protein kinase 4 is involved in the regulation of mitotic and cytokinetic microtubule transitions in *Arabidopsis thaliana*. *New Phytol* **189**, 1069-83.

Becker Y., Eaton C. J., Brasell E., May K. J., Becker M., Hassing B., Cartwright G. M., Reinhold L., and Scott B. (2015): The Fungal Cell-Wall Integrity MAPK Cascade Is Crucial for Hyphal Network Formation and Maintenance of Restrictive Growth of Epichloe festucae in Symbiosis With Lolium perenne. *Mol Plant Microbe Interact* **28**, 69-85.

Bekešová S., Komis G., Křenek P., Vyplelová P., Ovečka M., Luptovčiak I., Illés P., Kuchařová A., Šamaj J. (2015): Monitoring protein phosphorylation by acrylamide pendant Phos-Tag™ in various plants. *Front Plant Sci* **6**, 336.

Betzig E., Patterson G. H., Sougrat R., Lindwasser O. W., Olenych S., Bonifacino J. S., Davidson M. W., Lippincott-Schwartz J., Hess H. F. (2006): Imaging intracellular fluorescent proteins at nanometer resolution. *Science* **313**, 1642-5.

Bieling P., Telley I. A., Surrey T. (2010): A minimal midzone protein module controls formation and length of antiparallel microtubule overlaps. *Cell* **142**, 420-432.

Binarova P., Cenklova V., Prochazkova J., Doskocilova A., Volc J., Vrlik M. and Bogre L. (2006): Gamma-tubulin is essential for acentrosomal microtubule nucleation and coordination of late mitotic events in Arabidopsis. *Plant Cell* **18**, 1199-212.

Blume Y. B., Krasylenko Y. A., Demchuk O. M. and Yemets A. I. (2013): Tubulin tyrosine nitration regulates microtubule organization in plant cells. *Frontiers in plant science* **4**, 530.

Boruc J., Weimer A. K., Stoppin-Mellet V., Mylle E., Kosetsu K., Cedeño C., Jaquinod M., Njo M., De Milde L., Tompa P., Gonzalez N., Inzé D., Beeckman T., Vantard M., Van Damme D. (2017): Phosphorylation of MAP65-1 by Arabidopsis Aurora Kinases Is Required for Efficient Cell Cycle Progression. *Plant Physiol* **173**, 582-599.

Bratman S. V., Chang F. (2008): Mechanisms for maintaining microtubule bundles. *Trends Cell Biol* **18**, 580-586.

Braun M., Lansky Z., Fink G., Ruhnow F., Diez S., Janson M. E. (2011): Adaptive braking by Ase1 prevents overlapping microtubules from sliding completely apart. *Nat Cell Biol* **13**, 1259-64.

Caillaud M. C., Lecomte P., Jammes F., Quentin M., Pagnotta S., Andrio E., de Almeida Engler J., Marfaing N., Gounon P., Abad P., Favery B. (2008): MAP65-3 microtubule-associated protein is essential for nematode-induced giant cell ontogenesis in Arabidopsis. *Plant Cell* **20**, 423-37.

Chan J., Jensen C. G., Jensen L. C. W., Bush M., and Lloyd C. W. (1999): The 65-kDa carrot microtubule-associated protein forms regularly arranged filamentous cross-bridges between microtubules. *Proc. Natl. Acad. Sci. USA* **96**, 14931-14936.

Chan J., Mao G., Smertenko A., Hussey P. J., Naldrett M., Bottrill A., Lloyd C. W. (2003): Identification of a MAP65 isoform involved in directional expansion of plant cells. *FEBS Lett* **534**, 161-163.

Chan J., Rutten T., and Lloyd C. (1996): Isolation of microtubule-associated proteins from carrot cytoskeletons: a 120 kDa map decorates all four microtubule arrays and the nucleus. *Plant J* **10**, 251-259.

Chang H. Y., Smertenko A. P., Igarashi H., Dixon D. P., Hussey P. J. (2005): Dynamic interaction of NtMAP65-1a with microtubules in vivo. *J Cell Sci* **118**, 3195-201.

Chang-Jie J. and Sonobe S. (1993): Identification and preliminary characterization of a 65 kDa higher-plant microtubule-associated protein. *J. Cell Sci* **105**, 891-901.

Chen S., Jia H., Zhao H., Liu D., Liu Y., Liu B., Bauer S., Somerville C. R. (2016): Anisotropic Cell Expansion Is Affected through the Bidirectional Mobility of Cellulose Synthase Complexes and Phosphorylation at Two Critical Residues on CESA3. *Plant Physiology* **171**, 242-50.

Choi M. C., Raviv U., Miller H. P., Gaylord M. R., Kiris E., Ventimiglia D., Needleman D. J., Kim M. W., Wilson L., Feinstein S. C., Safinya C. R. (2009): Human microtubule-associated-protein tau regulates the number of protofilaments in microtubules: a synchrotron x-ray scattering study. *Biophys J* **97**, 519-527.

Combs C. A. (2010): Fluorescence microscopy: a concise guide to current imaging methods. *Curr Protoc Neurosci* Chapter **2**:Unit2.1.

Courtheoux T., Gay G., Gachet Y., Tournier S. (2009): Ase1/Prc1-dependent spindle elongation corrects merotely during anaphase in fission yeast. *J Cell Biol* **187**, 399-412.

Cyr R. J. (1991): Microtubule-associated proteins in higher plants. In: *The cytoskeletal basis of plant growth and form*. (Lloyd CW). Academic Press, London, 57–67.

Cyr R. J., Palevitz B. A. (1995): Organization of cortical microtubules in plant cells. *Curr Opin Cell Biol* **7**, 65-71.

de Keijzer J., Mulder B. M., and Janson M. E. (2014). Microtubule networks for plant cell division. *Syst Synth Biol* **8**, 187-194.

De S., Tsimounis A., Chen X. and Rotenberg S. A. (2014): Phosphorylation of alpha-tubulin by protein kinase C stimulates microtubule dynamics in human breast cells. *Cytoskeleton* **71**, 257-72.

Deeks M. J., Fendrych M., Smertenko A., Bell K. S., Oparka K., Cvrčková F., Žárský V., Hussey P. J. (2010): The plant formin AtFH4 interacts with both actin and microtubules, and contains a newly identified microtubule-binding domain. *J Cell Sci* **123**, 1209-15.

Deinum E. E., Tindemans S. H., Lindeboom J. J., Mulder B. M. (2017): How selective severing by katanin promotes order in the plant cortical microtubule array. *Proc Natl Acad Sci U S A.* **114**, 6942-6947.

Demmerle J., Innocent C., North A. J., Ball G., Müller M., Miron E., Matsuda A., Dobbie I. M., Markaki Y., Schermelleh L. (2017): Strategic and practical guidelines for successful structured illumination microscopy. *Nat Protoc* **12**, 988-1010.

Dhonukshe P., Gadella T. W. Jr. (2003): Alteration of microtubule dynamic instability during preprophase band formation revealed by yellow fluorescent protein-CLIP170 microtubule plus-end labeling. *Plant Cell* **15**, 597-611.

Dhonukshe P., Vischer N. and Gadella T. W., Jr. (2006): Contribution of microtubule growth polarity and flux to spindle assembly and functioning in plant cells. *Journal of Cell Science* **119**, 3193-205.

Diefenbach R. J., Mackay J. P., Armati P. J., Cunningham A. L. (1998): The C-terminal region of the stalk domain of ubiquitous human kinesin heavy chain contains the binding site for kinesin light chain. *Biochemistry* **37**, 16663-70.

Dimitrov A., Quesnoit M., Moutel S., Cantaloube I., Pous C., and Perez F. (2008): Detection of GTP-tubulin conformation in vivo reveals a role for GTP remnants in microtubule rescues. *Science* **322**, 1353-1356.

Dinarina A., Pugieux C., Corral M. M., Loose M., Spatz J., Karsenti E. and Nedelec F. (2009): Chromatin shapes the mitotic spindle. *Cell* **138**, 502-13.

Dixit R., and Cyr R. (2004): The cortical microtubule array: from dynamics to organization. *Plant Cell* **16**, 2546-2552.

Dryková D., Cenklová V., Sulimenko V., Volc J., Draber P. and Binarová P. (2003): Plant gamma-tubulin interacts with alphabeta-tubulin dimers and forms membrane-associated complexes. *Plant Cell* **15**, 465-80.

Endow S. A. and Waligora K. W. (1998): Determinants of kinesin motor polarity. *Science* **281**, 1200-1202.

Fache V., Gaillard J., Van Damme D., Geelen D., Neumann E., Stoppin-Mellet V., Vantard M. (2010): Arabidopsis kinetochore fiber-associated MAP65-4 cross-links microtubules and promotes microtubule bundle elongation. *Plant Cell* **22**, 3804-15.

Farache D., Emorine L., Haren L., Merdes A. (2018): Assembly and regulation of γ-tubulin complexes. *Open Biol* **8**, 170266.

Feng K., Liu F., Zou J., Xing G., Deng P., Song W., Tong W., and Nie X. (2016): Genome-Wide Identification, Evolution, and Co-expression Network Analysis of Mitogen-Activated Protein Kinase Kinase Kinases in Brachypodium distachyon. *Front Plant Sci* **7**, 1400.

Fiore R. S., Bayer V. E., Pelech S. L., Posada J., Cooper J. A., Baraban J. M. (1993): p42 mitogen-activated protein kinase in brain: prominent localization in neuronal cell bodies and dendrites. *Neuroscience* 55, 463-472.

Fišerová J., Efenberková M., Sieger T., Maninová M., Uhlířová J., Hozák P. (2017): Chromatin organization at the nuclear periphery as revealed by image analysis of structured illumination microscopy data. *J Cell Sci* **130**, 2066-2077.

Fitzgibbon J., Bell K., King E., Oparka K. (2010): Super-resolution imaging of plasmodesmata using three-dimensional structured illumination microscopy. *Plant Physiol* **153**, 1453-63.

Frickey T., Lupas A. N. (2004): Phylogenetic analysis of AAA proteins. J Struct Biol. 146(1-2):2-10.

Gaillard J., Neumann E., Van Damme D., Stoppin-Mellet V., Ebel C., Barbier E., Geelen D., Vantard M. (2008): Two microtubule-associated proteins of Arabidopsis MAP65s promote antiparallel microtubule bundling. *Mol Biol Cell* **19**, 4534-44.

Ghosh D., Dasgupta D., Guha A. (2012): Models, Regulations, and Functions of Microtubule Severing by Katanin. *ISRN Mol Biol* **2012**, 596289.

Griffiths J. S., Sola K., Kushwaha R., Lam P., Tateno M., Young R., Voiniciuc C., Dean G., Mansfield S. D., DeBolt S., Haughn G. W. (2015): Unidirectional movement of cellulose synthase complexes in Arabidopsis seed coat epidermal cells deposit cellulose involved in mucilage extrusion, adherence, and ray formation. *Plant Physiology* **168**, 502-20.

Gu Y., Deng Z., Paredez A. R., De Bolt S., Wang Z. Y., Somerville C. (2008): Prefoldin 6 is required for normal microtubule dynamics and organization in Arabidopsis. *Proc. Nat. Ac. Sci* **105**, 18064-18069.

Gu Y., Kaplinsky N., Bringmann M., Cobb A., Carroll A., Sampathkumar A., Baskin T. I., Persson S., Somerville C. R. (2010): Identification of a cellulose synthase-associated protein required for cellulose biosynthesis. *Proc. Natl. Acad. Sci*, **107**, 12866-12871.

Gunawardane R. N., Lizarraga S. B., Wiese C., Wilde A. and Zheng Y. (2000): gamma-Tubulin complexes and their role in microtubule nucleation. *Current Topics in Developmental Biology* **49**, 55-73.

Gunning B. E., Hardham A. R., Hughes J. E. (1978): Pre-prophase bands of microtubules in all categories of formative and proliferative cell division in Azolla roots. *Planta* **143**, 145-60.

Gustafsson M. G. (2000): Surpassing the lateral resolution limit by a factor of two using structured illumination microscopy. *J Microsc* **198**, 82-7.

Gutierrez R., Lindeboom J. J., Paredez A. R., Emons A. M., Ehrhardt D. W. (2009): Arabidopsis cortical microtubules position cellulose synthase delivery to the plasma membrane and interact with cellulose synthase trafficking compartments. *Nature Cell Biology* **11**, 797-806.

Hammond J. W., Cai D. and Verhey K. J. (2008): Tubulin modifications and their cellular functions. *Current Opinion in Cell Biology* **20**, 71-6.

Hardham A. R. and Gunning B. E. S. (1978): Structure of cortical microtubule arrays in plant cells. *J. Cell Biol* **77**, 14-34.

Hartman J. J., Mahr J., McNally K., Okawa K., Iwamatsu A., Thomas S., Cheesman S., Heuser J., Vale R. D., McNally F. J. (1998): Katanin, a microtubule-severing protein, is a novel AAA ATPase that targets to the centrosome using a WD40-containing subunit. *Cell* **93**, 277-87.

Hartman J. J., Vale R. D. (1999): Microtubule disassembly by ATP-dependent oligomerization of the AAA enzyme katanin. *Science* **286**, 782-785.

Hell S. W., Wichmann J. (1994): Breaking the diffraction resolution limit by stimulated emission: stimulated-emission-depletion fluorescence microscopy. *Opt Lett* **19**, 780-2.

Herrmann A., Livanos P., Lipka E., Gadeyne A., Hauser M. T., Van Damme D., Müller S. (2018): Dual localized kinesin-12 POK2 plays multiple roles during cell division and interacts with MAP65-3. *EMBO Rep* **19,** pii: e46085.

Higaki T., Kutsuna N., Sano T., Kondo N., Hasezawa S. (2010): Quantification and cluster analysis of actin cytoskeletal structures in plant cells: role of actin bundling in stomatal movement during diurnal cycles in Arabidopsis guard cells. *Plant J* **61**, 156-65.

Hino M., Kijima-Suda I., Nagai Y. and Hosoya H. (2003): Glycosylation of the alpha and beta tubulin by sialyloligosaccharides. *Zoological science* **20**, 709-15.

Hirokawa N., Noda Y., Tanaka Y., and Niwa S. (2009): Kinesin superfamily motor proteins and intracellular transport. *Nat Rev Mol Cell Biol* **10**, 682-696.

Hirokawa N., Pfister K. K., Yorifuji H., Wagner M. C., Brady S. T., Bloom G. S. (1989): Submolecular domains of bovine brain kinesin identified by electron microscopy and monoclonal antibody decoration. *Cell* **56**, 867-78.

Ho C. M., Hotta T., Guo F., Roberson R. W., Lee Y. R., Liu B. (2011): Interaction of antiparallel microtubules in the phragmoplast is mediated by the microtubule-associated protein MAP65-3 in Arabidopsis. *Plant Cell* **23**, 2909-23.

Ho C. M., Lee Y. R., Kiyama L. D., Dinesh-Kumar S. P., Liu B. (2012): Arabidopsis Microtubule-Associated Protein MAP65-3 Cross-Links Antiparallel Microtubules toward Their Plus Ends in the Phragmoplast via Its Distinct C-Terminal Microtubule Binding Domain. *The Plant Cell* **24**, 2071-2085.

Ho C. M., Lee Y. R., Kiyama L. D., Dinesh-Kumar S. P., Liu B. (2012): Arabidopsis microtubule-associated protein MAP65-3 cross-links antiparallel microtubules toward their plus ends in the phragmoplast via its distinct C-terminal microtubule binding domain. *Plant Cell* **24**, 2071-85.

Horio T., and Murata T. (2014). The role of dynamic instability in microtubule organization. *Front Plant Sci* **5**, 511.

Howard J., and Hyman A. A. (2007). Microtubule polymerases and depolymerases. *Curr Opin Cell Biol* **19**, 31-35.

Hussey P. J., Hawkins T. J., Igarashi H., Kaloriti D., Smertenko A. (2002): The plant cytoskeleton: recent advances in the study of the plant microtubule-associated proteins MAP-65, MAP-190 and the Xenopus MAP215-like protein, MOR1. *Plant Mol Biol* **50**, 915-924.

Jalmi S. K., and Sinha A. K. (2016): Functional Involvement of a Mitogen Activated Protein Kinase Module, OsMKK3-OsMPK7-OsWRK30 in Mediating Resistance against Xanthomonas oryzae in Rice. *Sci Rep* **6**, 37974.

Janson M. E., Loughlin R., Loïodice I., Fu C., Brunner D., Nédélec F. J., Tran P. T. (2007): Crosslinkers and motors organize dynamic microtubules to form stable bipolar arrays in fission yeast. *Cell* **128**, 357-68.

Jiang W., Jimenez G., Wells N. J., Hope T. J., Wahl G. M., Hunter T., Fukunaga R. (1998): PRC1: a human mitotic spindle-associated CDK substrate protein required for cytokinesis. *Mol Cell* **2**, 877-885.

Jinushi-Nakao S., Arvind R., Amikura R., Kinameri E., Liu A. W., Moore A. W. (2007): Knot/Collier and cut control different aspects of dendrite cytoskeleton and synergize to define final arbor shape. *Neuron* **56**, 963-978.

Juanes M. A., ten Hoopen R., Segal M. (2011): Ase1p phosphorylation by cyclin-dependent kinase promotes correct spindle assembly in *S. cerevisiae*. *Cell Cycle* **10**, 1988-97.

Jürgens G. (2005): Cytokinesis in higher plants. *Annu. Rev. Plant Biol* **56**, 281-299.

Kanai Y., Dohmae N., Hirokawa N. (2004): Kinesin transports RNA: isolation and characterization of an RNA-transporting granule. *Neuron* **43**, 513-25.

Kao Y. L., Deavours B. E., Phelps K. K., Walker R. A., Reddy A. S. (2000): Bundling of microtubules by motor and tail domains of a kinesin-like calmodulin-binding protein from Arabidopsis: regulation by Ca(2+)/Calmodulin. *Biochem Biophys Res Commun* **267**, 201-7.

Kikkawa M. (2013): Big steps toward understanding dynein. *The Journal of cell biology* **202**, 15-23.

Kimata Y., Higaki T., Kawashima T., Kurihara D., Sato Y., Yamada T., Hasezawa S., Berger F., Higashiyama T., Ueda M. (2016): Cytoskeleton dynamics control the first asymmetric cell division in Arabidopsis zygote. *Proc Natl Acad Sci U S A.* **113**, 14157-14162.

Kohoutová L., Kourová H., Nagy S. K., Volc J., Halada P., Meszaros T., Meskiene I., Bögre L., Binarová P. (2015): The Arabidopsis mitogen-activated protein kinase 6 is associated with γ-tubulin on microtubules, phosphorylates EB1c and maintains spindle orientation under nitrosative stress. *New Phytologist* **207**, 1061-74.

Kojo K. H., Higaki T., Kutsuna N., Yoshida Y., Yasuhara H., Hasezawa S. (2013): Roles of cortical actin microfilament patterning in division plane orientation in plants. *Plant Cell Physiol* **54**, 1491-503.

Kollman J. M., Merdes A., Mourey L., Agard D. A. (2011): Microtubule nucleation by γ-tubulin complexes. *Nat. Rev. Mol. Cell Biol* **12**, 709-721.

Kollman J. M., Polka J. K., Zelter A., Davis T. N., Agard D. A. (2010): Microtubule nucleating gamma-TuSC assembles structures with 13-fold microtubule-like symmetry. *Nature* **466**, 879-882.

Komis G., Luptovčiak I., Doskočilová A., Šamaj J. (2015c): Biotechnological aspects of cytoskeletal regulation in plants. *Biotechnology Advances* **33**, 1043-62.

Komis G., Luptovčiak I., Ovečka M., Samakovli D., Šamajová O., Šamaj J. (2017): Katanin Effects on Dynamics of Cortical Microtubules and Mitotic Arrays in *Arabidopsis thaliana* Revealed by Advanced Live-Cell Imaging. *Front Plant Sci* **8**, 866.

Komis G., Mistrik M., Šamajová O., Doskočilová A., Ovečka M., Illés P., Bartek J., Šamaj J. (2014): Dynamics and organization of cortical microtubules as revealed by superresolution structured illumination microscopy. *Plant Physiol* **165**, 129-48.

Komis G., Mistrik M., Šamajová O., Ovečka M., Bartek J., Šamaj J. (2015a): Superresolution live imaging of plant cells using structured illumination microscopy. *Nat Protoc* **10**, 1248-63.

Komis G., Novák D., Ovečka M., Šamajová O., Šamaj J. (2018): Advances in Imaging Plant Cell Dynamics. *Plant Physiol* **176**, 80-93.

Komis G., Šamajová O., Ovečka M., Šamaj J. (2015b): Super-resolution Microscopy in Plant Cell Imaging. *Trends Plant Sci* **20**, 834-843.

Kong, Z., Hotta, T., Lee, Y. R. J., Horio, T., Liu, B. (2010): The γ-tubulin complex protein GCP4 is required for organizing functional microtubule arrays in Arabidopsis thaliana. *Plant Cell*, **22**, 191-204.

Kopczak S. D., Haas N. A., Hussey P. J., Silflow C. D. and Snustad D. P. (1992): The small genome of Arabidopsis contains at least six expressed alpha-tubulin genes. *The Plant Cell* **4**, 539-47.

Korolev A. V., Buschmann H., Doonan J. H., Lloyd C. W. (2007): AtMAP70-5, a divergent member of the MAP70 family of microtubule-associated proteins, is required for anisotropic cell growth in Arabidopsis. *J Cell Sci* **120**, 2241-7.

Kosetsu K., Matsunaga S., Nakagami H., Colcombet J., Sasabe M., Soyano T., Machida Y. (2010): The MAP kinase MPK4 is required for cytokinesis in *Arabidopsis thaliana*. *Plant Cell* **22**, 3778-3790.

Kraus F., Miron E., Demmerle J., Chitiashvili T., Budco A., Alle Q., Matsuda A., Leonhardt H., Schermelleh L., Markaki Y. (2017): Quantitative 3D structured illumination microscopy of nuclear structures. *Nat Protoc* **12**, 1011-1028.

Kuo Y. W., Trottier O., Mahamdeh M., Howard J. (2019): Spastin is a dual-function enzyme that severs microtubules and promotes their regrowth to increase the number and mass of microtubules. *Proc Natl Acad Sci U S A.* **116**, 5533-5541.

Lancelle S. A., Callaham D. A. and Hepler P. K. (1986): A method for rapid freeze fixation of plant cells. *Protoplasma* **131**, 153-165.

Lansky Z., Braun M., Lüdecke A., Schlierf M., ten Wolde P. R., Janson M. E., Diez S. (2015): Diffusible crosslinkers generate directed forces in microtubule networks. *Cell* **160**, 1159-68.

Lawrence C. J., Dawe R. K., Christie K. R., Cleveland D. W., Dawson S. C., Endow S. A., Goldstein L. S., Goodson H. V., Hirokawa N., Howard J., Malmberg R. L., McIntosh J. R., Miki H., Mitchison T. J., Okada Y., Reddy A. S., Saxton W. M., Schliwa M., Scholey J. M., Vale R. D., Walczak C. E., Wordeman L. (2004): A standardized kinesin nomenclature. *J Cell Biol* **167**, 19-22.

Lee Y. R., Li Y., and Liu B. (2007): Two Arabidopsis phragmoplast-associated kinesins play a critical role in cytokinesis during male gametogenesis. *Plant Cell* **19**, 2595-2605.

Lee Y. R., Qiu W., Liu B. (2015): Kinesin Motors in Plants: from Subcellular Dynamics to Motility Regulation. *Current Opinion in Plant Biology* **28**, 120-126.

Li H., Mao T., Zhang Z., Yuan M. (2007): The AtMAP65-1 cross-bridge between microtubules is formed by one dimer. *Plant Cell Physiol* **48**, 866-74.

Li H., Sun B., Sasabe M., Deng X., Machida Y., Lin H., Julie Lee Y. R., Liu B. (2017): Arabidopsis MAP65-4 plays a role in phragmoplast microtubule organization and marks the cortical cell division site. New Phytol. **215**, 187-201.

Li H., Zeng X., Liu Z.Q., Meng, Q.T., Yuan, M. and Mao, T.L. (2009): Arabidopsis microtubule-associated protein AtMAP65-2 acts as a microtubule stabilizer. *Plant Mol. Biol* **69**, 313-324.

Li S., Lei L., Yingling Y. G., Gu Y. (2015): Microtubules and cellulose biosynthesis: the emergence of new players. *Current Opinion in Plant Biology* **28**, 76-82.

Li Y., Shen Y., Cai C., Zhong C., Zhu L., Yuan M., and Ren H. (2010): The type II Arabidopsis formin14 interacts with microtubules and microfilaments to regulate cell division. *Plant Cell* **22**, 2710-2726.

Lin F., Krishnamoorthy P., Schubert V., Hause G., Heilmann M., Heilmann I. (2019): A dual role for cell plate-associated PI4Kβ in endocytosis and phragmoplast dynamics during plant somatic cytokinesis. *EMBO J.* **38**, pii: e100303.

Lindeboom J. J., Nakamura M., Hibbel A., Shundyak K., Gutierrez R., Ketelaar T., Emons A. M., Mulder B. M., Kirik V., Ehrhardt D. W. (2013): A mechanism for reorientation of cortical microtubule arrays driven by microtubule severing. *Science* **342**:1245533.

Lipka E., Gadeyne A., Stockle D., Zimmermann S., De Jaeger G., Ehrhardt D. W., Kirik V., Van Damme D., and Muller S. (2014): The Phragmoplast-Orienting Kinesin-12 Class Proteins Translate the Positional Information of the Preprophase Band to Establish the Cortical Division Zone in *Arabidopsis thaliana. Plant Cell* **26**, 2617-2632.

Lipka E., Herrmann A., Mueller S. (2015): Mechanisms of plant cell division. *Wiley Interdiscip Rev Dev Biol* **4**, 391-405.

Liu B., Joshi H. C., Wilson T. J., Silflow C. D., Palevitz B. A., Snustad D. P. (1994): gamma-Tubulin in Arabidopsis: gene sequence, immunoblot, and immunofluorescence studies. *Plant Cell* **6**, 303-314.

Loïodice I., Staub J., Setty T. G., Nguyen N. P., Paoletti A., Tran P. T. (2005): Ase1p organizes antiparallel microtubule arrays during interphase and mitosis in fission yeast. *Mol Biol Cell* **16**, 1756-68.

Lucas J. R., Courtney S., Hassfurder M., Dhingra S., Bryant A., Shaw S. L. (2011): Microtubule-associated proteins MAP65–1 and MAP65–2 positively regulate axial cell growth in etiolated Arabidopsis hypocotyls. *Plant Cell* **23**, 1889-1903.

Lucas J. R., Shaw S. L. (2012): MAP65-1 and MAP65-2 promote cell proliferation and axial growth in Arabidopsis roots. *Plant J* **71**, 454-63.

Ma Q., Sun J., and Mao T. (2016): Microtubule bundling plays a role in ethylene-mediated cortical microtubule reorientation in etiolated Arabidopsis hypocotyls. *J Cell Sci* **129**, 2043-2051.

Mace A., Wang W. (2015): Modelling the role of catastrophe, crossover and katanin-mediated severing in the self-organisation of plant cortical microtubules. *IET Syst Biol* **9**, 277-84.

Magiera M. M., Janke C. (2014): Post-translational modifications of tubulin. *Curr Biol* **24**, R351-4.
Mandelkow E. M., Drewes G., Biernat J., Gustke N., Van Lint J., Vandenheede J. V., Mandelkow E. (1992): Glycogen synthase kinase-3 and the Alzheimer-like state of microtubule-associated protein tau. *FEBS letters* **314**, 315-321.
Mandelkow E. M., Mandelkow E. and Milligan R. A. (1991): Microtubule dynamics and microtubule caps: a time-resolved cryo-electron microscopy study. *Journal of Cell Biology* **114**, 977-91.
Mandelkow E., and Mandelkow E. M. (2002): Kinesin motors and disease. *Trends in Cell Biology* **12**, 585-591.
Mao G., Chan J., Calder G., Doonan J. H., Lloyd C. W. (2005): Modulated targeting of GFP-AtMAP65-1 to central spindle microtubules during division. *Plant J* **43**, 469-78.
Mao T., Jin L., Li H., Liu B., Yuan M. (2005): Two Microtubule-Associated Proteins of the Arabidopsis MAP65 Family Function Differently on Microtubules. *Plant Physiology* **138**, 65-662.
Marangoni P., Charles C., Tafforeau P., Laugel-Haushalter V., Joo A., Bloch-Zupan A., Klein O. D., and Viriot L. (2015): Phenotypic and evolutionary implications of modulating the ERK-MAPK cascade using the dentition as a model. *Sci Rep* **5**, 11658.
Marcus A. I., Moore R. C., Cyr R. J. (2001): The role of microtubules in guard cell function. *Plant Physiol* **125**, 387-95.
Martinez P., Allsman L. A., Brakke K. A., Hoyt C., Hayes J., Liang H., Neher W., Rui Y., Roberts A. M., Moradifam A., Goldstein B., Anderson C. T., Rasmussen C. G. (2018): Predicting Division Planes of Three-Dimensional Cells by Soap-Film Minimization. *Plant Cell* **30**, 2255-2266.
Martinez P., Luo A., Sylvester A., Rasmussen C. G. (2017): Proper division plane orientation and mitotic progression together allow normal growth of maize. *Proc Natl Acad Sci U S A.* **114**, 2759-2764.
Marx A., Muller J., and Mandelkow E. (2005): The structure of microtubule motor proteins. *Adv Protein Chem* **71**, 299-344.
McNally F. J., Okawa K., Iwamatsu A., Vale R. D. (1996): Katanin, the microtubule-severing ATPase, is concentrated at centrosomes. *J Cell Sci* **109**, 561-7.
McNally F. J., Vale R. D. (1993): Identification of katanin, an ATPase that severs and disassembles stable microtubules. *Cell* **75**, 419-429.
McNally K., Audhya A., Oegema K., McNally F. J. (2006): Katanin controls mitotic and meiotic spindle length. *J Cell Biol* **175**, 881-891.
Means A. R., Tash J. S., Chafouleas J. G., Lagace L., Guerriero V. (1982): Regulation of the cytoskeleton by Ca2+-calmodulin and cAMP. *Annals of the New York Academy of Science* **383**, 69-84.
Meng Q., Du J., Li J., Lu X., Zeng X., Yuan M. and Mao T. (2010): Tobacco microtubule-associated protein, MAP65-1c, bundles and stabilizes microtubules. *Plant Mol. Biol* **74**, 537-547.
Miart F., Desprez T., Biot E., Morin H., Belcram K., Höfte H., Gonneau M., Vernhettes S. (2014): Spatio-temporal analysis of cellulose synthesis during cell plate formation in Arabidopsis. *Plant Journal* **77**, 71-84.
Miki H., Okada Y., and Hirokawa N. (2005): Analysis of the kinesin superfamily: insights into structure and function. *Trends in Cell Biology* **15**, 467-476.
Miki T., Naito H., Nishina M., Goshima G. (2014): Endogenous localizome identifies 43 mitotic kinesins in plant cell. *Proc Natl Acad Sci U S A.* **111**, 1053-1061.
Mitchison T., Kirschner M. (1984): Dynamic instability of microtubule growth. *Nature* **312**, 237-242.
Mitchison T. J, Salmon E. D. (2001): Mitosis: a history of division. *Nat. Cell. Biol* **3**, E17–E21.
Mitra T., Menon S. N., Sinha S. (2018): Emergent memory in cell signaling: Persistent adaptive dynamics in cascades can arise from the diversity of relaxation time-scales. *Sci Rep.* **8**, 13230.
Mollinari C., Kleman J. P., Jiang W., Schoehn G., Hunter T. and Margolis R. L. (2002): PRC1 is a microtubule binding and bundling protein essential to maintain the mitotic spindle midzone. *J. Cell Biol* **157**, 1175-1186.
Müller S., Fuchs E., Ovečka M., Wysocka-Diller J., Benfey P. N., Hauser M. T. (2002): Two new loci, PLEIADE and HYADE, implicate organ-specific regulation of cytokinesis in Arabidopsis. *Plant Physiol* **130**, 312-24.

Müller S., Smertenko A., Wagner V., Heinrich M., Hussey P. J., Hauser M.T. (2004): The plant microtubule associated protein, AtMAP65-3/PLE, is essential for cytokinetic phragmoplast function. *Curr. Biol* **14**, 412-417.

Muller-Reichert T., Chretien D., Severin F., and Hyman A. A. (1998): Structural changes at microtubule ends accompanying GTP hydrolysis: information from a slowly hydrolyzable analogue of GTP, guanylyl (alpha, beta)methylenediphosphonate. *Proc Natl Acad Sci U S A.* **95**, 3661-6.

Murata T. and Hasebe M. (2007): Microtubule-dependent microtubule nucleation in plant cells. *Journal of Plant Research* **120**, 73-8.

Murata T., Sano T., Sasabe M., Nonaka S., Higashiyama T., Hasezawa S., Machida Y. and Hasebe M. (2013): Mechanism of microtubule array expansion in the cytokinetic phragmoplast. *Nature Communications* **4**, 1967.

Murata T., Sonobe S., Baskin T. I., Hyodo S., Hasezawa S., Nagata T., Horio, T and Hasebe M. (2005): Microtubule-dependent microtubule nucleation based on recruitment of gamma-tubulin in higher plants. *Nature Cell Biology* **7**, 961-8.

Nagy N., Goldstein A. M. (2017): Enteric nervous system development: A crest cell's journey from neural tube to colon. *Seminars in Cell and Developmental Biology* **66**, 94-106.

Nakamura M., Ehrhardt D. W., Hashimoto T. (2010): Microtubule and katanin-dependent dynamics of microtubule nucleation complexes in the acentrosomal Arabidopsis cortical array. *Nat Cell Biol* **12**, 1064-1070.

Naylor R. W., Davidson A. J. (2017): Pronephric tubule formation in zebrafish: morphogenesis and migration. *Journal of Pediatric Nephrology* **32**, 211-216.

Nogami A. and Mineyuki Y. (1999): Loosening of a preprophase band of microtubules in onion (Allium cepa L.) root tip cells by kinase inhibitors. *Cell Structure and Function* **24**, 419-24.

Oakley B. R., Oakley C. E., Yoon Y. and Jung M. K. (1990): Gamma-tubulin is a component of the spindle pole body that is essential for microtubule function in *Aspergillus nidulans*. *Cell* **61**, 1289-301.

Ogawa T., Nitta R., Okada Y., Hirokawa N. (2004): A common mechanism for microtubule destabilizers-M type kinesins stabilize curling of the protofilament using the class-specific neck and loops. *Cell* **116**, 591-602.

Ovečka M., Takáč T., Komis G., Vadovič P., Bekešová S., Doskočilová A., Šamajová V., Luptovčiak I., Šamajová O., Schweighofer A., Meskiene I., Jonak C., Křenek P., Lichtscheidl I., Škultéty L., Hirt H., Šamaj J. (2014): Salt-induced subcellular kinase relocation and seedling susceptibility caused by overexpression of Medicago SIMKK in Arabidopsis. *J Exp Bot* **65**, 2335-2350.

Ovečka M., von Wangenheim D., Tomančák P., Šamajová O., Komis G., Šamaj J. (2018): Multiscale imaging of plant development by light-sheet fluorescence microscopy. *Nat Plants* **4**, 639-650.

Paganelli L., Caillaud M.-C., Quentin M., Damiani I., Govetto B., Lecomte P., Karpov P. A., Abad P., Chabouté M.-E. and Favery B. (2015): Three BUB1 and BUBR1/MAD3-related spindle assembly checkpoint proteins are required for accurate mitosis in Arabidopsis. *New Phytol* **205**, 202-215.

Paluh J. L., Nogales E., Oakley B. R., McDonald K., Pidoux A. L., and Cande W. Z. (2000): A mutation in gamma-tubulin alters microtubule dynamics and organization and is synthetically lethal with the kinesin-like protein pkl1p. *Molecular Biology of the Cell* **11**, 1225-39.

Panteris E., Adamakis I. D., Daras G., Hatzopoulos P., Rigas S. (2013): Differential responsiveness of cortical microtubule orientation to suppression of cell expansion among the developmental zones of *Arabidopsis thaliana* root apex. *PLoS One* **8**, e82442.

Panteris E., Adamakis I. D., Tzioutziou N. A. (2009): Abundance of actin filaments in the preprophase band and mitotic spindle of brick1 Zea mays mutant. *Protoplasma* **236**, 103-6

Paredez A. R., Somerville C. R. and Ehrhardt D. W. (2006): Visualization of cellulose synthase demonstrates functional association with microtubules. *Science* **312**, 1491-5.

Petrovská B., Jerábková H., Kohoutová L., Cenklová V., Pochylová Ž., Gelová Z., Kocárová G., Váchová L., Kurejová M., Tomastíková E., Binarová P. (2013): Overexpressed TPX2 causes ectopic formation of microtubular arrays in the nuclei of acentrosomal plant cells. *J Exp Bot* **64**, 4575-4587.

Petry S., Vale R.D. (2015): Microtubule nucleation at the centrosome and beyond. *Nat. Cell Biol* **17**, 1089-1093.

Pickett-Heaps J. D. and Northcote D. H. (1966): Organization of microtubules and endoplasmic reticulum during mitosis and cytokinesis in wheat meristems. *Journal of Cell Science* **1**, 109-20.

Piedra F. A., Kim T., Garza E. S., Geyer E. A., Burns A., Ye X., and Rice L. M. (2016): GDP-to-GTP exchange on the microtubule end can contribute to the frequency of catastrophe. *Mol Biol Cell* **27**, 3515-3525.

Pincus D., Ryan C. J., Smith R. D., Brent R., Resnekov O. (2013): Assigning quantitative function to post-translational modifications reveals multiple sites of phosphorylation that tune yeast pheromone signaling output. *PLoS One* **8**, e56544.

Pleskot R., Li J., Zarský V., Potocký M., Staiger C. J. (2013): Regulation of cytoskeletal dynamics by phospholipase D and phosphatidic acid. *Trends in Plant Science* **18**, 496-504.

Portran D., Zoccoler M., Gaillard J., Stoppin-Mellet V., Neumann E., Arnal I., Martiel J. L., Vantard M. (2013): MAP65/Ase1 promote microtubule flexibility. *Mol Biol Cell* **24**, 1964-73

Prabakaran S., Lippens G., Steen H., Gunawardena J. (2012): Post-translational modification: nature's escape from genetic imprisonment and the basis for dynamic information encoding. *Wiley Interdisciplinary Reviews: Systems Biology and Medicine* **4**, 565-83.

Pringle J., Muthukumar A., Tan A., Crankshaw L., Conway L., Ross J. L. (2013): Microtubule organization by kinesin motors and microtubule crosslinking protein MAP65. *J Phys Condens Matter* **25**, 374103.

Rasi M. Q., Parker J. D. K., Feldman J. L., Marshall W. F., Quarmby L. M. (2009): Katanin knockdown supports a role for microtubule severing in release of basal bodies before mitosis in Chlamydomonas. *Mol Biol Cell* **20**, 379–388.

Rasmussen C. G., Bellinger M. (2018): An overview of plant division-plane orientation. *New Phytol.* **219**, 505-512.

Rasmussen C.G., Wright A. J., and Muller S. (2013): The role of the cytoskeleton and associated proteins in determination of the plant cell division plane. *Plant J* **75**, 258-269.

Ray L. B., Sturgill T. W. (1988): Insulin-stimulated microtubule-associated protein kinase is phosphorylated on tyrosine and threonine in vivo. *Proc. Nat. Ac. Sci* **85**, 3753-3757.

Raynaud-Messina B. and Merdes A. (2007): Gamma-tubulin complexes and microtubule organization. *Current Opinion in Cell Biology* **19**, 24-30.

Ribeiro T., Marques A., Novák P., Schubert V., Vanzela A. L., Macas J., Houben A., Pedrosa-Harand A. (2017): Centromeric and non-centromeric satellite DNA organisation differs in holocentric Rhynchospora species. *Chromosoma* **126**, 325-335.

Rice L. M., Montabana E. A. and Agard D. A. (2008): The lattice as allosteric effector: structural studies of alphabeta- and gamma-tubulin clarify the role of GTP in microtubule assembly. *Proc Natl Acad Sci U S A.* **105**, 5378-83.

Richardson D. N., Simmons M. P., and Reddy A. S. (2006): Comprehensive comparative analysis of kinesins in photosynthetic eukaryotes. *BMC Genomics* **7**, 18.

Robert H. S., Crhak Khaitova L., Mroue S., Benkova E. (2015): The importance of localized auxin production for morphogenesis of reproductive organs and embryos in Arabidopsis. *Journal of Experimental Botany* **66**, 5029-42.

Rochlin M. W., Dailey M. E. and Bridgman P. C. (1999): Polymerizing microtubules activate site-directed F-actin assembly in nerve growth cones. *Molecular Biology of the Cell* **10**, 2309-2327.

Rodríguez-Milla M. A., Salinas J. (2009): Prefoldins 3 and 5 play an essential role in Arabidopsis tolerance to salt stress. *Mol. Plant* **2**, 526-534.

Roll-Mecak A., McNally F. J. (2010) Microtubule-severing enzymes. Curr Opin Cell Biol. **22**, 96-103.

Roll-Mecak A., Vale R. D. (2008): Structural basis of microtubule severing by the hereditary spastic paraplegia protein spastin. *Nature* **451**, 363-367.

Roostalu J., Surrey T. (2017): Microtubule nucleation: beyond the template. *Nat. Rev. Mol. Cell Biol* **91**, 321.

Rust M. J., Bates M., Zhuang X. (2006): Sub-diffraction-limit imaging by stochastic optical reconstruction microscopy (STORM). *Nat Methods* **3**, 793-5.

Šamaj J., Baluška F., Hirt H. (2004): From signal to cell polarity: mitogen-activated protein kinases as sensors and effectors of cytoskeleton dynamicity. *J. Exp. Bot* **55**, 189-198.
Sanchez A. D., Feldman J. L. (2016): Microtubule-organizing centers: from the centrosome to non-centrosomal sites. *Curr. Opin. Cell Biol* **44**, 93-101.
Sasabe M., Kosetsu K., Hidaka M., Murase A., Machida Y. (2011): Arabidopsis thaliana MAP65-1 and MAP65-2 function redundantly with MAP65-3/PLEIADE in cytokinesis downstream of MPK4. *Plant Sign. Beh* **6**, 743-747.
Sato M., Toda T. (2010): Space shuttling in the cell: nucleocytoplasmic transport and microtubule organization during the cell cycle. *Nucleus* **1**, 231-236.
Sauer M., Paciorek T., Benkova E., Friml J. (2006): Immunocytochemical techniques for whole-mount *in situ* protein localization in plants. *Nature Protocols* **1**, 98-103.
Schaefer E., Belcram K., Uyttewaal M., Duroc Y., Goussot M., Legland D., Laruelle E., de Tauzia-Moreau M. L., Pastuglia M., Bouchez D. (2017): The preprophase band of microtubules controls the robustness of division orientation in plants. *Science* **356**, 186-189.
Schmid V. J., Cremer M., Cremer T. (2017): Quantitative analyses of the 3D nuclear landscape recorded with super-resolved fluorescence microscopy. *Methods* **123**, 33-46.
Schubert V. (2014): RNA polymerase II forms transcription networks in rye and Arabidopsis nuclei and its amount increases with endopolyploidy. *Cytogenet Genome Res* **143**, 69-77.
Schubert V. (2017): Super-resolution Microscopy - Applications in Plant Cell Research. *Front Plant Sci* **8**, 531.
Schubert V., Lermontova I., Schubert I. (2013): The Arabidopsis CAP-D proteins are required for correct chromatin organisation, growth and fertility. *Chromosoma* **122**, 517-33.
Schubert V., Lermontova I., Schubert I. (2014): Loading of the centromeric histone H3 variant during meiosis-how does it differ from mitosis? *Chromosoma* **123**, 491-7.
Schuyler S. C., Liu J. Y., and Pellman D. (2003): The molecular function of Ase1p: evidence for a MAP-dependent midzone-specific spindle matrix. Microtubule-associated proteins. *J Cell Biol* **160**, 517-528.
Seagull R. W. and Heath I. B. (1980): The organization of cortical microtubule arrays in the radish root hair. *Protoplasma* **103**, 205-229.
Shao W., Dong J. (2016): Polarity in plant asymmetric cell division: Division orientation and cell fate differentiation. *Developmental Biology* **419**, 121-131.
Shaw S. L. (2013): Reorganization of the plant cortical microtubule array. *Curr Opin Plant Biol* **16**, 693-697.
Shaw S. L., Kamyar R., Ehrhardt D. W. (2003): Sustained microtubule treadmilling in Arabidopsis cortical arrays. *Science* **300**, 1715-8.
Sherwood N. T., Sun Q., Xue M., Zhang B., Zinn K. (2004): Drosophila spastin regulates synaptic microtubule networks and is required for normal motor function. *PLoS Biol* **2**, e429.
Smékalová V., Doskočilová A., Komis G., and Šamaj J. (2014): Crosstalk between secondary messengers, hormones and MAPK modules during abiotic stress signalling in plants. *Biotechnology Advances* **32**, 2-11.
Smékalová V., Luptovčiak I., Komis G., Šamajová O., Ovečka M., Doskočilová A., Takáč T., Vadovič P., Novák O., Pechan T., Ziemann A., Kosutová P., Šamaj J. (2014): Involvement of YODA and mitogen activated protein kinase 6 in Arabidopsis post-embryogenic root development through auxin up-regulation and cell division plane orientation. *New Phytologist* **203**, 1175-93.
Smertenko A. P., Chang H. Y., Sonobe S., Fenyk S. I., Weingartner M., Bögre L., Hussey P. J. (2006): Control of the AtMAP65-1 interaction with microtubules through the cell cycle. *Journal of Cell Scienc*e **119**, 3227-37.
Smertenko A. P., Chang H. Y., Wagner V., Kaloriti D., Fenyk S., Sonobe S., Lloyd C., Hauser M. T., Hussey P. J. (2004): The Arabidopsis microtubule-associated protein AtMAP65-1: molecular analysis of its microtubule bundling activity. *Plant Cell* **16**, 2035-47.
Smertenko A. P., Kaloriti D., Chang H. Y., Fiserová J., Opatrný Z., Hussey P. J. (2008): The C-terminal variable region specifies the dynamic properties of Arabidopsis microtubule-associated protein MAP65 isotypes. *Plant Cell* **20**, 3346-58.

Smertenko A., Saleh N., Igarashi H., Mori H., Hauser-Hahn I., Jiang C. J., Sonobe S., Lloyd C. W. and Hussey P. J. (2000): A new class of microtubule associated proteins in plants. *Nat. Cell Biol* **2**, 750-753.

Smith L. G. (2001): Plant cell division: building walls in the right places. *Nat. Rev. Mol. Cell Bioll* **2**, 33-9.

Šnaurová R. (2017): Role of GSK inhibitors on mitotic progression of plants, bachelor thesis, UPOL, Czech Republic.

Snustad D. P., Haas N. A., Kopczak S. D. and Silflow C. D. (1992): The small genome of Arabidopsis contains at least nine expressed beta-tubulin genes. *Plant Cell* **4**, 549-56.

Söllner R., Glässer G., Wanner G., Somerville C. R., Jürgens G., Assaad F. F. (2002): Cytokinesis-defective mutants of Arabidopsis. *Plant Physiol* **129**, 678-90.

Staehelin L. A., Hepler P. K. (1996): Cytokinesis in higher plants. *Cell* **84**, 821-4.

Steiner A., Rybak K., Altmann M., McFarlane H. E., Klaeger S., Nguyen N., Facher E., Ivakov A., Wanner G., Kuster B., Persson S., Braun P., Hauser M. T., Assaad F. F. (2016): Cell cycle-regulated PLEIADE/AtMAP65-3 links membrane and microtubule dynamics during plant cytokinesis. *The Plant Journal* **88**, 531-541.

Stoppin V., Vantard M., Schmit A. C., and Lambert A. M. (1994): Isolated Plant Nuclei Nucleate Microtubule Assembly: The Nuclear Surface in Higher Plants Has Centrosome-like Activity. *The Plant Cell* **6**, 1099-1106.

Stoppin-Mellet V., Fache V., Portran D., Martiel J.-L., Vantard M. (2013): MAP65 Coordinate Microtubule Growth during Bundle Formation. *PLoS ONE* **8**, e56808.

Subramanian R., Wilson-Kubalek E. M., Arthur C. P., Bick M. J., Campbell E. A., Darst S. A., Milligan R. A., Kapoor T. M. (2010): Insights into antiparallel microtubule crosslinking by PRC1, a conserved nonmotor microtubule binding protein. *Cell* **142**, 433-43.

Sulimenko V., Hájková Z., Klebanovych A., Dráber P. (2017): Regulation of microtubule nucleation mediated by γ-tubulin complexes. *Protoplasma* **254**, 1-13.

Szczurek A., Contu F., Hoang A., Dobrucki J., Mai S. (2018): Aqueous mounting media increasing tissue translucence improve image quality in Structured Illumination Microscopy of thick biological specimen. *Sci Rep* **8**, 13971.

Takahashi Y., Soyano T., Kosetsu K., Sasabe M., Machida Y. (2010): HINKEL kinesin, ANP MAPKKKs and MKK6/ANQ MAPKK, which phosphorylates and activates MPK4 MAPK, constitute a pathway that is required for cytokinesis in *Arabidopsis thaliana*. *Plant Cell Physiol* **51**, 1766-1776.

Takahashi Y., Soyano T., Sasabe M. and Machida Y. (2004): A MAP kinase cascade that controls plant cytokinesis. *J. Biochem* **136**, 127-132.

Takeuchi M., Karahara I., Kajimura N., Takaoka A., Murata K., Misaki K., Yonemura S., Staehelin L. A., Mineyuki Y. (2016): Single microfilaments mediate the early steps of microtubule bundling during preprophase band formation in onion cotyledon epidermal cells. *Mol Biol Cell* **27**, 1809-20.

Teixidó-Travesa N., Roig J., Lüders J. (2012): The where, when and how of microtubule nucleation - one ring to rule them all. *J. Cell Sci* **125**, 4445-4456.

Tilney L. G., Bryan J., Bush D. J., Fujiwara K., Mooseker M. S., Murphy D. B., and Snyder D. H. (1973): Microtubules: evidence for 13 protofilaments. *J Cell Biol* **59**, 267-275.

Tiwari S. C., Wick S. M., Williamson R. E., Gunning B. E. S. (1984): Cytoskeleton and integration of cellular function in cells of higher plants. *J Cell Biol* **99**, 63-69.

Tovey C. A., Conduit P. T. (2018): Microtubule nucleation by γ-tubulin complexes and beyond. *Essays Biochem* **62**, 765-780.

Trotta N., Orso G., Rossetto M. G., Daga A., Broadie K. (2004): The hereditary spastic paraplegia gene, spastin, regulates microtubule stability to modulate synaptic structure and function. *Curr Biol* **14**, 1135-1147.

Tulin A., McClerklin S., Huang Y., Dixit R. (2012): Single-molecule analysis of the microtubule cross-linking protein MAP65-1 reveals a molecular mechanism for contact-angle-dependent microtubule bundling. *Biophys J* **102**, 802-9

Vale R. D. (2003): The molecular motor toolbox for intracellular transport. *Cell* **112**, 467-480.

Vale R. D., Funatsu T., Pierce D. W., Romberg L., Harada Y., Yanagida T. (1996): Direct observation of single kinesin molecules moving along microtubules. *Nature* **380**, 451-3.
Vale R. D., Reese T. S., Sheetz M. P. (1985): Identification of a novel force-generating protein, kinesin, involved in microtubule-based motility. *Cell* **42**, 39-50.
Van Damme D., Van Poucke K., Boutant E., Ritzenthaler C., Inzé D., Geelen D. (2004): In vivo dynamics and differential microtubule-binding activities of MAP65 proteins. *Plant Physiol* **136**, 3956-67.
Van Damme D., Vanstraelen M., Geelen D. (2007): Cortical division zone establishment in plant cells. *Trends Plant Sci* **12**, 458-64.
Vaughan K. T. (2005): Microtubule plus ends, motors, and traffic of Golgi membranes. *Biochimica et Biophysica Acta* **1744**, 316-24.
Vavrdová T., Šamajová O., Křenek P., Ovečka M., Floková P., Šnaurová R., Šamaj J., Komis G. (2019): Multicolour three dimensional structured illumination microscopy of immunolabeled plant microtubules and associated proteins. *Plant Methods* **15**, 22.
Vleugel M., Kok M., and Dogterom M. (2016): Understanding force-generating microtubule systems through in vitro reconstitution. *Cell Adh Migr* **10**, 475-494.
Vos J. W., Dogterom M., Emons A. M. (2004): Microtubules become more dynamic but not shorter during preprophase band formation: a possible "search-and-capture" mechanism for microtubule translocation. *Cell Motil Cytoskeleton* **57**, 246-58.
Vyplelová P., Ovečka M., Komis G., Šamaj J. (2018): Advanced microscopy methods for bioimaging of mitotic microtubules in plants. *Methods Cell Biol* **145**, 129-158.
Wade R. H. (2009): On and around microtubules: an overview. *Mol Biotechnol* **43**, 177-191.
Wade R. H., and Hyman A. A. (1997): Microtubule structure and dynamics. *Curr Opin Cell Biol* **9**, 12-17.
Wasteneys G. O. (2002): Microtubule organization in the green kingdom: chaos or self-order?. *Journal of Cell Science* **115**, 1345-54.
Wasteneys G. O., and Ambrose J. C. (2009): Spatial organization of plant cortical microtubules: close encounters of the 2D kind. *Trends Cell Biol* **19**, 62-71.
Wickstead B., and Gull K. (2007): Dyneins across eukaryotes: a comparative genomic analysis. *Traffic* **8**, 1708-1721.
Wightman R., Turner S. R. (2007): Severing at sites of microtubule crossover contributes to microtubule alignment in cortical arrays. *Plant J.* **52**, 742-51
Woehlke G., Ruby A. K., Hart C. L., Ly B., Hom-Booher N., Vale R. D. (1997): Microtubule interaction site of the kinesin motor. *Cell* **90**, 207-16.
Woehlke G., Schliwa M. (2000): Directional motility of kinesin motor proteins. *Biochim Biophys Acta* **1496**, 117-27.
Yamada M., and Goshima G. (2017): Mitotic Spindle Assembly in Land Plants: Molecules and Mechanisms. *Biology* **6**, 6.
Yamagishi M. and Yajima J. (2018): Plus-end directionality is present in the catalytic core of kinesin-14 minus-end directed motors. *BioRxiv* https://doi.org/10.1101/292375.
Yamashita A., Sato M., Fujita A., Yamamoto M. and Toda T. (2005): The roles of fission yeast ase1 in mitotic cell division, meiotic nuclear oscillation, and cytokinesis checkpoint signaling. *Mol. Biol. Cell* **16**, 1378–1395.
Yang Y., Mahaffey C. L., Bérubé N., Nystuen A., Frankel W. N. (2005): Functional characterization of fidgetin, an AAA-family protein mutated in fidget mice. *Exp Cell Res* **304**, 50-8.
Yu I., Garnham C. P., Roll-Mecak A. (2015): Writing and Reading the Tubulin Code. *The Journal of Biological Chemistry* **290**, 17163-72.
Zhang D. H., Wadsworth P., and Hepler P. K. (1990): Microtubule dynamics in living dividing plant cells: Confocal imaging of microinjected fluorescent brain tubulin. *Proc. Natl. Acad. Sci. USA* **87,** 8820-8824.
Zhang D., Rogers G. C., Buster D. W., Sharp D. J. (2007): Three microtubule severing enzymes contribute to the "Pacman-flux" machinery that moves chromosomes. *J Cell Biol* **177**, 231-242.
Zhang H., Deng X., Sun B., Lee Van S., Kang Z., Lin H., Lee Y. J., Liu B. (2018): Role of the BUB3 protein in phragmoplast microtubule reorganization during cytokinesis. *Nat Plants* **4**, 485-494.

Zhang Q., Fishel E., Bertroche T., Dixit R. (2013): Microtubule severing at crossover sites by katanin generates ordered cortical microtubule arrays in Arabidopsis. *Curr Biol* **23**, 2191-5.
Zhang Q., Lin F., Mao T., Nie J., Yan M., Yuan M., Zhang W. (2012): Phosphatidic acid regulates microtubule organization by interacting with MAP65-1 in response to salt stress in Arabidopsis. *Plant Cell* **24**, 4555-76.
Zhang Y., Dong J. (2018): Cell polarity: compassing cell division and differentiation in plants. *Curr Opin Plant Biol* **45**(Pt A):127-135.
Zhang Y., Iakovidis M., and Costa S. (2016): Control of patterns of symmetric cell division in the epidermal and cortical tissues of the Arabidopsis root. *Development* **143**, 978-982.

7 List of Abbreviations

+TIPs	(+) end tracking proteins
AAA	ATPases Associated with diverse cellular Activities
ANP	Mitogen-activated protein kinase kinase kinase
Ase1	Anaphase Spindle Elongation 1
AtFH4	Formin-like protein 4
BSA	Bovine serum albumine
CDK	Cyclin-dependent kinase
CESA	cellulose synthase enzyme
CGMC	Group of Protein Kinases (CDK, MAPK, GSK3 and CLK)
CLASPs	CLIP-associated proteins
CLK	CDC-like Kinase
CSI	Cellulose synthase interactive protein 1
Col-0	Wild Type Ecotype of *Arabidopsis thaliana*
DAPI	4',6-diamidino-2-phenylindole
dH_2O	Distilled water
DMSO	Dimethyl Sulfoxide
DNA	Deoxyribonucleic acid
EB1a	End Binding 1a protein
EB1a	End Binding 1a protein
EB1c	END BINDING protein 1c
eGFP	enhanced green fluorescent protein
EGTA	Ethylene glycol-bis(β-aminoethyl ether)-N,N,N',N'-tetraacetic acid
Feo	fascetto; the Drosophila homolog of PRC1
FOV	Field of view
G2 phase	Gap 2
GCPs	γ-tubulin complex proteins
GDP	guanosine diphosphate
GTP	guanosine triphosphate
KCBP	kinesin calmodulin binding protein
KHC	Kinesin heavy chain
KLC	Kinesin light chain
KOH	Potassium Hydroxide
MAP2	Microtubule-associated protein 2
MAP2K	MAP kinase kinase
MAP3K	MAP kinase kinase kinase
MAP65-1-9	65-kDa microtubule-associated protein 1-9
MAP65s	65-kDa microtubule-associated proteins
MAP70	70 kDa microtubule-associated protein
MAP70-5	70 kDa microtubule-associated protein 5
MAPK	mitogen-activated protein kinase
MAPs	microtubule-associated proteins
MBD	Microtubule binding domain
$MgSO_4 \times 7\ H_2O$	Magnesium Sulfate Heptahydrate
Milli-Q®	Ultrapure Water
MKK6	Mitogen-activated protein kinase kinase 6
MPK4	Mitogen-activated protein kinase 4
MPK6	Mitogen-activated protein kinase 6

MS	Murashige and Skoog
MTOC	microtubule organizing center
MTs	microtubules
MTSB	Microtubule-stabilizing Buffer
$NaBH_4$	Sodium Borohydride
NaClO	sodium hypochlorite
PALM	photoactivation localization microscopy
PBS	Phosphate Buffered Saline
PCR	polymerase chain reaction
PFA	Paraformaldehyde
PIPES	Piperazine-N,N′-bis(2-ethanesulfonic acid)
PLE	65-kDa microtubule-associated protein 3
POK2	PHRAGMOPLAST ORIENTING KINESIN 2
PPase	phosphatase
PPB	preprophase band
PRC1	Protein Regulator of Cytokinesis 1
PTM	Post-translational modification
ROI	Region of interest
RT	Room Temperature
SAC	spindle assembly checkpoint protein
SIM	structure illumination microscopy
SIM	structured illumination microscopy
STED	stimulated emission depletion microscopy
STORM	stochastic optical reconstruction microscopy
TAE	tris-acetate-EDTA
tagRFP	red fluorescent protein
TBB2	Tubulin beta-2
TIRF	Total Internal Reflection Fluorescence Microscopy
Tris	Tris(hydroxymethyl)aminomethane
TUA6	Tubulin α-6
WT	Wild Type
γ-TuRCs	γ-tubulin ring complexes

8 Addendum

Parts of the thesis were contributed to the publication "Vavrdová T., Šamajová O., Křenek P., Ovečka M., Floková P., Šnaurová R., Šamaj J., Komis G. Multicolour three dimensional structured illumination microscopy of immunolabeled plant microtubules and associated proteins. Plant Methods 2019 15:22. doi: 10.1186/s13007-019-0406-z".